Chaotic Vibration in Machine Systems and Its Implications for Design

by

Pengyun Gu

B.S., Shanghai Jiao Tong University, 1982
M.S., Shanghai Jiao Tong University, 1984

Submitted to the
Department of Mechanical Engineering
in partial fulfillment of the requirements for the degree of

Doctor of Philosophy

at the

Massachusetts Institute of Technology

June 1994

Signature of Author_____
Department of Mechanical Engineering
June 1, 1994

Certified by_____
Professor Steven Dubowsky
Thesis Supervisor

Accepted by_____
Professor Ain A. Sonin
Chairman, Departmental Graduate Committee

Chaotic Vibration in Machine Systems and Its Implications for Design

by

Pengyun Gu

Submitted to the Department of Mechanical Engineering
On June 1, 1994, in partial fulfillment of the requirements
for the degree of Doctor of Philosophy

Abstract

Accurate prediction of machine performance is a key to the design of high performance machines. Due to the existence of clearance connections and component flexibility, the dynamic behavior of machine systems exhibits sensitivities to small variations of system parameters. These sensitivities limit the usefulness of predictions from computer-based simulations for design. Certain sensitivities are associated with chaotic behavior of the systems. This thesis investigates the design implications of chaotic behavior in machine systems with clearance connections and component flexibility. It also proposes a design methodology to most effectively use the predictions of machine models at the design stage.

The dynamic behaviors of two systems, called the Impact Beam System and the Spatial Slider Crank, are investigated. The existence of chaotic vibrations in these two systems is confirmed both numerically and experimentally. The dynamic responses of these systems can be classified into three characteristic types. These classifications are useful guidelines for design.

While Type I Response is well-behaved, Type II and Type III Responses are sensitive to small variations of the system parameters, presenting important design problems. The dynamic behavior of such machine systems could be quite different from model-based predictions due to these sensitivities. In particular, the periodicity of the Type II Response may lead designers to overlook the sensitivities. Design guidelines are developed for classifying these three types of responses and for evaluating the fatigue life and the reliability of machine systems at the design stage.

Thesis Supervisor: Dr. Steven Dubowsky
Title: Professor of Mechanical Engineering

To my wife

Acknowledgments

I would like to thank my thesis advisor, Professor Steven Dubowsky, for his guidance, inspiration, and financial support throughout this work. His depth of knowledge and keen insights into the subject have been my sure guide in this research. His enthusiasm for exploring new concepts and new approaches will always be a positive influence on my professional career.

I wish to express my gratitude to Professors Stephen Crandall and Steve Strogatz for serving as members of my thesis committee and for their valuable critical comments at various stages of the research. Professor Crandall, listening to your lectures during AV Lab lunch meetings has been a very enjoyable learning experience. I wish I could take more courses taught by you. Professor Strogatz, thank you for teaching me chaos in your class. I really like your teaching style.

I wish to express my thanks to Dr. Ming-Kai Tse for guidance and encouragement as well as financial support for my early years at MIT.

I am very grateful to Professor Richard Lyon for teaching me Statistical Energy Analysis and many useful discussions on noise and vibration issues as well as for helping me in my career planning.

I thank my Chinese friends at MIT: Drs. Zhong Cai, Fuquan Gao, Xiaojun Liu, Li Lin, Jie Ren, Hong Tian and Youhong Gong. I would like to thank Professor Zhao Chunsheng and his family for their friendship. Professor Zhao, thank you for beautiful flowers and for taking many memorable pictures after my thesis defense. Good luck for your research in China.

I would like to thank Fred Coté for his help for my experimental setup. With his assistance, I could have my work done and keep my ten fingers well.

I would like to express my thanks to my colleagues, both past and present, in Dr. D's group. All of you have created an enjoyable, yet productive, atmosphere. I would to says: thanks for many jokes and helpful hands. Thanks to Jeff Cole, Tom Corrigan, Dr. Dinos Mavroidis, Nate Rutman, Craig Sunada, Michele Tesciuba, Richard Wang, Dr. Kazuya Yoshida for many useful suggestions when I prepared my thesis defense. In particularly, to Dinos for many suggestions and discussions since you joined this group.

I would like to thank members of "Machine Dynamics Group": Dr. Joe Deck, Erin O'Connell, and Dr. Charles Oppenheimer. Charles gave many suggestions for my research. We had many discussions on SEA. Thank you for recommending me to serve as AV Lab manager. I learned a lot from this job. Joe has helped me in many ways. He is a very knowledgeable colleague. From the day I walked into room 3-443, my "one question strategy" for Joe has been working very well. His patience and generosity have made me very comfortable to work with him for many years. He taught me how to run his program which has been used extensively in this research. He gave me many constructive suggestions for my research. I remember many, many discussions we had. I am very grateful to Joe for his critical reading on both the English and technical aspects of my thesis. Thank you Joe, I wish you good luck in your life. For Uwe Müller, although you were not a member of this sub-group, I appreciate your help for my experiments. I am glad you were MIT when I served lunch for the group. Good luck in Germany. I will see you there.

Thanks to Kate Melvin for providing technical support and helping my English.

Thanks to Laureen Luszcz for her assistance since she came back to this group.

I would like to thank other professors of the Acoustics & Vibration/Machine Dynamics Laboratory: Triantaphyllos Akylas, Patrick Leehey, Frank Feng. They listened to my presentations in Lab lunch meetings and made suggestions. Thanks to Professor Frank Feng for friendship and for coming to my thesis defense. I wish you good luck at MIT. I thank student members of the Lab: Djamil Boulahbal, Dr. Jangbom Chai, John Chi, Sophie Debost, Hua He, Dr. Kay Herbert, Chris Lerch, Dr. Dan McCarthy, Roni Shlomi, In-Soo Suh for their cooperation and support when I worked as lab manager.

I thank Mary Toscano and Laurie McLaughlin for their help during my tenure as AV lab manager.

I thank Leslie Regan for effective administration and her help whenever I walked into her office.

Thanks to my cousin, Shengming Lin, and his family, for their help to my family.

I am especially grateful to my uncle and aunt, Institute Professor and Mrs. C. C. Lin for their generosity, concern, encouragement and guidance. Uncle's advice on "Why, What and How" has a great influence on my research and my future career. Aunt has helped our family whenever we needed.

I would like to thank my "family-in-law" for their support and for having faith that I would one day be able to provide for my wife. Thanks to my parents-in -law for taking care of my son and for everything they have done for me and my family.

My mother and father deserve a great of thanks for their love, encouragement, and support through my long education. Mom and dad, thank you for firm supports whenever I pursue my goals. Your expectation has been a continuous source of motivation. You should be proud of my achievements. To my young sister, thank you for your love and encouragement. I wish you good luck in your pursuits.

My son Steve has helped me in many ways he is still too young to understand. Steve, thank you to make my life more enjoyable.

Finally, I would like to thank my lovely wife, Dr. Hui Xie, who has sustained me throughout this many years at MIT. Hui, thank you for enduring so long and having great inspiration and faith. You have provided all the support and encouragement to keep me going when it all seemed hopeless. In many ways, this accomplishment is yours as well as mine. Without your love, talent and support in times of struggle, this dissertation would not exist today. Now, I am done. Let us enjoy our new, wonderful life.

The support of this research by the National Science Foundation under grant number MSS-9023487 is greatly appreciated.

Table of Contents

List of Figures

List of Tables

Chapter 1
Introduction

This chapter explains the motivation for this research, reviews previous work in the related areas, highlights the contributions of the thesis, and finally, outlines the organization of this thesis.

1.1 Motivation

Over the decades, many analytical design models have been developed to predict the dynamic performance of machines with non-ideal characteristics such as clearance connections and component flexibility [3-10,12-14,25,27,28,34,40,41,57-59]. The effects of such non-ideal characteristics often degrade a machine's dynamic performance by causing impacts, vibration and noise, component fatigue, and poor precision. These developed models have focused on *predicting* this dynamic behavior.

Recently, it has been found that the dynamic responses of machine systems with clearance connections could exhibit both a large variation and high sensitivity to small parameter changes and operating conditions [3,4]. The findings have suggested that there are limitations on predictions of the responses based on machine models for design analysis, due to the sensitivity of the responses to small variations of machine parameters. Since every real engineering design, when manufactured and used, is subject to variations in its parameters, such as in its component dimensions and material properties, the real dynamic behavior of a machine could be quite different from the behavior predicted using an analytical modeling method.

The sensitivity of the dynamic behavior in responding to small variations in the parameters may indicate the existence of the chaotic

behavior in the systems since a characteristic of a chaotic system is the sensitivity of its dynamic response to small changes of initial conditions and system parameters [16,36,61]. In fact, chaotic behavior has been found in simulations of systems with non-ideal elements such as clearance connections [1,21,26,29-30,32-33,37-39,44,49-56,60,62,67]. Most of the research has focused on chaos *itself* and usually concerned with demonstrating the existence of the chaos, rather than with the effects of chaotic behavior on machine performance. Yet, the ability to predict accurately the performance of real systems needs to remain the goal of their design analysis.

New approaches need to be developed to use the predictions of machine models at the design stage effectively. In this thesis, the following important issues will be addressed: 1) how does a designer effectively test for the potential existence of chaotic vibrations in a machine design? 2) what are the effects of chaotic vibrations on a machine's performance? and 3) what is the relationship between chaotic vibrations and design parameters?

1.2 Background and Literature Review

1.2.1 Modeling Clearance Connections and Component Flexibility

Over the past three decades, the effects of clearance connections and component flexibility in machines have been studied extensively. Research in this area has been focused on the dynamic characteristics of a single clearance connection [5,12,27], a rigid-link system with clearance connections [9-10,13-14,25,34,57], and a flexible-link system with clearance connections [3,6-8,28]. A brief review will be given here; a comprehensive review can be found in reference [3].

Three different approaches have been proposed for modeling a single clearance connection or its equivalent effects. The first approach models the

connection as having compliance and friction but no clearance gap [25]. The second approach treats a clearance impact as an instantaneous event, characterized by conservation of momentum and energy dissipation described by a restitution coefficient. [28,34,57]. These two models cannot directly predict the clearance impact force. The third approach models the impact force in the clearance connection as a function of the relative motion, internal geometry, and material properties of the connection [5,27]. This approach is capable of predicting a detailed time history of the contact force during the impact. These connection models have been combined with rigid-body and flexible-body models of machine components [3-10,25,28,34,57] in order to predict an integrated machine's dynamics.

1.2.2 Chaotic Behavior of Simple Impact Oscillators

The clearance models described above, often called either the impact pair or impact oscillator by researchers, have been applied to analyze the chaotic behavior of the clearance connections. A bilinear system, a model of an asymmetrical clearance, was studied by Shaw and Holmes [51-53] using bifurcation theory and other tools of modern dynamical systems theory. Harmonic, subharmonic and chaotic vibrations were found to exist. Shaw [50] extended the analysis to a system having two-sided amplitude constraints. He found that in certain parameter regions no simple stable motions exist. In these regions complicated bifurcation sequences result in chaotic motions.

Moon and Shaw [38] studied forced vibrations of a nonlinear elastic beam. The nonlinearity arose from bi-modal boundary conditions applied at the end of the cantilevered beam. This system was numerically analyzed using a simple single-mode model. They showed that the system exhibits

chaotic behavior for a sinusoidal excitation. The numerical results were experimentally confirmed later by Shaw [51].

Shaw and his coworkers studied pendulum-type-impact problems [39,48-49,55]. In their studies, the system consisted of an inverted pendulum with rigid barriers which limited the amplitude variation of the pendulum from the unstable upright position. When subjected to a periodic excitation the system response can be quite complicated and may include subharmonics and/or chaotic motions. Their analytical results were verified by the experiments [39].

Li, Rand and Moon [30] studied space truss structures having pin joints with play, using a simple model called zero-stiffness model. They analyzed simple symmetric and asymmetric motions of the model under small forcing amplitudes. For large forcing amplitudes, it was numerically shown that the system exhibits chaotic behavior. The chaotic behavior in such space truss structures was confirmed experimentally [37].

For compliant off-shore structures, subharmonic and chaotic motions were also predicted using an impact oscillator model by Thompson and his coworkers [60,62]. They delineated cascades of period-doubling bifurcation leading to chaotic regimes.

Heiman, Bajaj and Sherman [21] investigated the dynamics of an inclined impact pair, consisting of a harmonically moved primary mass and a secondary mass moving in an inclined slot within the primary mass. They found that harmonic, subharmonic and chaotic motions can exist for various values of parameters.

Mahfouz and Badrakhan [33] studied three systems with clearance. Chaotic motions and subharmonics of various orders were observed. It was shown that chaos is, in general, preceded and/or followed by a subharmonic

motion of order 3. They also noticed that decreasing the viscous damping level increases the chances of having chaotic motions.

Peterka and Vacík [44] explored the mechanisms of the transitions from periodic to chaotic motions in impact systems. They studied the impact behaviors of a one DOF impact oscillator and a multiple DOF oscillator. The behaviors of the two systems included period-doubling and chaos. The global behavior of one dimensional, harmonically excited impact oscillators was studied by Kleczka and his coworkers [29] and Whiston [67]. Aidanpää and Gupta [1] recently investigated a two-degree-of-freedom impact oscillator with proportional damping. The dynamic behavior of the system includes period-doubling, period halving, and chaos. Their results may be applied to the design of impact tools.

Païdoussis and Li [43] studied the chaotic dynamics of heat exchanger tubes impacting on the loose baffle plate which supports the tubes. Their numerical solutions showed that the amplitude of motion grew until impacting with the loose support occurred; more complex motions arose leading to chaos at a sufficiently high flow velocity. Furthermore, they used a impact oscillator model with negative damping to study the complex behavior of the system.

In general, it has been found both analytically [1,26,29,30,49-50,52-55,60,62,67] and experimentally [32,37,39,51] that even under periodic excitation, a simple impact system can exhibit very complex dynamics such as subharmonic and chaotic vibrations.

1.2.3 Chaotic Behavior of Mechanisms

There has been a series of studies on impact printers. Chaotic motion was found in impact printers at the high speeds at which impact print

hammers operate [22]. In this case, strict periodicity of the actuator motion is lost and randomness sets in. The chaotic motion causes print force variations, resulting in unacceptable print quality. To improve the impact printer's performance, Tung and Shaw [65,66] established printer performance criteria and proposed a control method to increase the printer speeds retaining acceptable print quality, based on the simulation results of their mathematical model.

Recently, the study of chaotic behavior in more realistic machine systems with multiple clearance connections and nonlinear kinematics has become an active topic. Seneviratne and Earles [46,47] studied a four-bar mechanism using a massless-link model for a clearance joint to predict contact loss in the mechanism. Based on their numerical simulation, certain cases were found where the response was non-periodic and sensitive to initial conditions, indicating chaotic behavior. Farahanchi and Shaw [11] used a one-degree of freedom model for a slider crank mechanism, with a clearance in the sliding joint. They found numerically that chaotic motion is prevalent over a range of parameters which corresponds to high crank speed and/or low values of bearing friction.

To investigate the existence of chaos in more realistic systems having rigid members, as opposed to the highly flexible structures often seen in chaotic demonstrations [38,51], Peurach and Tongue [45] used a slider-crank mechanism to approximate the single mode response of a continuous beam under a periodic excitation [38]. The experimental setup displayed complicated dynamic responses, including chaos, while the idealized theoretical model only supported the existence of a period-one response. However, it was shown that an extremely small external perturbation would cause the response of the model to be chaotic.

Mevel and Guyader [35] studied the dynamic motion of a lightly loaded ball bearing system in order to find out the mechanisms involved in transitions from periodic to chaotic behavior. The period-doubling route and the quasiperiodic route to chaotic behavior were observed. They also noticed that loss of contact always occurred when chaos took place under the two routes and suggested that contact loss is a necessary condition for chaotic behavior.

1.3 Objective and Approach

Up to now, however, research on chaotic behavior in realistic machines has been limited mainly to numerical analysis. There have not been experiments to confirm the existence of chaotic behavior in mechanisms with nonlinear kinematics. Furthermore, there has not been a systematic investigation to study the chaotic vibrations of machine systems from a design point of view.

The objectives of this research are to confirm experimentally the existence of chaotic vibrations in machine systems, to study the effects of this behavior on the system performance, to develop practical methods for testing chaotic behavior of machine models at the design stage, and to propose design guidelines for dealing with potential chaotic behavior of machine systems.

Two systems have been investigated systematically in this research: an Impact Beam System [3,42] and a Spatial Slider Crank mechanism [3,41]. The Impact Beam System was designed to provide physical insights into the dynamic behavior of machines with clearance connections and component flexibility. It represents the features found in common machines. For simplicity, this system excludes the interactions among multiple nonlinearities, such as nonlinear nominal kinematic motions and multiple

clearance connections. This system is used to suggest the basic characteristics of chaotic behavior in machines with clearance connections and component flexibility.

The Spatial Slider Crank mechanism is chosen to further explore chaotic phenomenon in more complex machine systems. This mechanism, as a prototype machine, has multiple clearance connections as well as nonlinearities associated with full spatial nonlinear kinematic motions.

These two systems are modeled using techniques for modeling machines with clearance connections and component flexibility [3,7,58,59]. Extensive numerical analyses are performed for each system. The numerical results are compared with experiments. The global behaviors of these systems are studied as functions of the major system parameters, such as clearance size, excitation frequency, and component dimensions. From the studies, the parameter regions causing chaotic vibrations are identified. The effects of chaotic vibrations on machine performance are studied and understood.

Based on the characteristics of dynamic responses common to the Impact Beam System and the Spatial Slider Crank mechanism, design guidelines for dealing with chaotic vibrations in this class of systems are formulated and evaluated.

1.4 Contributions of the Research

The major contribution of this research is an exploration of the design implications of chaotic behavior in machine systems through extensive analytical and experimental studies of two systems with clearance connections and component flexibility. The principal results of this research are summarized as follows:

- The existence of chaotic vibrations in machine systems with clearance connections and component flexibility is confirmed both numerically and experimentally. The Two-Step Test method and the Matrix Update Test method are developed for testing chaotic vibrations of computer-based dynamic simulation of machine models.
- Empirical predictive criteria are presented for the regions of system parameters that result in chaotic vibrations. Chaotic vibrations are found to be associated with large clearances, high operating speeds, and low values of damping.
- Based on the characteristics of the dynamic response of machine systems, the responses are classified into Type I, Type II, and Type III for design purposes. Design guidelines are developed for classifying these three types of responses and for evaluating fatigue life and reliability of the machine systems which exhibit each of three response types.
- A design methodology, which implements the developed methods and guidelines, is developed to effectively use the predictions of the machine models at the design stage.

1.5 Thesis Overview

The thesis is organized as follows.

Chapter 2 reviews both a modeling technique for complex machine systems with clearance connections and component flexibility and basic concepts of chaotic dynamics. This modeling technique was originally developed by Sunada [56,57] to model flexible spatial machine systems and was later extended to include clearance joints by Deck [3,7]. It has been used to model the two systems studied in this thesis. The purpose of including the

basic concepts of chaotic dynamics is to clarify definitions and notations used in the thesis.

Chapter 3 presents the experimental and analytical studies of a simplified machine system called the Impact Beam System. The study of the Impact Beam System provides physical insights into the chaotic vibration of machine systems with clearance connections and component flexibility. The Impact Beam System was designed and constructed by Deck [3], Oppenheimer [42], and the author. The system, its experimental setup and dynamic model are described. Numerical results and experimental data demonstrate the chaotic vibrations of the system. The sensitivity of the dynamic response to small variations of system parameters is investigated. Based on the characteristics of the dynamic responses of the system, the responses are classified into Type I, Type II and Type III for design purposes. The comparison between numerical results and experimental measurements indicate that the numerical model captures much of the qualitative dynamic behavior of the system.

Chapter 4 presents the experimental and analytical studies of a more complex machine system call the Spatial Slider Crank mechanism. The mechanism was originally designed and constructed by Deck [3] and O'Connell [41]. While the Impact Beam System has only one clearance connection, the Spatial Slider Crank mechanism has two clearance connections and other nonlinearities associated with full spatial, nonlinear kinematic motions. The existence of chaotic vibrations in this mechanism is confirmed both numerically and experimentally. The sensitivity of the dynamic response to small variations of system parameters is studied. The three identifiable types of responses are observed in different parameter regions of the mechanism.

Chapter 5 provides a design methodology to effectively use the predictions of machine models at the design stage. The Two-Step Test method and the Matrix Update Test method for testing chaotic vibrations of computer-based dynamic simulation of machine models are developed. The guidelines for classifying the response as Type I, Type II or Type III and for evaluating fatigue life and reliability of the machines are formulated and evaluated.

Finally, Chapter 6 concludes the thesis with a brief summary of the results.

Chapter 2
Basic Tools and Concepts

2.1 Introduction

This chapter presents a modeling technique for machine systems with clearance connections and component flexibility and basic concepts of chaotic dynamics. The primary intent of this chapter is to clarify definitions, and notations for readers who may be unfamiliar with the terminology used.

2.2 Dynamic Modeling of Machine Systems

In this section, an analytical modeling technique, developed for complex machine systems with component flexibility and clearance connections, is briefly reviewed. The technique was originally developed by Sunada [58,59] to model flexible spatial machine systems with ideal joints and later extended by Deck [3,7] to include clearance joints. This technique models the distributed mass and flexibility of the machine components, large, nonlinear kinematic motions, and clearance connections of the machine system.

2.2.1 The Dynamic Modeling Technique

Using the finite element method, this technique models the distributed mass and flexibility of machine components, which are called links. The standard finite element models of the machine's links are combined with Hartenberg-Denavit descriptions of the links' nominal motions to derive equations of motion that include the effects of large kinematic motions on the elastic deformations of the links.

The FE nodal displacement coordinates are called perturbation coordinates, and they describe the motions of the FE nodes of the link with respect to a reference frame attached to the link's nominal motion. The dynamic equations of motion for a given link are derived using Lagrange's formulation, in which perturbation coordinates are the generalized coordinates. The dynamic equations of motion for the i^{th} link are given as:

$$\mathbf{M}_i\ddot{\mathbf{p}}_i + \mathbf{G}_i\dot{\mathbf{p}}_i + \mathbf{K}_i\mathbf{p}_i = \mathbf{f}_i \tag{2.1}$$

where the vector $\mathbf{p}_i$ is the perturbation coordinate vector of the i^{th} link. The $\dot{\mathbf{p}}_i$ and $\ddot{\mathbf{p}}_i$ are the perturbation velocities and accelerations, respectively. The matrices $\mathbf{M}_i$, $\mathbf{G}_i$, and $\mathbf{K}_i$ are the mass, damping and stiffness matrices. The vector $\mathbf{f}_i$ includes the external forces applied to the link, the dynamic forces resulting from the velocities and accelerations of the nominal link motion, and the gravity force. The elements of the $\mathbf{M}_i$, $\mathbf{G}_i$, and $\mathbf{K}_i$ matrices and the force vector $\mathbf{f}_i$ are, in general, nonlinear functions of the nominal motions of the machine components. These functions represent the nonlinear kinematics of the machine system, including configuration-dependent mass and stiffness properties and corrections for the accelerated motions of the link reference frames.

In general, the detailed FE model of each link makes the equations of motion, Eq. (2.1), a very large set. The numerical integration of such a large set of equations for nonlinear analysis would be prohibitively expensive in terms of computational time. The Component Mode Synthesis (CMS) technique is used to reduce the size of the Eq. (2.1) without a serious loss of dynamic accuracy[24]. The perturbation coordinate vector, $\mathbf{p}_i$, is transformed into a vector, $\mathbf{a}_i$, which contains the interface coordinates and mode coordinates of the link, through a CMS transformation matrix:

$$\mathbf{p}_i = \mathbf{A}_i \mathbf{a}_i, \tag{2.2}$$

where $\mathbf{A}_i$ is the CMS transformation matrix. Now the size of the vector $\mathbf{a}_i$ is much small than that of the vector $\mathbf{p}_i$. The number of modal coordinates included in the vector $\mathbf{a}_i$ depends on the requirement of the frequency consideration.

A reduced set of equations of motion is produced for each link by substituting Eq. (2.2) and its derivatives into Eq. (2.1). Furthermore, by introducing the connection constraints between the links in the machine, the reduced vector $\mathbf{a}_i$ is written as:

$$\mathbf{a}_i = \mathbf{B}_i \mathbf{q}_i, \tag{2.3}$$

where the matrix $\mathbf{B}_i$ is the compatibility matrix among link (i-1), link i, and link (i+1). The vector $\mathbf{q}$ is the global independent generalized displacement vector. The reduced link equations of motion are combined with Eq. (2.3) of each link to form global dynamic equations of the machine system:

$$\overline{\mathbf{M}}\ddot{\mathbf{q}} + \overline{\mathbf{G}}\dot{\mathbf{q}} + \overline{\mathbf{K}}\mathbf{q} = \mathbf{Q}, \tag{2.4}$$

in which the $\overline{\mathbf{M}}$, $\overline{\mathbf{G}}$, and $\overline{\mathbf{K}}$ describe the mass, damping and stiffness matrices of the system and , in general, are time varying. The vectors $\mathbf{q}$, $\dot{\mathbf{q}}$, and $\ddot{\mathbf{q}}$ are the global independent displacement vector, velocity vector and acceleration vector. The vector $\mathbf{Q}$ describes the force applied to the system, including actuator force/torques and external loads. The matrices $\overline{\mathbf{M}}$, $\overline{\mathbf{G}}$, and $\overline{\mathbf{K}}$ and vector $\mathbf{Q}$ are given as follows [3,58]:

$$\overline{\mathbf{M}} = \sum_{i=1}^{NL} \mathbf{B}_i^T \mathbf{A}_i^T \mathbf{M}_i \mathbf{A}_i \mathbf{B}_i, \tag{2.5}$$

$$\overline{\mathbf{K}} = \sum_{i=1}^{NL} \mathbf{B}_i^T \mathbf{A}_i^T \mathbf{K}_i \mathbf{A}_i \mathbf{B}_i + \sum_{i=1}^{NL} \sum_{j=1}^{NL} \mathbf{B}_i^T \mathbf{A}_i^T \mathbf{G}_i \mathbf{A}_i \mathbf{B}_{ij} \dot{\theta}_j + \sum_{i=1}^{NL} \sum_{j=1}^{NL} \mathbf{B}_i^T \mathbf{A}_i^T \mathbf{M}_i \mathbf{A}_i \left[\sum_{k=1}^{NL} \mathbf{B}_{ijk} \dot{\theta}_j \dot{\theta}_k + \mathbf{B}_{ij} \ddot{\theta}_j \right], \quad (2.6)$$

$$\overline{\mathbf{G}} = \sum_{i=1}^{NL} \left\{ 2\mathbf{B}_i^T \mathbf{A}_i^T \mathbf{M}_i \sum_{j=1}^{NL} \mathbf{B}_{ij} \dot{\theta}_j + \mathbf{B}_i^T \mathbf{A}_i^T \mathbf{G}_i \mathbf{A}_i \mathbf{B}_i \right\}, \quad (2.7)$$

$$\mathbf{Q} = \sum_{i=1}^{NL} \mathbf{B}_i^T \mathbf{f}_i, \quad (2.8)$$

where NL is the number of links in the machine system, $\mathbf{B}_{ij}$ is defined as $\frac{\partial \mathbf{B}_i}{\partial \theta_j}$, and $\mathbf{B}_{ijk}$ is defined as $\frac{\partial^2 \mathbf{B}_i}{\partial \theta_j \partial \theta_k}$. The forms of the compatibility matrices, $\mathbf{B}_i$, which are used to construct the equations of motion of the system, are determined by the nature of the system's joints. These joints may be ideal kinematic joints or non-ideal joints with compliance and clearances.

2.2.2 Connection Models

To form Eq. (2.4) from the dynamic equations of the motion for each individual link, connection information between adjacent links is needed. The flexible components of machine systems can have large relative motions, and are connected by different types of joints such as revolute, spherical or prismatic joints. The basic features of different connection models are briefly presented as follows.

Ideal joints

An ideal joint is defined as a joint without any internal clearance and compliance. When two links are connected through an ideal joint, certain motions of one link are made to match those of another due to the kinematic constraints of the joint. The relationships between the matched motions

change over time. In addition, the kinematic constraints are relaxed for motions that are permitted by the joint. For example, when two links are connected through a revolute joint, the translation motion of one link matches that of another link, but relative rotation is permitted by this joint. Therefore, an ideal joint model provides kinematic constraints between adjacent links. For ideal joints, the compatibility matrices, $\mathbf{B}_i$, which describe the connection constraints are, in general, nonlinear functions of the nominal motion vector θ and its derivatives.

Clearance Joints

A clearance joint consists of two parts that fit together with a clearance. The clearance is much smaller than the overall dimension of the joint. A clearance joint model has internal compliance and clearance, and may also have internal friction and other effects. Due to the existence of the clearance in the joint, some of the kinematic constraints are removed between the connected links. These relaxed motions of the links are constrained whenever the relative motions between the links reach limits of the clearance. The interaction forces and torques between the links constrain their motions. These forces and torques are functions of the relative motion between the links, and they are applied as reactions to both of the links. Therefore, a clearance joint model provides nonlinear force constraints. If the i^{th} link is connected to the $(i-1)^{th}$ at one end and the $(i+1)^{th}$ link at the other through two clearance joints, the elements of the $\mathbf{B}_i$ matrix are constant, either zeros or one. Then all the elements of i^{th} link's $\mathbf{a}_i$ vector are independent, and the $\mathbf{q}$ vector is simply a concatenation of the $\mathbf{a}_i$ vector. Different types of clearance connection models such as spherical, revolute, and prismatic joints can be found in reference [3,7].

A numerical simulation package called ASSET (Advanced Spatial Systems Emulation Technique) was developed by Deck [3] to implement this modeling technique and the connection models. ASSET has been used extensively throughout this research.

2.3 Basic Concepts of Chaotic Dynamics

Chaotic motions are complicated, unpredictable and seemingly random motions in deterministic physical systems. The time history of a chaotic motion in the deterministic physical system has a *sensitive dependence on initial conditions*. This class of motions is associated with a state of motion called a *strange attractor* [16,36,61].

2.3.1 Diagnostics of Chaotic Vibrations

There are many methods for determining whether or not a system is truly chaotic and they provide useful information on the system characteristics [36]: (a) Time histories, (b) Phase plane portraits, (c) Poincaré map, (d) Fourier spectrum, and (e) computation of Lyapunov exponents. These methods, as described in reference [36], are outlined as follows:

Time Histories

Non-repeatability or irregular variations in the time history of a dynamic response provide a first clue that the system may have chaotic vibrations. The nature of the response can not be concluded by this observation since a motion could have a long-period behavior beyond the observation period, or could be a quasiperiodic response. Other test methods should be used to confirm the nature of the response.

Phase Plane Portraits

A phase plane portrait is a graphical representation of the behavior of a dynamic system. When the motion is periodic, the phase plane portrait shows a closed orbit. When the motion is chaotic, the phase plane portrait shows an orbit that never closes or repeats. Thus, the trajectory of the orbit in the phase plane portrait will tend to fill up a section or a band-section of the phase plane. Phase plane portraits sometimes provide very little information and thus Poincaré maps have to be used.

Poincaré Map

A Poincaré map is a phase plane portrait in which the position of a system's trajectory is recorded only at given times, not continuously. The usual time interval used in a periodically excited system is equal to the excitation period. For a single periodic response, the Poincaré map will appear as a single point in the phase space. For subharmonic dynamic behavior, the Poincaré map will appear as a set of points, the number of which are equal to the number of external forcing periods contained in one period of the response. Chaotic motion produces a Poincaré map which usually has a fractal structure and represents a cross-section of the actual strange attractor associated with the system.

Frequency Spectrum

One of the clues to detecting chaotic response is the appearance of a broadband spectrum of frequencies in the responses when the input is a single frequency harmonic motion. This noise-like spectrum is a characteristic exhibited by all chaotic systems. In some systems, in addition to

the broadband components, the spectrum contains spikes indicating the predominant frequencies in the responses.

Sensitivity to Initial Conditions and Lyapunov Exponents

Chaotic behavior of a deterministic system implies a sensitivity of the response of the system to small changes in initial conditions. The accurate prediction of long term response becomes impossible because, in this case, a small initial condition uncertainty will be magnified exponentially as time evolves and, as a result, two originally indistinguishable initial conditions can lead to completely different long-term solutions.

In order to quantify this sensitivity to initial conditions, the Lyapunov exponents of the response need to be calculated. The Lyapunov exponent is an estimate of the rate of divergence or convergence and characterizes quantitatively the average exponential divergence or convergence of neighboring trajectories. Negative Lyapunov exponents indicate the closeness of neighboring trajectories with evolution of time, thereby signaling periodic responses. At least one positive Lyapunov exponent indicates a chaotic trajectory and divergence of initially closed trajectories. A technique for numerically calculating Lyapunov exponents of chaotic responses in experiments was given by Wolf and his coworkers [68].

While phase plane portraits and Poincaré maps can provide graphic evidence for chaotic behavior and the fractal properties of strange attractors, the Fourier spectrum and Lyapunov exponents can give quantitative measures of chaotic vibrations. The quantitative measures of chaotic vibrations are very important for the cases in which Poincaré maps may be

difficult to capture and the measures are the only hard evidence for chaotic behavior.

2.3.2 Routes to Chaos

The mechanisms of the transitions from periodic to chaotic are of fundamental importance for understanding the phenomenon of chaotic behavior. In many systems, as some parameters vary, several characteristic changes in the motion may occur due to bifurcations that can lead to chaos. The bifurcation types leading to chaos are the infinite period-doubling cascades, the intermittencies and the crises [36,61]. These routes to chaos are briefly described as follows.

Period-doubling

The period-doubling route to chaos is the most widely known and studied[16,36,61]. In this case, the variation of a typical system parameter leads the dynamical system through a sequence of successive bifurcations in which the period of all solutions at each step of the bifurcation is twice that at the previous step: thus this process is call a period-doubling cascade. A common feature of a chaos is a succession of bifurcations to higher and higher subharmonics as a parameter is varied. In some systems, chaos occurs as a sequence of period-doubling bifurcations with a limit point beyond which strange attractors occur.

Intermittency

Intermittent bifurcations to chaos are caused by discontinuous or catastrophic disappearance of a periodic attractor inside a phase space region of chaotic transients [16,36,61]. Bifurcations to chaos via intermittency are

usually found in the dynamical systems that have interrupted, or incomplete, sequences of period doubling. In this route, one observes long periods of periodic motion with bursts of chaos. As the parameter varies, the chaotic bursts become more frequent and longer. Finally, the response becomes complete chaotic.

Crises

A crisis is defined as a collision between a chaotic attractor and a coexisting unstable fixed point or periodic orbit [15]. In crises, discontinuous qualitative changes occur in the character of the long-time behavior of the system. Phenomena associated with crises include sudden changes in the size of chaotic attractors, sudden appearances of chaotic attractors, and sudden destruction of chaotic attractors. It has been observed that response takes longer time to settle down to steady state response when the parameter is close to the crisis point [15,61].

Chapter 3
Study of an Impact Beam System

3.1 Introduction

This chapter presents a study of the Impact Beam System, which provides physical insights into the chaotic vibration of machine systems with clearance connections and component flexibility. The system and its experimental setup are introduced in Section 3.2, and the dynamic model is described in Section 3.3. Numerical simulations of the system are presented in Section 3.4. The effects of variations of system parameters are investigated in Section 3.5. Experimental results are presented and compared with numerical simulations in Section 3.6 and 3.7, respectively. Major results from this study are summarized in Section 3.8.

Numerical results and experimental data demonstrate the chaotic vibrations of the system. Based on the characteristics of the dynamic responses of the system, the responses are classified into Type I, Type II and Type III for design purposes. The comparison between numerical results and experimental measurements indicate that the numerical model captures much of the qualitative dynamic behavior of the system.

3.2 The System

The Impact Beam System (IBS) [3,42], illustrated schematically in Figure 3.1, consists of a beam, a one-dimensional adjustable clearance connection, and a baseplate. One end of the beam is held by a zero-clearance bearing. The other end of the beam is inside the one-dimensional clearance connection. In operation, the beam is excited by an external force, F(t), as depicted in Figure

3.1. Impact forces are generated at the clearance connection when the beam end reaches the clearance.

The system has been used to study the basic characteristics of dynamic behavior in common machines with clearance connections and component flexibility. The elements of this system are designed to represent features in such machines. The beam represents a flexible component; the clearance connection represents a bearing with an internal clearance; and the baseplate represents a supporting structure. For simplicity, this system includes only one nonlinear element (i.e., one clearance connection) and excludes the interactions among multiple nonlinearities, such as multiple clearance connections and nonlinear kinematic motions.

The experimental IBS is illustrated in Figure 3.2. A steel beam is mounted to the beam support using a flexure pivot, which provides a zero clearance bearing. The beam is excited by sinusoidal forces, which are generated by an electromechanical shaker attached to the beam through a steel rod. The shaker's force magnitude is controlled by a signal generator and a power amplifier. Figure 3.3 shows the instrumented adjustable-clearance joint with two piezoelectric sensors. As the free end of the beam moves, it strikes sensors that measure the contact forces at their tips. The author proposed using piezoelectric ceramic materials to directly measure the impact force at impact locations. The sensors were designed by the author and Uwe Müller, and constructed by Deck [3]. These sensors have flat dynamic responses from near DC to 10 kHz [3].

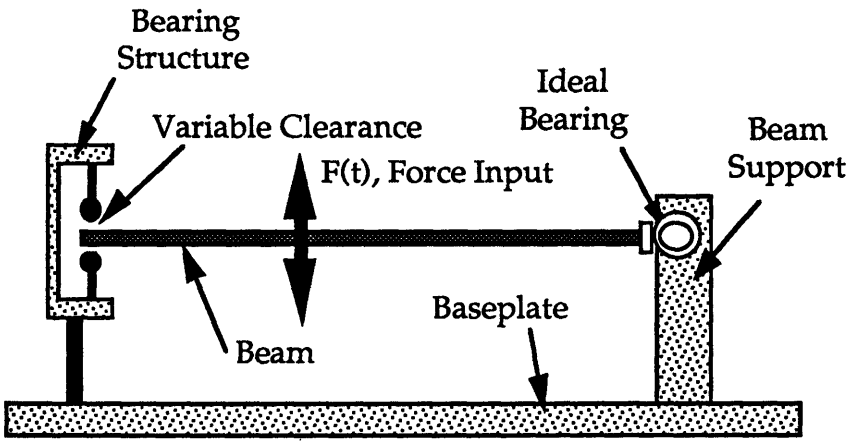

Figure 3.1 Schematic diagram of the Impact Beam System [4].

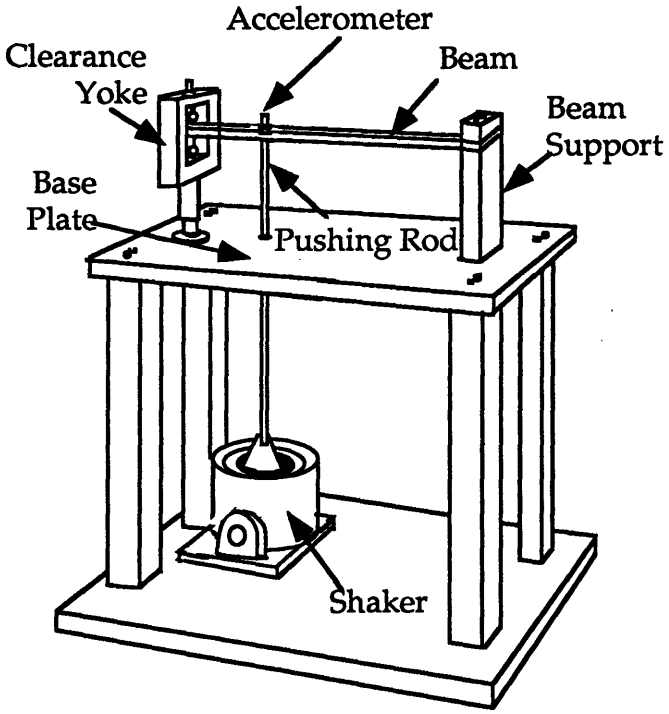

Figure 3.2 Experimental setup of the Impact Beam System.

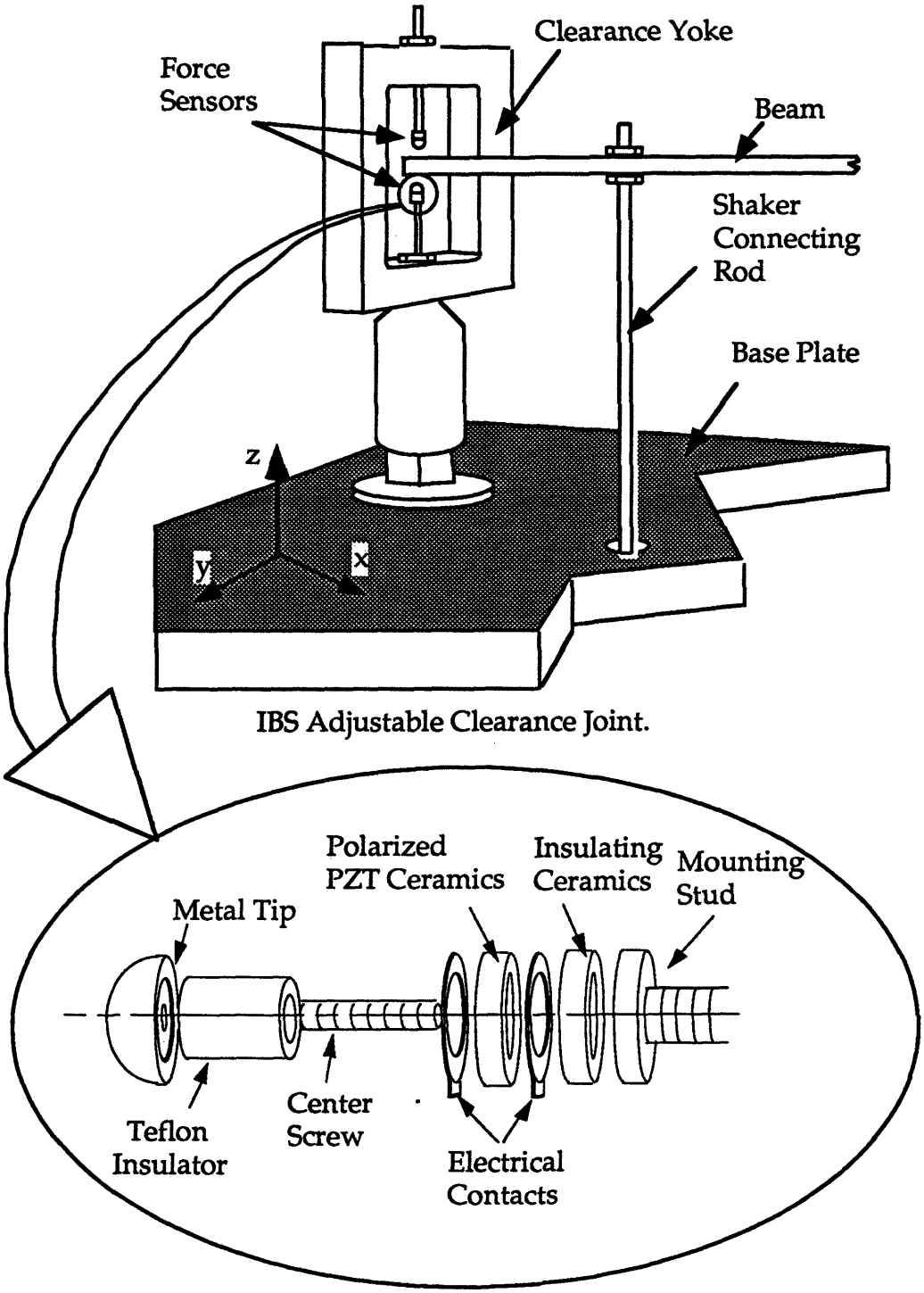

Figure 3.3 IBS adjustable clearance joint and contact sensor.

A schematical diagram of the experimental setup and data collection on the IBS is shown in Figure 3.4. The clearance gap is set using feeler gauges, which gives accuracy and repeatability of approximately ±0.0254 mm. An analog Spectral Dynamics signal generator produces a sinusoidal signal, which is monitored by a Hewlett-Packard period counter. The signal is amplified by a B&K 2702 power amplifier to drive a Ling 603 shaker. The shaker excites the beam through the pushing rod, so that the end of the beam inside the clearance moves back and forth to impact the contact force sensors.

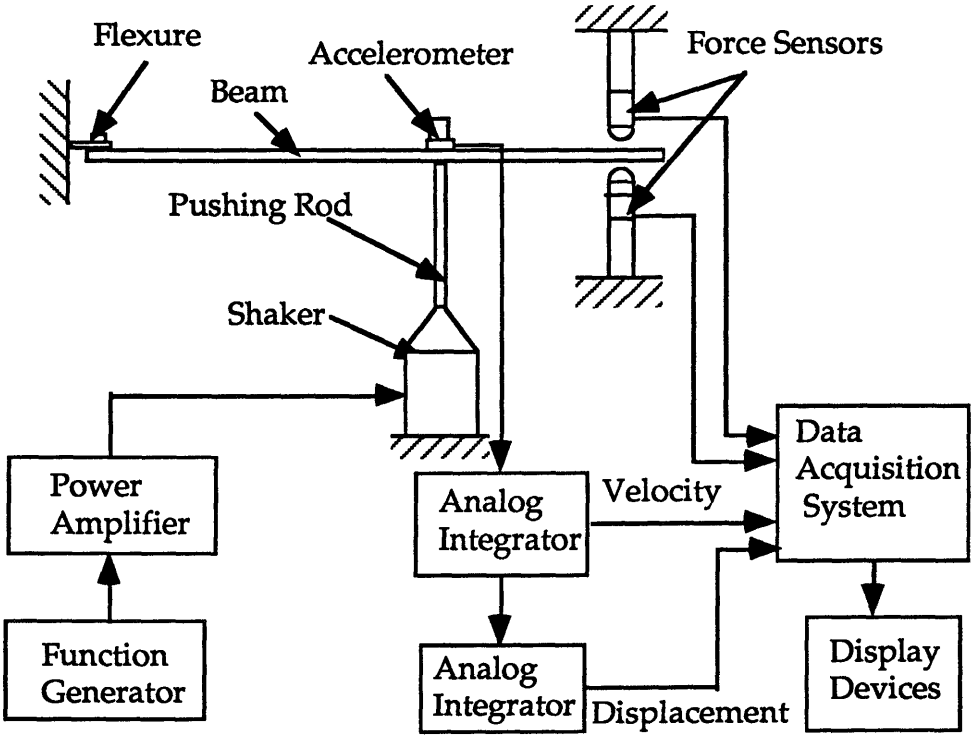

Figure 3.4 Schematic diagram of experimental measurement.

In the measurements, the signals generated by the contact force sensors are amplified by two PCB 462A charge amplifiers. A B&K accelerometer, mounted on the beam at the connection point of the pushing rod, measure

the beam's motion. The output of the accelerometer is integrated twice to obtain the displacement of the beam motion. The data collection is done using a Concurrent 6000 computer with laboratory data acquisition hardware and software called Laboratory Workbench [2].

3.3 Analytical Model of the Impact Beam System

The modeling technique presented in Section 2.1 was used to model the Impact Beam System. As shown in Figure 3.5, three major parts of the system, the beam, the clearance bearing, and the force input, were considered.

The beam was modeled using finite elements. The beam support post and the yoke holding the force sensors were assumed to be rigid. The flexure pivot mounting of the steel beam was modeled as two springs. One spring has finite stiffness in one rotational degree of freedom. The other has finite stiffness in one translation degree of freedom.

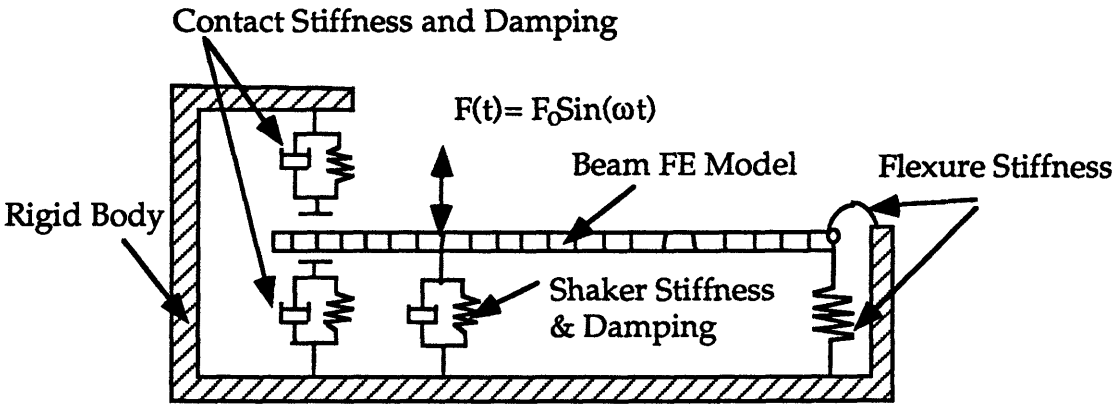

Figure 3.5 Dynamic Model of the Impact Beam System.

The clearance bearing was modeled as a zero force zone to represent the gap, and a non-zero force zone with linear contact stiffness and damping to represent the bearing surface. The stiffness was calculated using a linearized

Hertzian contact analysis [63]. The damping coefficient was determined by an assumed damping ratio, an equivalent beam mass, and calculated contact stiffness. The contact stiffness and damping coefficient in the model were 1.5×10^7 N/m and 20 N·s/m, respectively [3].

The shaker force was modeled as the force applied to the beam FE node which corresponded to the attachment point of the connecting rod. The shaker's internal suspension was represented by a linear spring and a damper. The numerical values of the spring and damper were provided by Deck [3] and Oppenheimer [42].

3.4 Simulations of Dynamic Responses of the System

The IBS model described above was numerically simulated using ASSET. Numerical simulations of the IBS predicted the existence of chaotic behavior. The model was found to have chaotic behavior for certain excitation frequencies and clearances, and to be periodic in other cases.

The time history, phase plane portrait, Poincaré map, and frequency spectrum of the beam motion were used to analyze the nature of the system's dynamic responses. The impact force in the clearance was also studied in characterizing the system's responses, since it is important in design, having a strong influence on system life, noise, etc.

For the results presented here, the system was excited by a sinusoidal force of 8.9 N peak amplitude and the clearance was set to ±0.127 mm.

Periodic Response

Figures 3.6 (a)-(c) show a periodic response of the IBS in the time, frequency, and phase domains at an excitation frequency of 19 Hz. The time history and phase plane portrait of the beam tip motion at the clearance joint

are shown in Figures 3.6 (a) and (b), respectively. The frequency spectrum of the beam displacement is given in Figure 3.6 (c). The time history and the phase diagram of the response clearly demonstrate the periodicity of the system's response. The frequency spectrum, with spikes corresponding to the excitation frequency and its harmonic components, also shows the feature of periodic response.

The time history of the predicted impact force on one side of the bearing is presented in Figure 3.6 (d). Because the impact force is periodic, the magnitude of the impacts can be obtained from just a few cycles of simulations.

Chaotic Response

Figures 3.7 (a)-(d) show a chaotic response of the IBS in the time, frequency, and phase domains at an excitation frequency of 30 Hz. The time history and phase plane portrait of the beam tip motion at the clearance joint are shown in Figures 3.7 (a) and (b), respectively. The frequency spectrum of the displacement and Poincaré map of the response are given in Figures 3.7 (c) and 3.7 (d). The Poincaré map is constructed by sampling the trajectory of the beam motion once per period of excitation, at fixed phases of excitation, over many periods.

From the time history, phase plane diagram, and Poincaré map of the response, it is clearly seen that the response is chaotic, exhibits irregular variations from one excitation cycle to another. This chaotic nature is also confirmed by the broad spectrum of frequencies in the response spectrum.

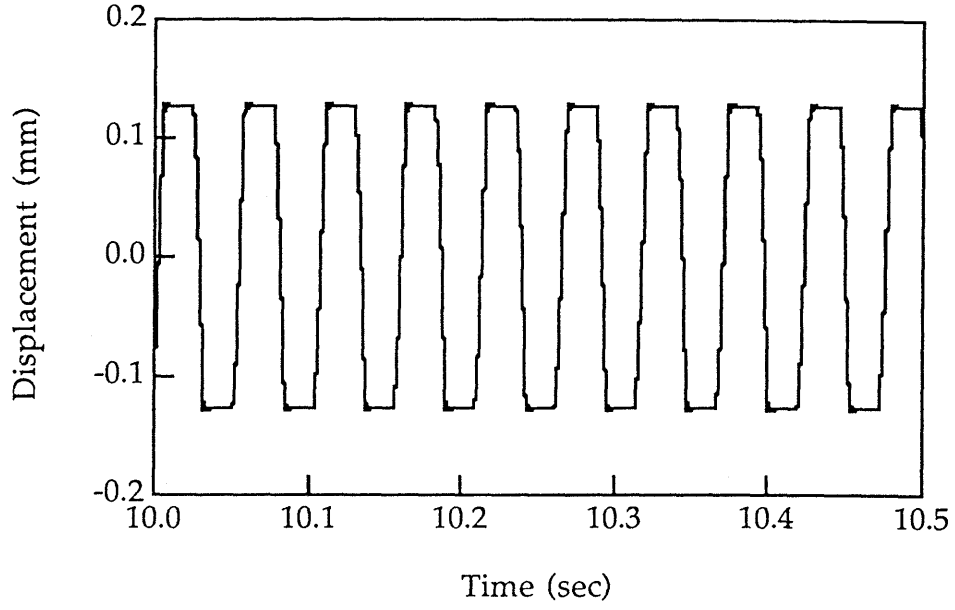

(a) Displacement of the beam tip motion.

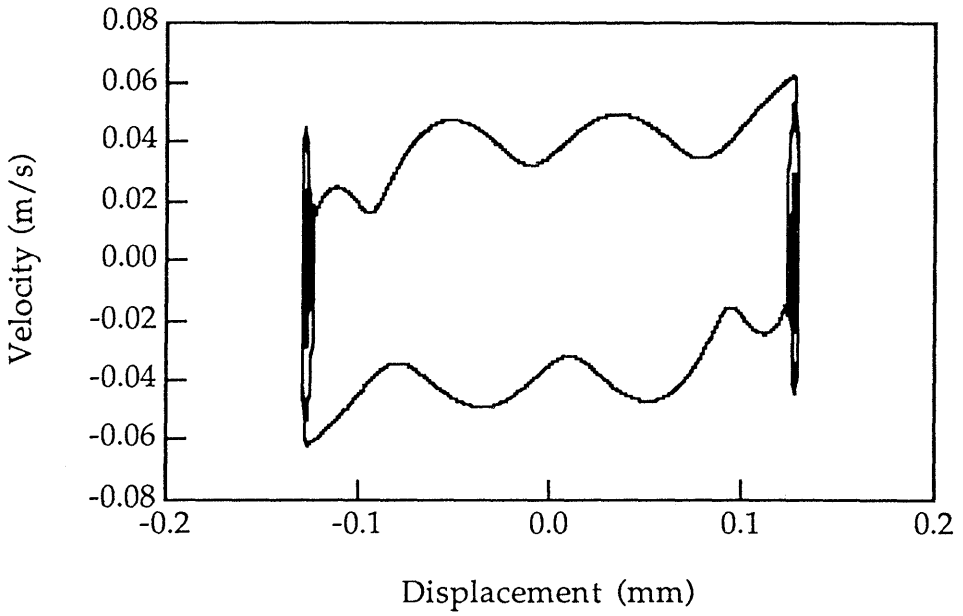

(b) Phase plane portrait of the beam tip motion.

Figure 3.6 A simulation result. A periodic response of the IBS. ±0.127 mm clearance, 19 Hz excitation frequency, and 8.9 N force amplitude.

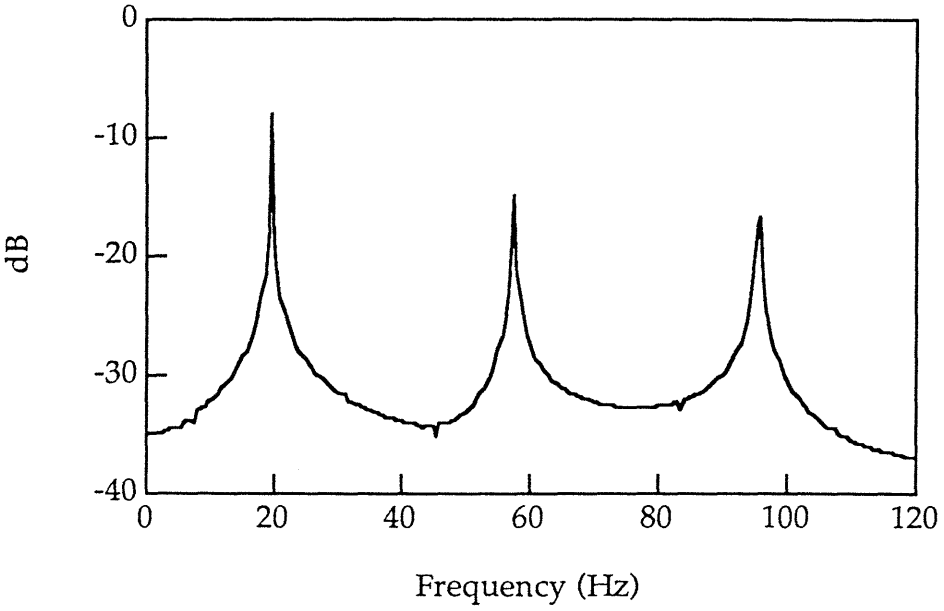

(c) Frequency spectrum of the displacement.

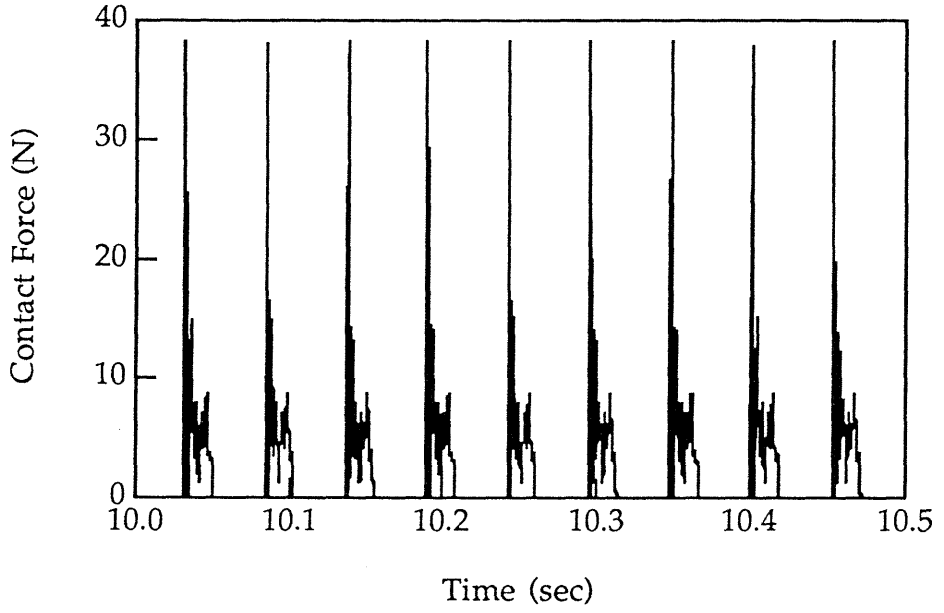

(d) Impact force on one side of the bearing.

Figure 3.6 (Continued).

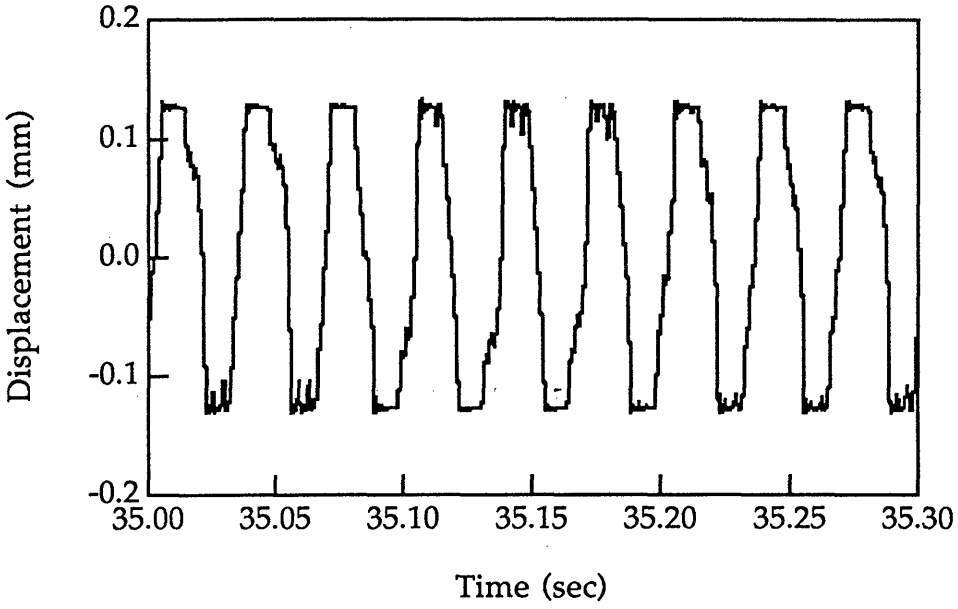

(a) Displacement of the beam tip motion.

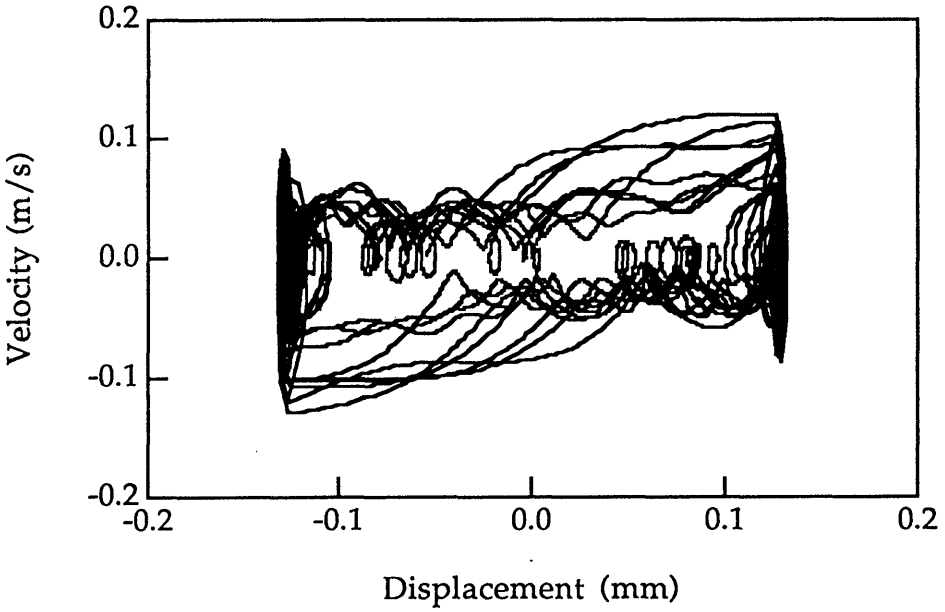

(b) Phase plane portrait of the beam tip motion.

Figure 3.7 A simulation result. A chaotic response of the IBS. ±0.127 mm Clearance, 30 Hz excitation frequency, and 8.9 N force amplitude.

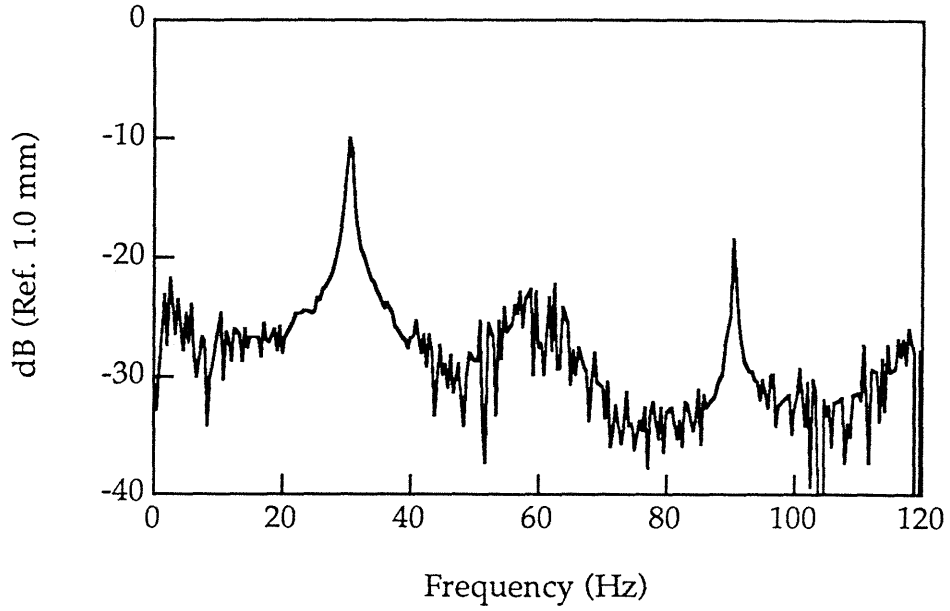

(c) Frequency spectrum of the displacement.

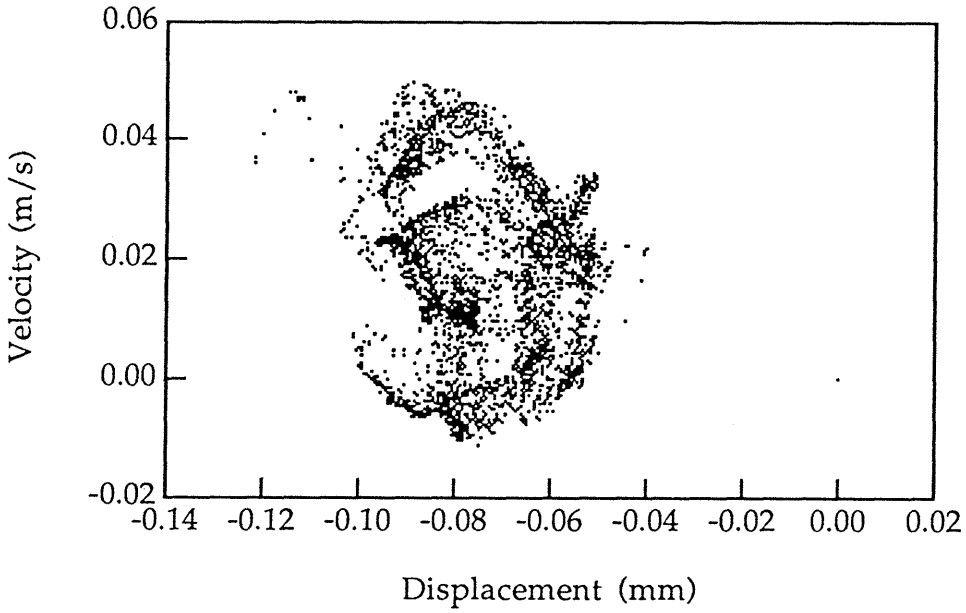

(d) Poincaré map of the beam tip motion.

Figure 3.7 (Continued).

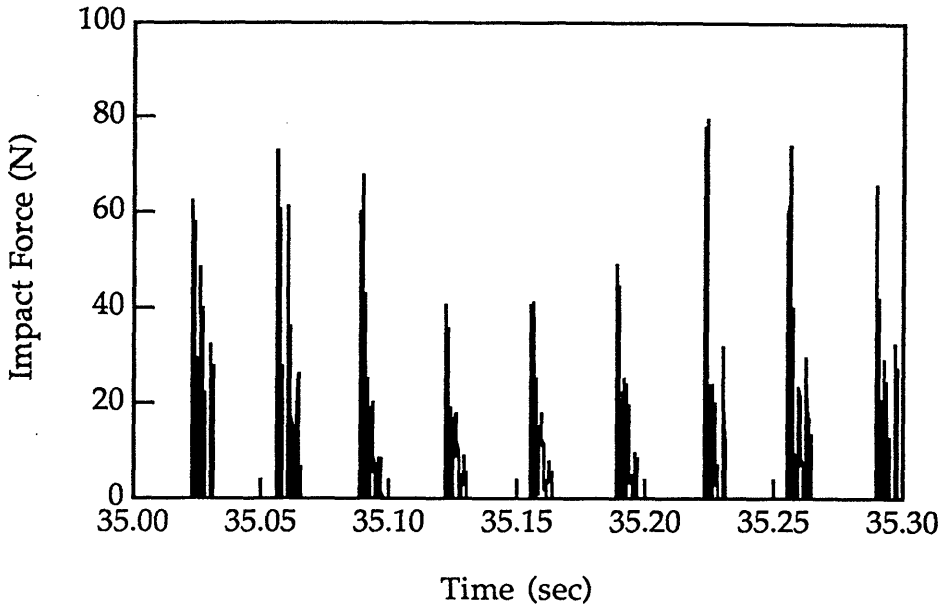

(e) Impact force on one side of the bearing.

Figure 3.7 (Continued).

The time history of the predicted impact force on one side of the bearing is presented in Figure 3.7 (e). Since the impact force varies from one excitation cycle to another for a chaotic response, looking at only a few cycles could result in a designer or analyst underestimating the peak impact force. Therefore, many cycles must be simulated to determine the range of the impact force for a chaotic response. A detailed discussion of the design issues for chaotic responses is given in Section 5.4.

3.5 Effects of System Parameters on the Dynamic Response

The clearance size, excitation frequency, beam dimension, and damping are four parameters that strongly affect the impact force in the bearing. The effects of each of these parameters on the dynamic response are discussed in this section.

3.5.1 The Effect of Clearance and Excitation Frequency

Figures 3.8 (a) and (b) show impact forces as functions of the excitation frequency for dimensionless clearances of ±0.01 (±0.032 mm clearance) and ±0.04 (±0.127 mm clearance), respectively. Dimensionless clearance is the actual clearance normalized by the displacement of the beam tip if a static force equal to peak magnitude of the excitation force were applied to the beam without the constraint of the clearance bearing. Curves in these figures record the peak impact forces for 100 cycles of machine operation at each excitation frequency. For a periodic response, a single point appears since the peak values of 100 cycles are the same. For a subharmonic response, a few discrete points appear. For a chaotic response, distributed points appear since the peak force varies from one excitation cycle to another. Based on the characteristics of the impact force shown in the figures, the responses are classified into three types.

Type I Response is periodic, and is not sensitive to initial conditions or small variations of system parameters. The predicted impact force increases smoothly as the excitation frequency increases in the range of 1 to 8 Hz, as shown in Figure 3.8. This well-behaved region permits the designer to predict trends accurately or without ambiguity.

Type II Response is periodic, and not sensitive to initial conditions, but it is sensitive to small variations of system parameters. This sensitivity is seen as the excitation frequency varies from 8 to 30 Hz in Figure 3.8 (a), and from 8 to 17 Hz in Figure 3.8 (b). Note that the peak impact force significantly fluctuates as the excitation frequency changes. For example, as the excitation frequency increases from 18 to 20 Hz, the corresponding peak impact forces are periodic, but change from 30.5 to 15.0 N (about 50% decrease), and then rises to 28 N (about 100% increase). For the Type II Response, the hidden

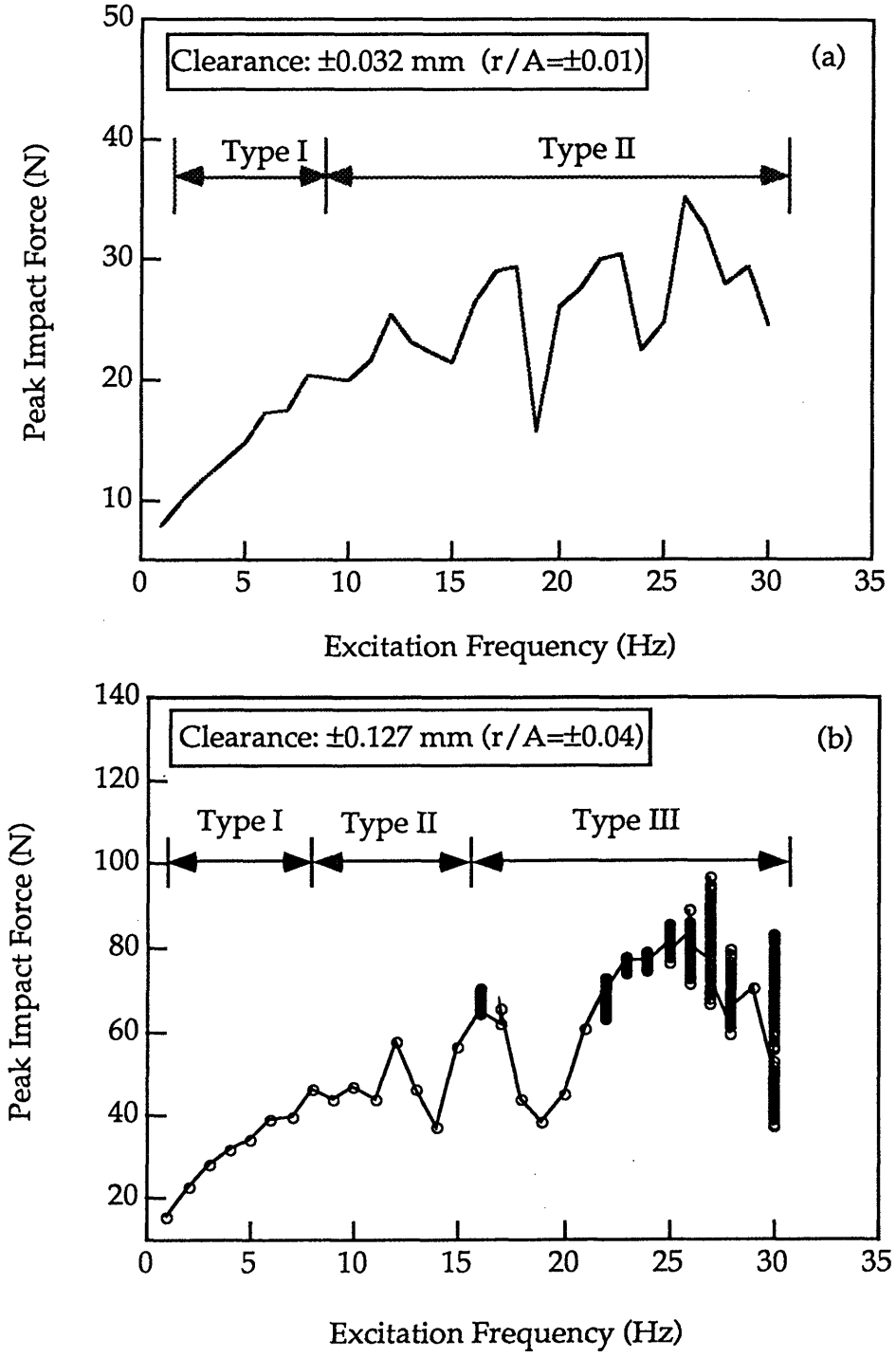

Figure 3.8 Simulation results. Peak impact force as a function of excitation frequency. 8.9 N force amplitude. (a) ±0.032 mm clearance. (b) ±0.127 mm clearance.

danger is its periodicity. The periodic response may lead designers to overlook its sensitivity to small variations of system parameters.

Type III Response is unpredictable, either chaotic or periodic, as shown in Figure 3.8 (b) for excitation frequencies from 16 to 30 Hz. When chaotic, the predicted impact force is sensitive to initial conditions. For example, at 30 Hz, the peak impact force varies between 30 Newton and 85 Newton, depending on the initial displacements and velocities. The peak impact force also fluctuates significantly as the excitation frequency changes. For example, while the response is periodic with a peak impact force of 70 N at 29 Hz, it becomes chaotic with peak impact force in the range of 30 - 85 N as the excitation frequency increases to 30 Hz. For the Type III Response, the variation range and statistical properties of the peak impact force in a chaotic response may be obtained through sufficient cycles of simulation. These statistical properties may be sufficient for designers to perform the necessary design analysis. However, the uncertainty and sensitivity of the responses present ambiguities for a designer or analyst using simulation predictions.

The above study is extended to different clearance sizes. The response nature of the system is plotted in Figure 3.9 against the dimensionless clearance and excitation frequency. In the figure, an open circle represents a periodic response, and a black dot represents a chaotic response. According to the above definitions for the three types of responses, the responses in this parameter space are classified into three types. The corresponding regions for these three types of responses are suggested in the figure using different shadings. Furthermore, this figure shows that large clearance and high frequency encourage a chaotic response. For example, chaotic vibrations occur when the dimensionless clearance is larger than 0.02 and the excitation frequency is higher than 16 Hz.

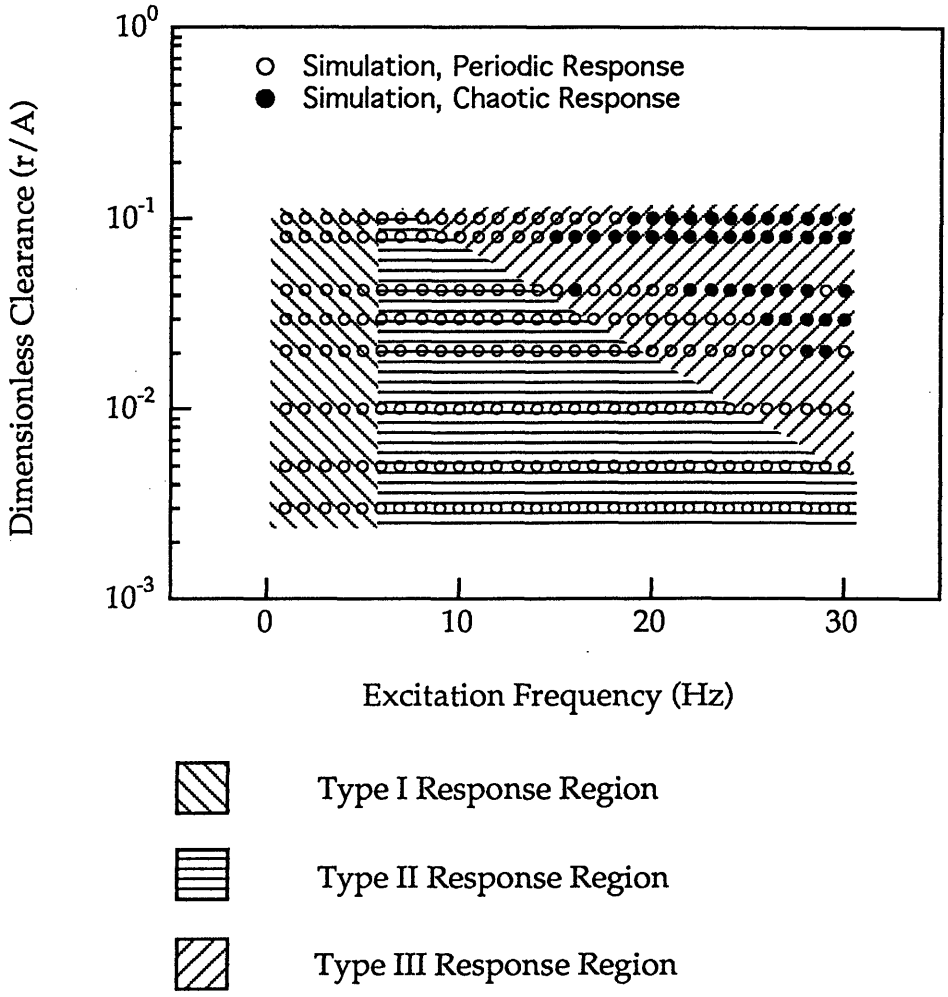

Figure 3.9 Simulation results. Response nature of the IBS in *Excitation frequency-Clearance space*. Regions of three types of responses are suggested using three different shadings.

The existence of the Type II Response is due to both the clearance and the beam flexibility. Impact forces generated at a clearance connection have a broadband, high frequency spectrum. The broadband impact force excites the high frequency modes of the beam, whose frequencies are much higher than the excitation frequency. The vibrations of the high frequency modes superpose on the rigid-body motion of the beam. The velocity of the beam tip

immediately prior to contact with the bearing is affected by the phase between the rigid-body motion and the vibrations of the high frequency modes. The velocity is higher than that of the rigid-body motion if the rigid-body motion and the vibrations are in phase, or less than that of the rigid-body motion if the rigid-body motion and the vibrations are out of phase. For the IBS, the phase between the rigid-body motion and the vibrations of the high frequency modes is a complicated function of the excitation frequency, clearance size, and beam flexibility.

Table 3.1 The first natural frequencies of the beam for different beam lengths

Beam length (mm)	Frequency (Hz)
279.0	298.4
281.5	293.2
284.0	288.2

The sensitivity of the Type II Response is examined by changing the beam flexibility. The original length of the beam is increased by 2.5 mm and 5.0 mm, respectively. The flexibility of the beam is quantified using its first pinned-pinned mode frequency. The first pinned-pinned mode frequencies of the beam for three different lengths are calculated and listed in Table 3.1. The simulation results of the beam for these three lengths with ±0.015 mm clearance are shown in Figure 3.10. In the figure, the peak impact force is plotted as a function of the excitation frequency. The results show similar patterns for all three lengths of the beam: the peak impact force fluctuates as the excitation frequency varies from 15 Hz to 30 Hz. For frequencies lower than 15 Hz, the impact force is too small to excite sufficiently large vibrations

of the high frequency modes. Such small vibrations do not affect the velocity of the beam tip before the impact. In this frequency range, the influence of the beam flexibility is not sufficient. The responses are, therefore, Type I.

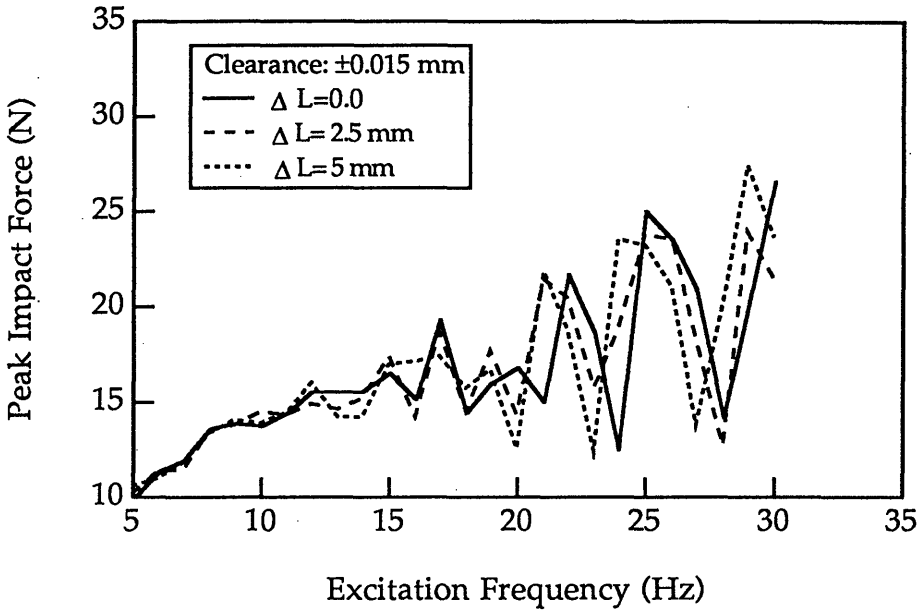

Figure 3.10 Simulation results. Peak impact force as a function of excitation frequency for different beam lengths. ±0.015 mm clearance and 8.9 N force amplitude.

When the peak impact force for each beam length is depicted as a function of the frequency ratio, (the ratio of the excitation frequency and the first pinned-pinned mode frequency of each beam length), as shown in Figure 3.11, the crests and valleys in the fluctuation of the peak impact forces coincide for all three lengths. These results indicate that the sensitivity of the Type II Response is related to the beam flexibility and that the variation of any system parameter, which can affect the beam flexibility, could result in a different fluctuation pattern of the peak impact force for the same range of excitation frequency. The results also show that there is an inherent

relationship between the fluctuation of the peak impact force and the system parameters, such as the excitation frequency, clearance size, and beam mode frequencies. However, it is very difficult to develop a closed formula to show explicitly the relationship because of the nonlinearity of the clearance.

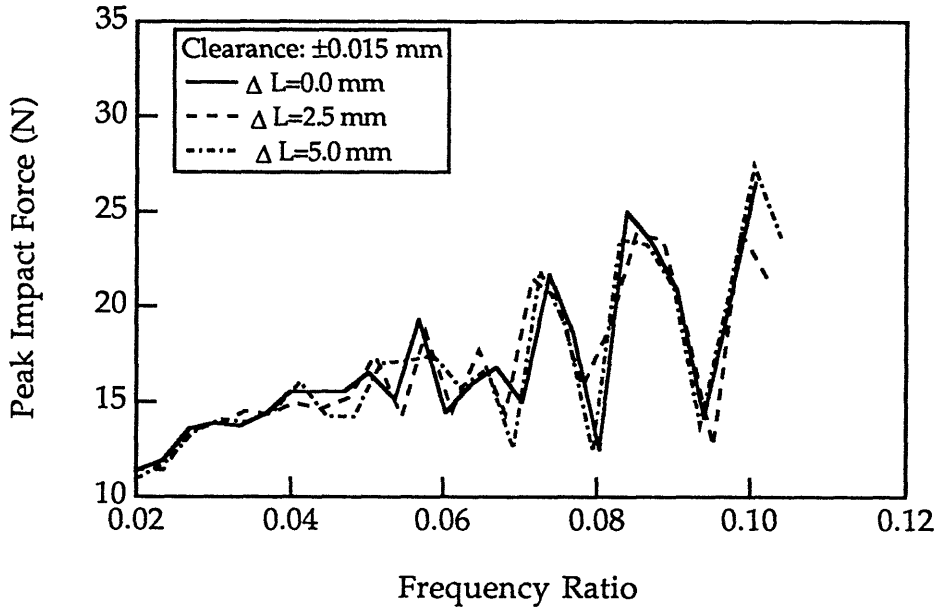

Figure 3.11 Simulation results. Peak impact force as a function of frequency ratio for different beam lengths. ±0.015 mm clearance and 8.9 N force amplitude.

3.5.2 The Effect of Beam Dimensional Variation

Virtually every engineering design is subject to dimensional variations when the design is manufactured. In some cases, the design is slightly modified in order to use a new designed part. The replacement of one component may cause small dimensional changes of other components that fit into the modified design. Therefore, it is important to evaluate the effects of dimensional variation on the dynamic response of machine systems. Beam length is one of the major design parameters for the impact beam

system, and was chosen for an investigation into the effect of dimensional variation on the dynamic response.

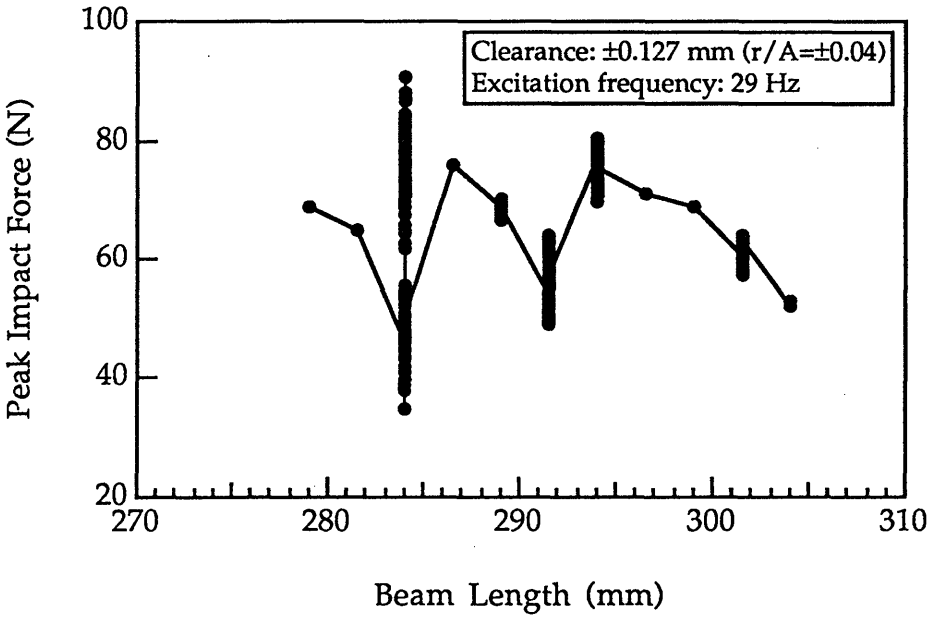

Figure 3.12 Simulation results. Peak impact force as a function of beam length variation.

Figure 3.12 shows the peak impact force as a function of the variation of the beam length at an excitation frequency of 29 Hz and a clearance of ±0.127 mm. The design length of the beam was assumed to be 279 mm. The length was change from 279 mm to 304 mm with ten increments. Each increment is 2.5 mm, which is about 1% of the original length. It is seen that the nature of the response changes from chaotic to periodic or vice versa even for a small variation of the beam length at different beam lengths. For example, when the beam length increases by about 1% at the length of 281.5 mm, from 281.5 mm to 284 mm, the response changes from periodic to

chaotic, and the maximum value of the peak impact force increases from 70 N to 95 N, almost a 30% increase.

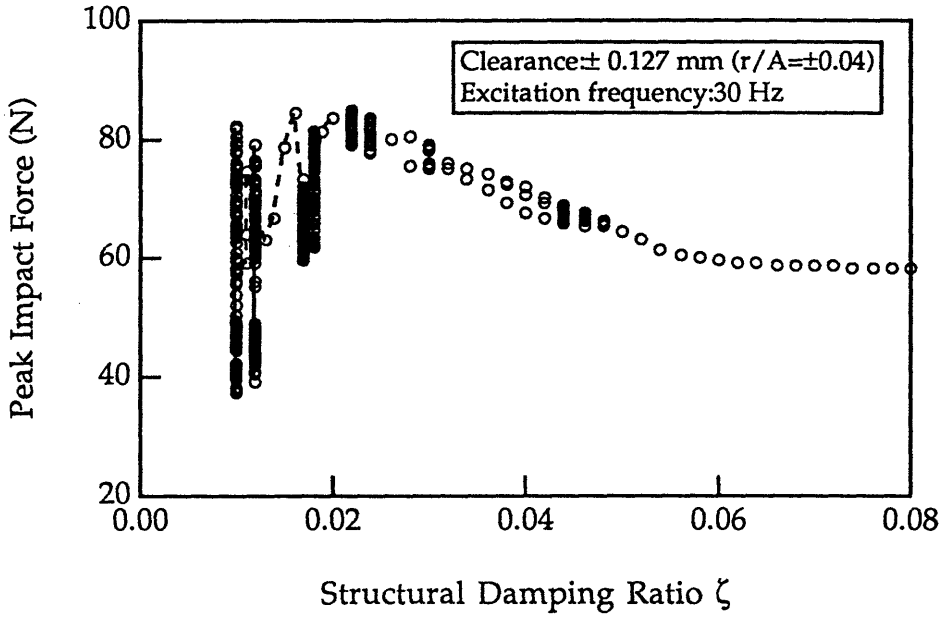

Figure 3.13 Simulation results. Peak impact force as a function of the structural damping ratio.

3.5.3 The Effect of Damping

In order to understand the effect of structural damping on a chaotic response, the structural damping ratio was varied in the numerical simulation. Figure 3.13 shows the peak impact force as a function of the damping ratio at an excitation frequency of 30 Hz and ±0.127 mm clearance. Note that the variation of the peak impact forces of chaotic responses decreases as the damping ratio increases from 1% to 8%. It is clearly shown that increasing damping is an effective way of minimizing the unsatisfactory chaotic responses.

3.6 Experimental Responses of the Impact Beam System

Extensive experiments were performed for different excitation frequencies and clearances. The dynamic responses of the IBS were found to be chaotic for certain excitation frequencies and clearances, and to be periodic in other cases. The response nature was determined based on the characteristics of the time history and phase portrait of the beam motion, and the variation of the peak impact force in response to the periodic excitation. For the two typical responses presented here, the peak magnitude of the excitation force was 8.9 N, and the clearance was set to ±0.127 mm.

A Periodic Response

Figure 3.14 shows the measured response of the system when it is excited at 10 Hz. Figures 3.14 (a) and (b) are the displacement and phase portrait of the beam motion at the location of the input force. Figure 3.14 (c) presents the time history of the impact force in the clearance bearing. These results indicate the characteristics of a periodic response. Except for minor deviation, the phase trajectory of the beam motion forms a closed orbit for each excitation cycle, and the peak impact force repeats from one excitation cycle to another. The slight deviations are due to experimental errors, such as the quantization error of the A/D conversion and non-repeatability in the sensors. These deviations are small; for example, the force variation was found to be less than 5% of the average peak value of the impact force.

A Chaotic Response

Figure 3.15 shows the measured response of the system when it is excited at 21 Hz. Figures 3.15 (a) and (b) are again the displacement and phase portrait of the beam motion at the location of the input force. Figure 3.15 (c)

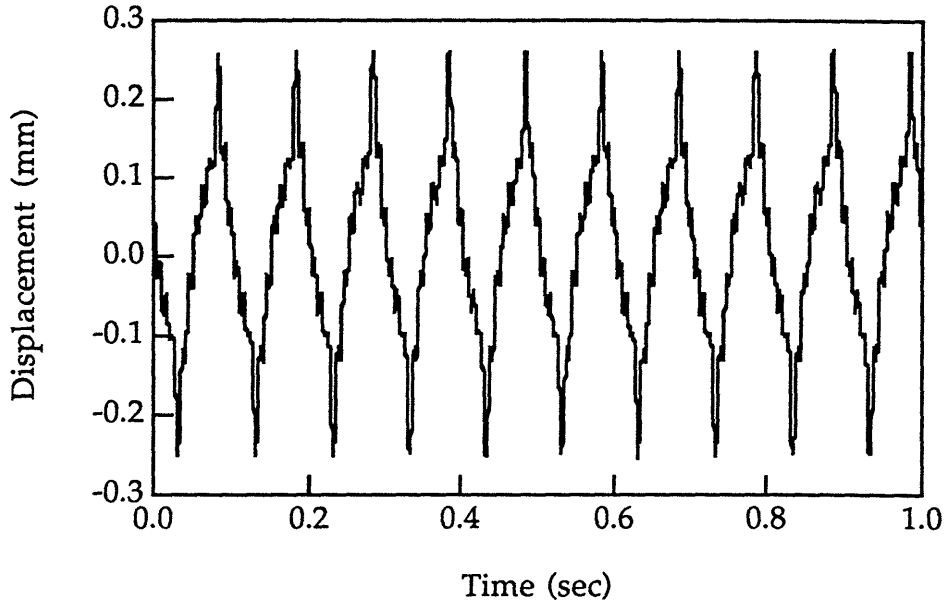

(a) Displacement of beam motion.

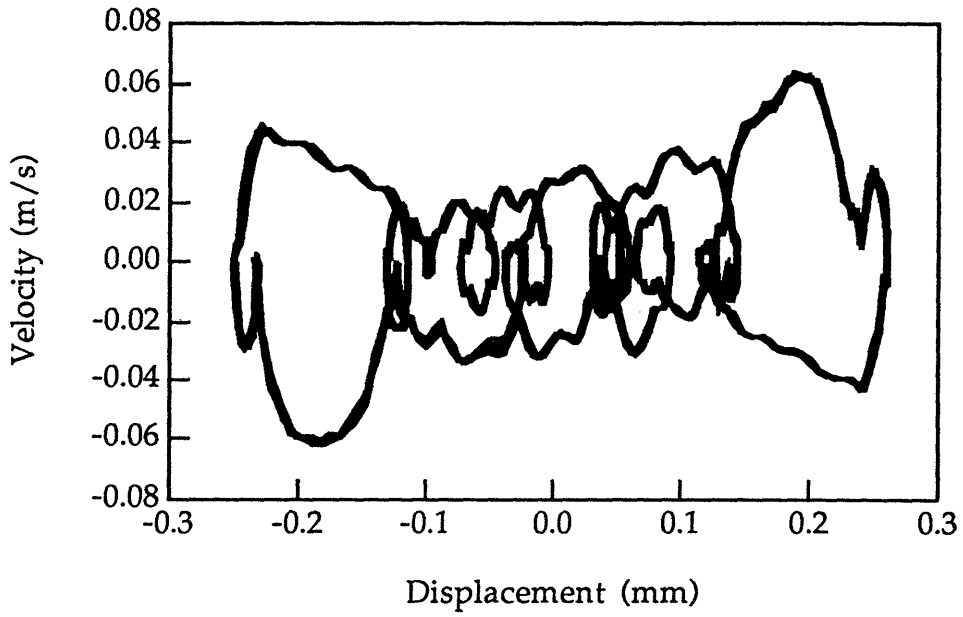

(b) Phase plane portrait of the beam motion.

Figure 3.14 An experimental result. A periodic response. ±0.127 mm clearance, 10 Hz excitation frequency, and 8.9 N force amplitude.

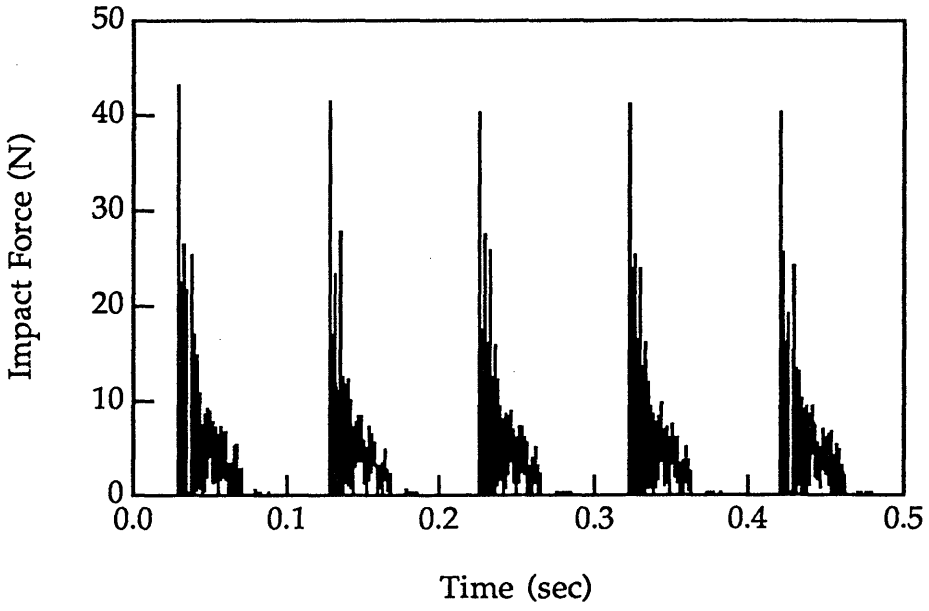

(c) Impact force on one side of the bearing.

Figure 3.14 (Continued).

presents the time history of the impact force. These figures show the characteristics of a chaotic response. The phase trajectory of the beam motion does *not* close for each excitation cycle, and the peak impact force irregularly fluctuates from one excitation cycle to another. This non-repeatability of the response indicates that system behavior is unpredictable at this excitation frequency. Although the exact value of a response parameter is unpredictable, its range which covers all possible values can, in principle, be obtained through sufficient measurements. For example, the range of the peak impact force for such a chaotic response can be determined by measuring the peak impact forces for a sufficient number of excitation cycles.

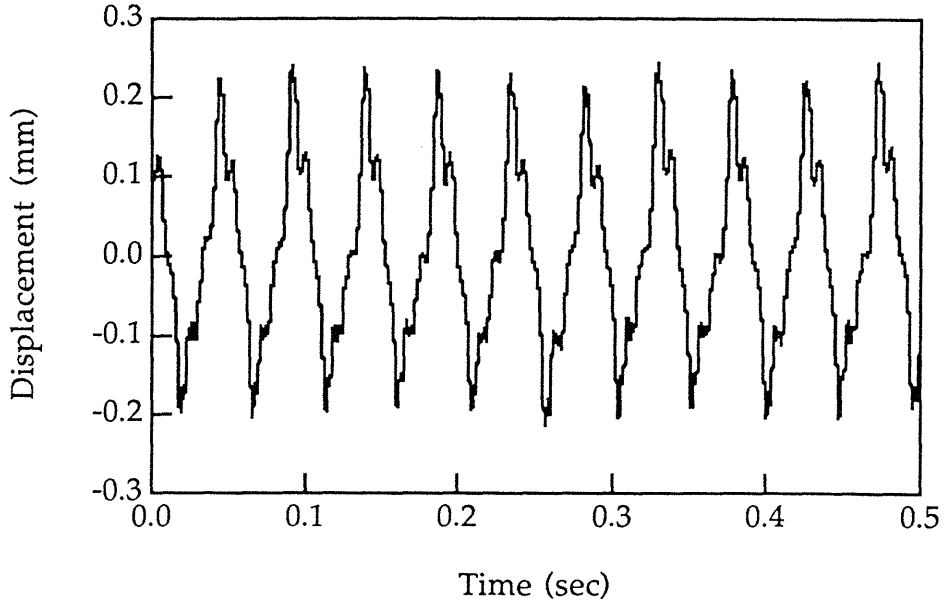

(a) Displacement of the beam motion.

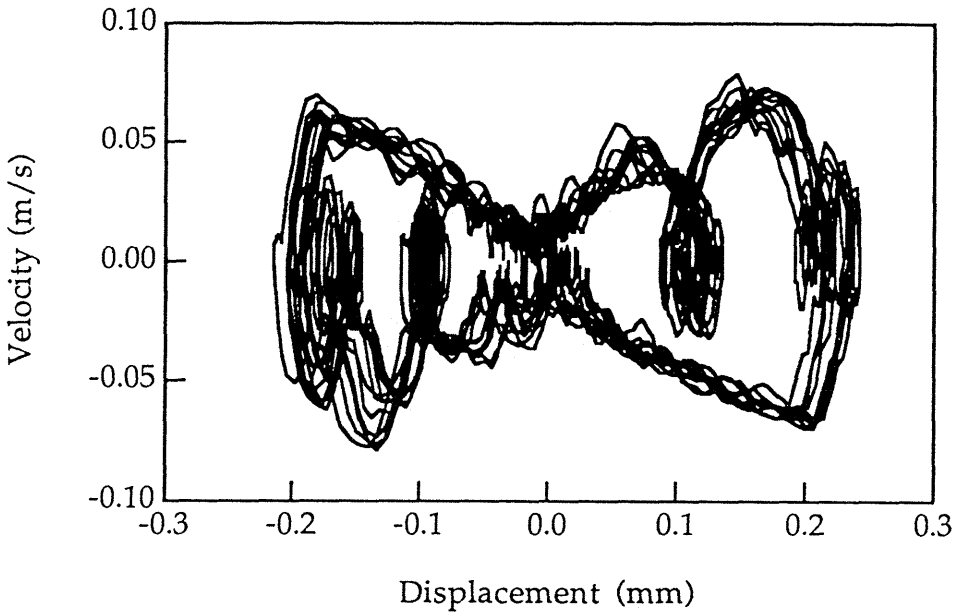

(b) Phase plane portrait of the beam motion.

Figure 3.15 An experimental result. A chaotic response. ±0.127 mm clearance, 21 Hz excitation frequency, and 8.9 N force amplitude.

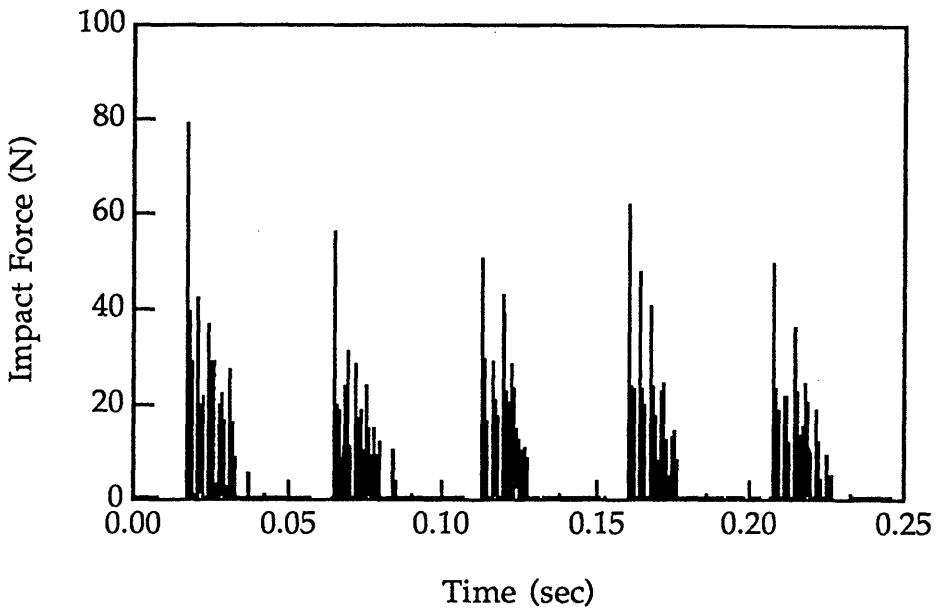

(c) Impact force on one side of the bearing.

Figure 3.15 (Continued).

Characteristics of Measured Responses

The measured peak impact forces as a function of the excitation frequency are presented in Figure 3.16. Figure 3.16 (a) is the results of ±0.016 mm clearance and Figure 3.16 (b) is the results of ±0.127 mm clearance. Data were collected in ensembles of 30 impact peaks at each excitation frequency. The solid lines are plotted through the mean value of the ensemble of the data at each excitation frequency.

In principle, a periodic response has zero variation in the ensemble and should produce a single point at a given frequency on this figure. Due to the non-repeatability of the sensor and other uncertainties in the measurement, the measured values for a periodic response exhibit small variations. On the other hand, a chaotic response produces irregular peak impacts from one excitation cycle to another, leading to a large variation in

the peak impact force, characterized by distributed points at a given frequency in the figure.

The non-repeatable error of the force sensor was found to be approximately ±3 N. This error value, the small variation of the impact force, is used to classify characteristics of system's responses. A response with force variation larger than ±3 N is classified as chaotic. In Figure 3.16 (a), the response is periodic for all excitation frequencies. For the excitation frequency in the range of 4-9 Hz, the response is classified as Type I because of the well-behave trend of the peak impact forces. For the excitation frequency in the range of 10-30 Hz, the response is classified as Type II rather than Type I, because its trend fluctuates with excitation frequency. In Figure 3.16 (b), the response is periodic for excitation frequencies less than 19 Hz. For the excitation frequency in the range of 4-9 Hz, the response is classified as Type I. For the excitation frequency in the range of 10-19 Hz, the response is classified as Type II rather than Type I, since its trend with excitation frequency is not well-behaved. For excitation frequencies larger than 19 Hz, the response is unpredictable (i.e. either periodic and chaotic) and is classified as Type III response. These classifications were cross checked using other methods, such as phase plane portraits and frequency spectra of the responses. The conclusions from these methods on the nature of the responses were found to be consistent.

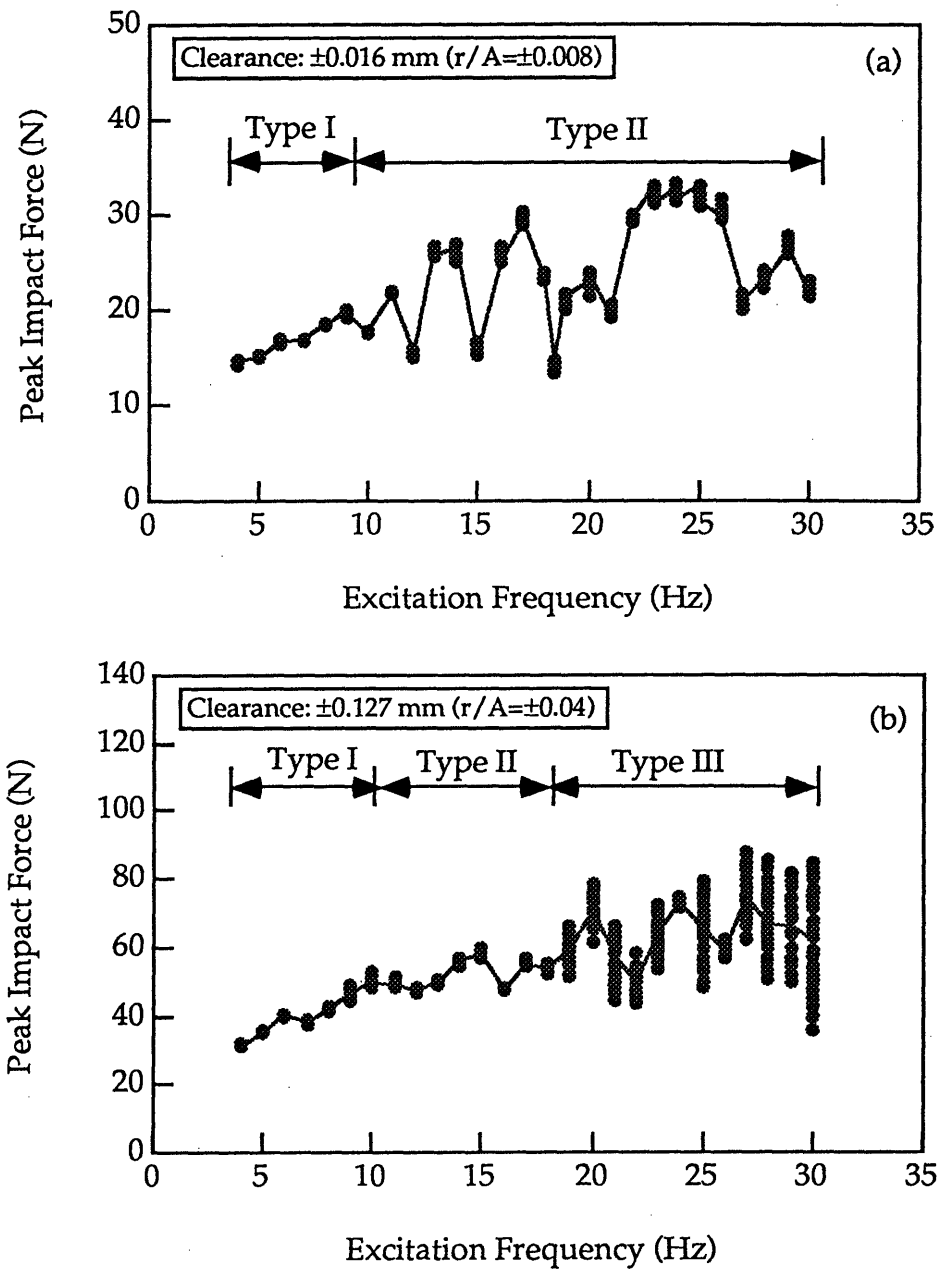

Figure 3.16 Experimental results. Peak impact force as a function of excitation frequency. These two figures show Type I, Type II, and Type III Responses.

3.7 Comparison of Experimental and Numerical Results

The previous sections have discussed numerical and experimental evidence for the existence of chaotic responses in the IBS. This section directly compares results from the numerical model with experimental measurements.

Figure 3.17 is a comparison between experimental and numerical results for an excitation frequency of 30 Hz at ±0.127 mm clearance. The parameters used for this comparison are the same as those for Figure 3.6, but the beam motion presented here is at the location of the force input instead of the beam tip. Figures 3.17 (a) and (b) give the comparisons between simulation and measurements for the displacement and phase portrait of beam motion, respectively. Figure 3.17 (c) presents both results for time histories of the impact force. These figures show an excellent agreement between the numerical results and the experimental data in three aspects. First, both indicate that the response is chaotic. Second, both show that the beam vibration has the similar pattern as well as the same variation range (i.e. the displacement from -0.2 to 0.2 mm and the velocity from -0.1 to 0.1 m/s). Third, both show that the peak impact force has the same variation range (i.e. from 40 to 100 N).

While the predictions and measurements are in an excellent agreement for some sets of system parameters, the numerical model provides a qualitatively good prediction for the whole parameter space. This can be seen from the following two comparisons: 1) characteristics of the impact force as a function of the excitation frequency for a given clearance, and 2) characteristics of the impact force over the *Excitation Frequency-Clearance* space.

Experiment Result

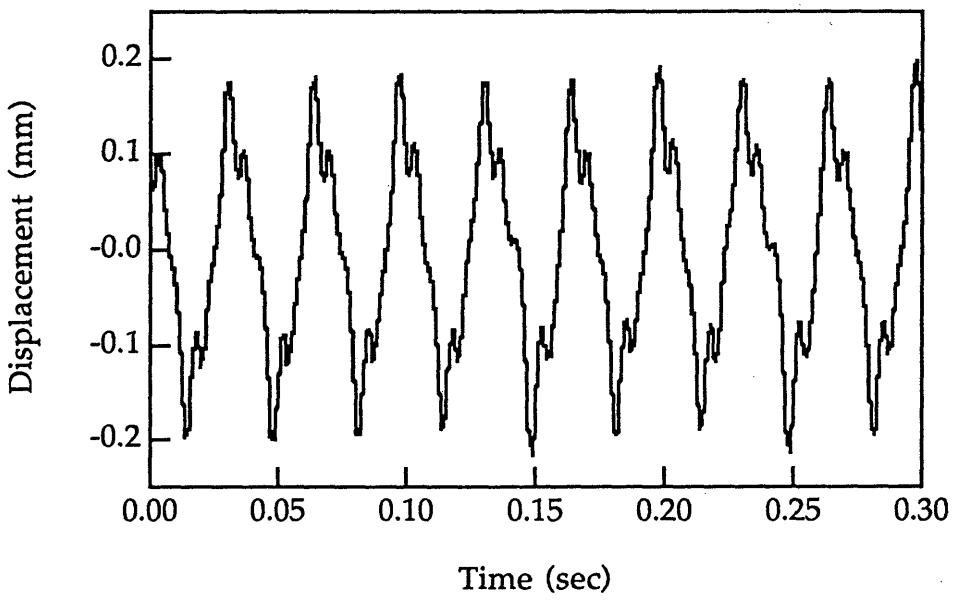

Numerical Result

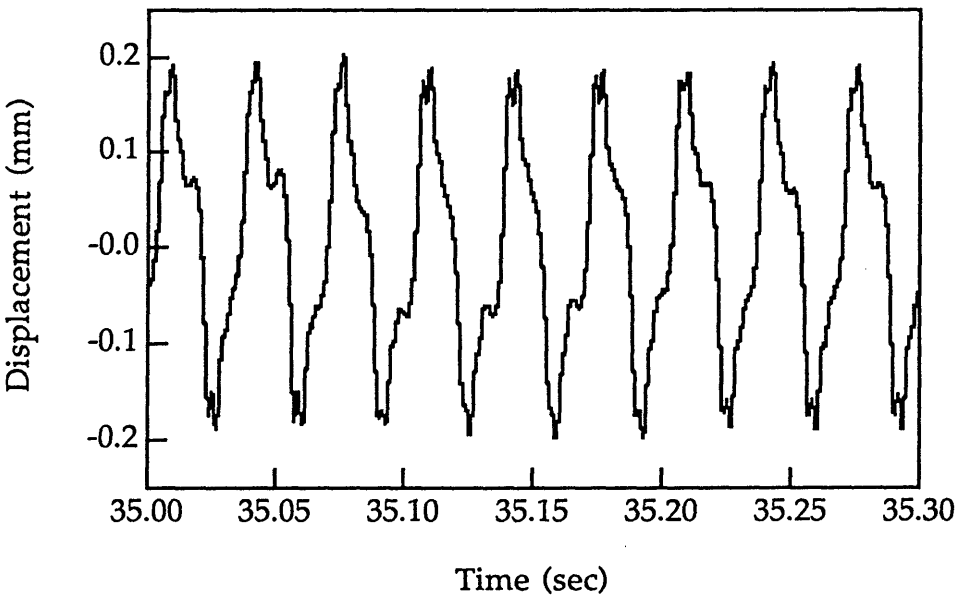

(a) Displacement of the beam motion.

Figure 3.17 Comparison between experimental and numerical results. ±0.127 mm clearance, 30 Hz excitation frequency, and 8.9 N force amplitude.

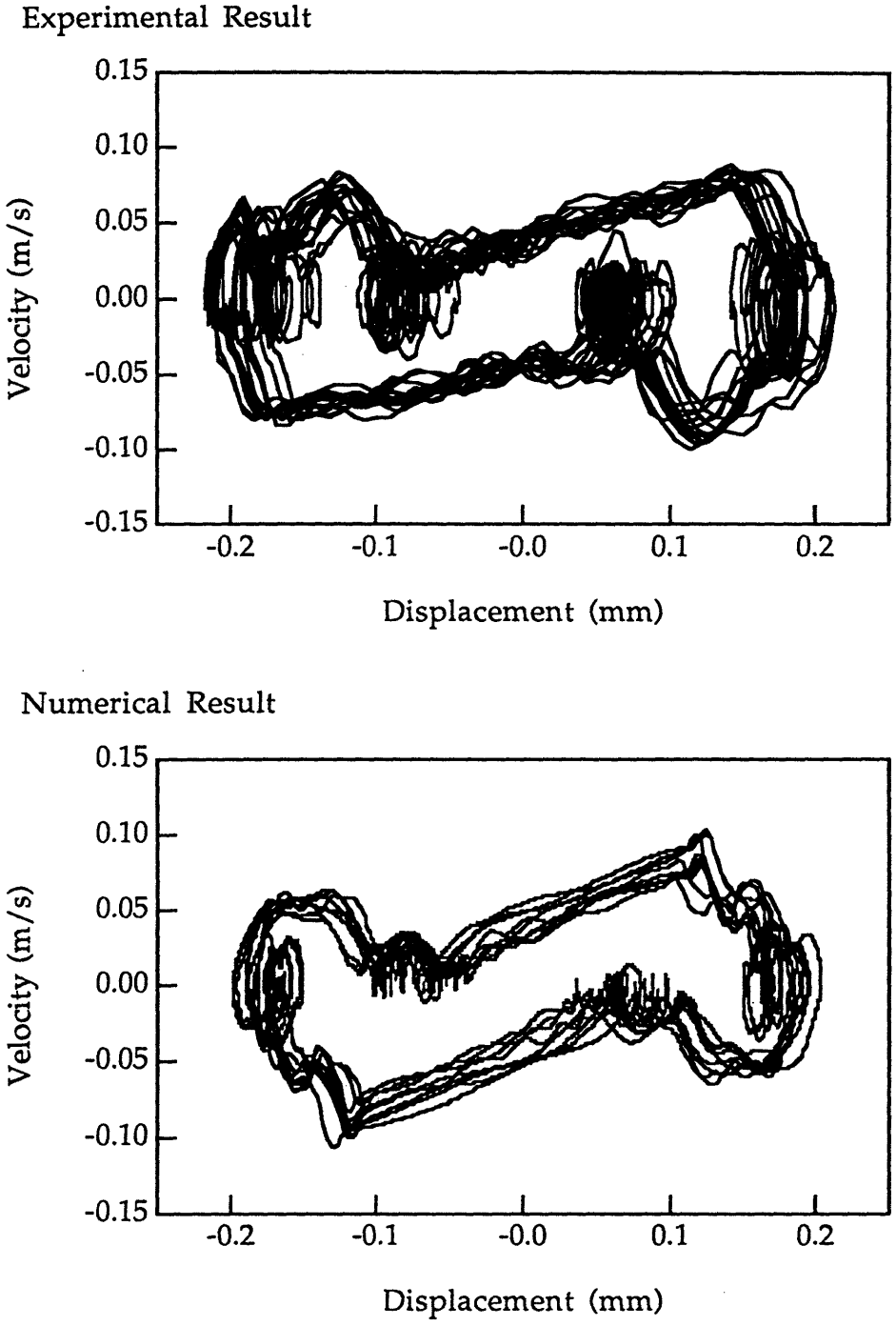

(b) Phase plane portraits of the beam motion.

Figure 3.17 (Continued).

Experimental Result

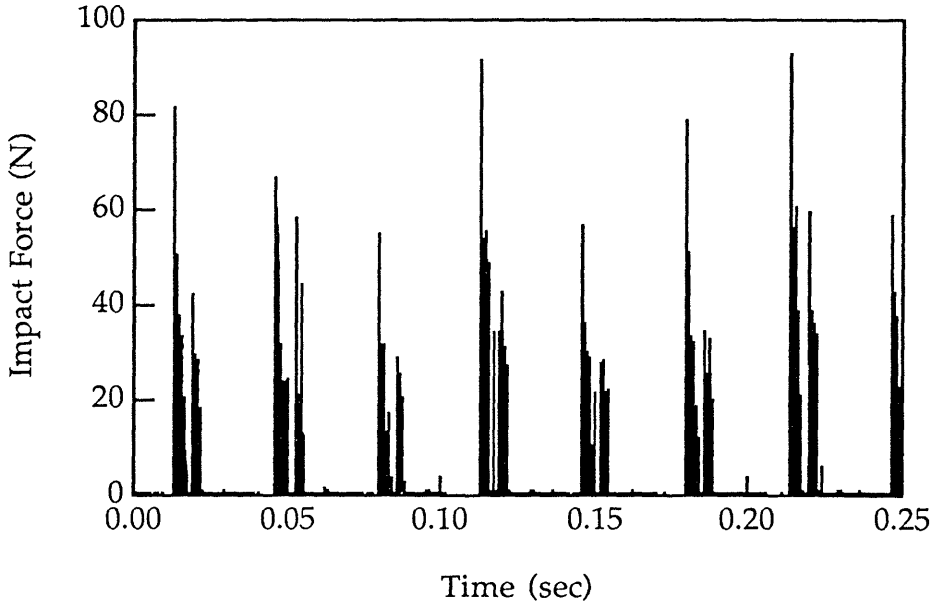

Numerical Result

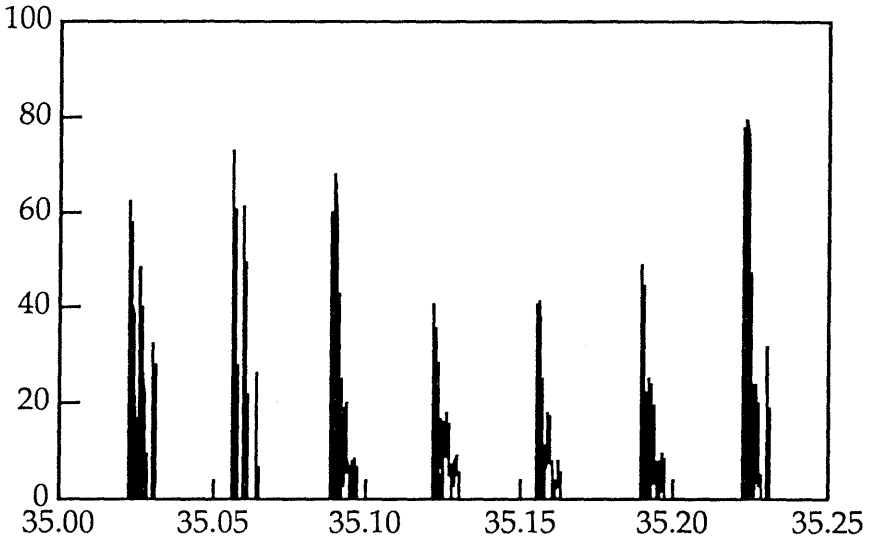

(c) Impact force on one side of the bearing.

Figure 3.17 (Continued).

For a given ±0.127 mm clearance (±0.04 dimensionless clearance), Figures 3.8 (b) and 3.16 (b) are used for the comparison. Compared with the numerical results shown in Figure 3.8 (b), the experimental data shown in Figure 3.16 (b) exhibit similar patterns of the impact forces except for a small difference in the frequency boundary between the Type II and Type III regions (i.e. 16 Hz from simulation and 19 Hz from experiments). The similarity of the numerical results and experimental data indicate that the numerical model captures much of the qualitative dynamic behavior of the IBS.

Over the *Excitation Frequency-Clearance* space, Figure 3.18 reproduces Figure 3.9, and adds two curves. The solid curve is a measured predictable-unpredictable boundary curve. The curve was obtained experimentally such that the responses are surely periodic when the clearance and excitation frequency are in the region below the curve, but are either periodic or chaotic in the region above the curve. In other words, the curve is a boundary between the predictable- and unpredictable-response parameter regions or a boundary between the Type I and Type II and the Type III Responses. The dashed curve is a measured boundary between the Type I and Type II Responses. The experimental results are qualitatively consistent with the numerical data over the studied region.

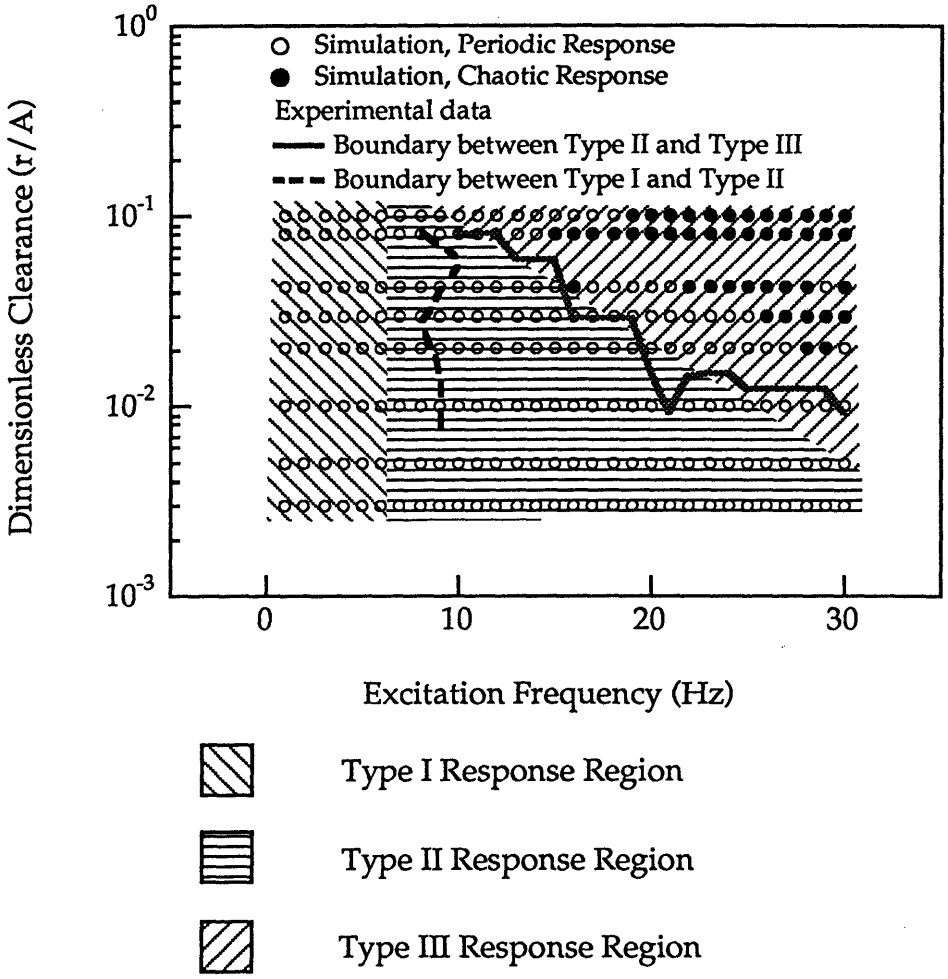

Figure 3.18 Comparison between experimental and numerical results. The nature of responses in *Excitation frequency-Clearance space.* 8.9 N force amplitude.

3.8 Summary

Interesting results from both numerical simulation and experimental measurements of the Impact Beam System are:

- The existence of chaotic vibrations in the system is confirmed both numerically and experimentally.
- Chaotic vibration usually occurs for large clearance and/or high frequency of the excitation force.

- Chaotic phenomena can be minimized by increasing the damping.
- Dynamic response of the system is found to consist of three identifiable types:

  Type I response is periodic, and is not sensitive to initial conditions or small parameter variations;

  Type II response is periodic and not sensitive to initial conditions, but it is sensitive to small parameter variations;

  Type III response is either chaotic or periodic, sensitive to both initial conditions and small variations of the system parameters such as clearance size, excitation frequency, component dimension, and damping.

Chapter 4
Study of a Spatial Slider Crank Mechanism

4.1 Introduction

Chapter 3 discusses the dynamic behavior of the IBS. Here dynamic characteristics of complex machine systems with clearance connections and component flexibility are explored. A Spatial Slide Crank (SSC) mechanism, is studied. While the IBS has only one nonlinear element (its one clearance connection), the SSC has multiple clearance connections and other nonlinearities associated with spatial, large rotational motions. An experimental Spatial Slider Crank was designed and constructed by Deck [3] and O'Connell [41] as a testbed to study the dynamic behavior of more realistic machines with clearance connections and component flexibility.

The experimental SSC is described in Section 4.2, and its numerical model is presented in Section 4.3. Numerical simulations of dynamic responses of the mechanism are presented in Section 4.4. In Section 4.5, the effects of parameter variations on the dynamic behavior of the mechanism are investigated. Experimental results are presented and compared with numerical simulations in Sections 4.6 and 4.7, respectively. The conclusions of this study are summarized in Section 4.8.

4.2 The Spatial Slider Crank Mechanism

The Spatial Slider Crank mechanism, shown schematically in Figure 4.1, consists of a motor and a crank, a ball joint which connects the crank to a connecting rod, a universal joint, which connects the connecting rod to a slider, and a slider guide rod. The slider and slider guide rod compose a sliding prismatic joint. In operation, the slider moves along the guide rod as

the crank turns. The slider's stroke can be adjusted by changing the motor angle, which is the angle between the motor axis and the axis perpendicular to the guide rod axis. The mechanism operates with spatial kinematic motion when the motor angle is different from zero degrees, and with planar kinematic motion when the motor angle is zero degrees. This mechanism is widely used in manufacturing processes and assembly lines for feeding and packing applications.

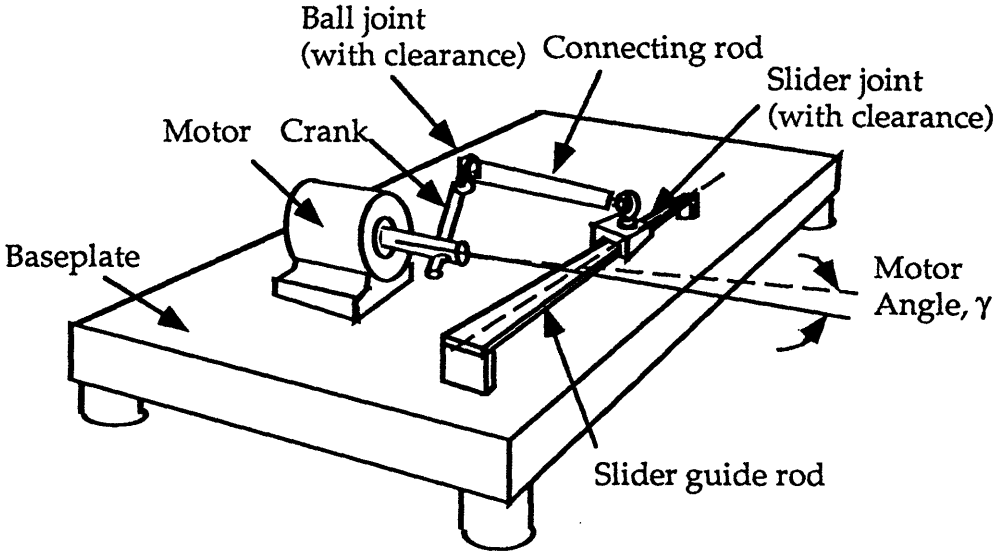

Figure 4.1 Schematic diagram of a spatial slider crank mechanism [3].

An experimental SSC was designed and developed as a testbed to study machine dynamics associated with clearance connections and component flexibility [3,41]. Two views of the experimental SSC are shown in Figures 4.2 (a) and (b), with 25° motor angle representing a spatial slider crank mechanism; and with 0° motor angle representing a planer slider crank mechanism, respectively.

A flywheel is used to stabilize the machine's speed and also acts as the crank. The ball joint is mounted on the flywheel. One end of the connecting

rod is attached to the housing of the ball joint. The other end of the rod is attached through a ball bearing to a yoke with a pair of ball bearings that allows the slider to pivot. The slider moves along the slider guide rod as the flywheel turns. The motor angle can be adjusted between 0° and 25°, causing the slider stroke to vary between 100 mm and 90 mm. The interference of the ball joint housing with the flywheel limits the motor angle to 25°. The entire SSC mechanism is mounted on an aluminum baseplate, which is 12.7 mm thick, 560 mm long and 457 mm wide. The operation speed of the SSC ranges from 50 to 300 rpm.

The ball joint and sliding prismatic joint in the mechanism were designed as instrumented, adjustable clearance joints with contact force sensors. The force sensors used in these two joints have the same design as those used in the clearance joint of the IBS. The ball joint is illustrated in Figure 4.3 (a), and the geometrical configuration of its contact force sensors is shown in Figure 4.3 (b). The ball joint has four force sensors placed symmetrically so that they retain a 15.9 mm diameter hard steel ball. The force sensors used in the ball joint have steel tips, ground to flat surfaces.

The sliding prismatic joint is illustrated in Figure 4.4 (a), and the geometrical configuration of its contact force sensors is shown in Figure 4.4 (b). It has eight sensors, set off-center symmetrically. This pattern prevents the slider from rotating due to torques parallel to the guide rod axis. Four of the sensors are oriented vertically, and the other four are horizontal. The force sensors are like those of the ball joint, except that their tips are made of brass, machined to an approximately hemispherical shape of 4.8 mm diameter.

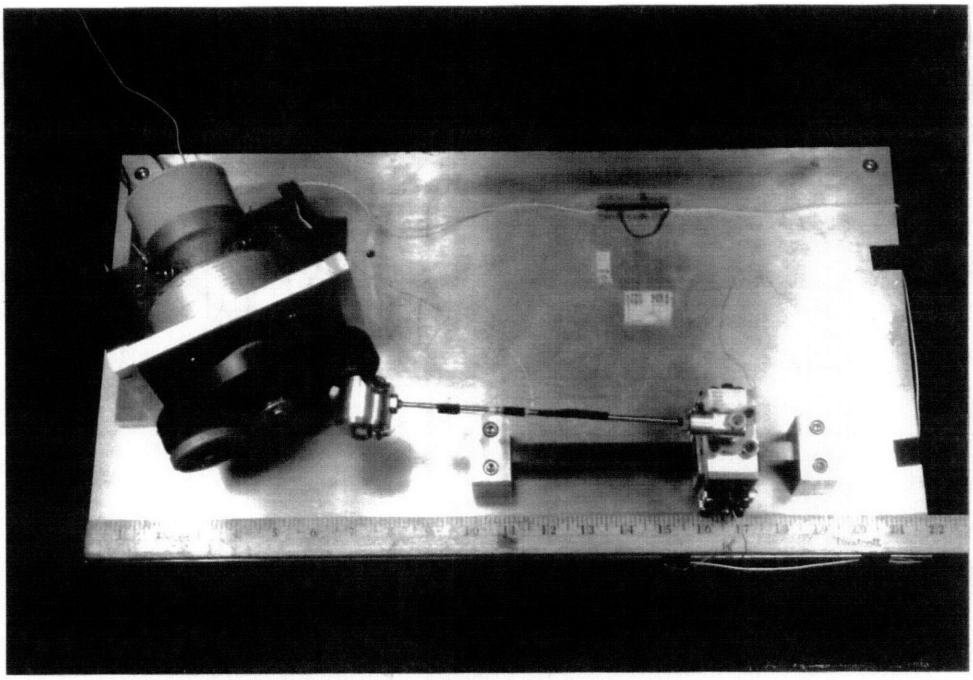

(a) Top view, 25° motor angle.

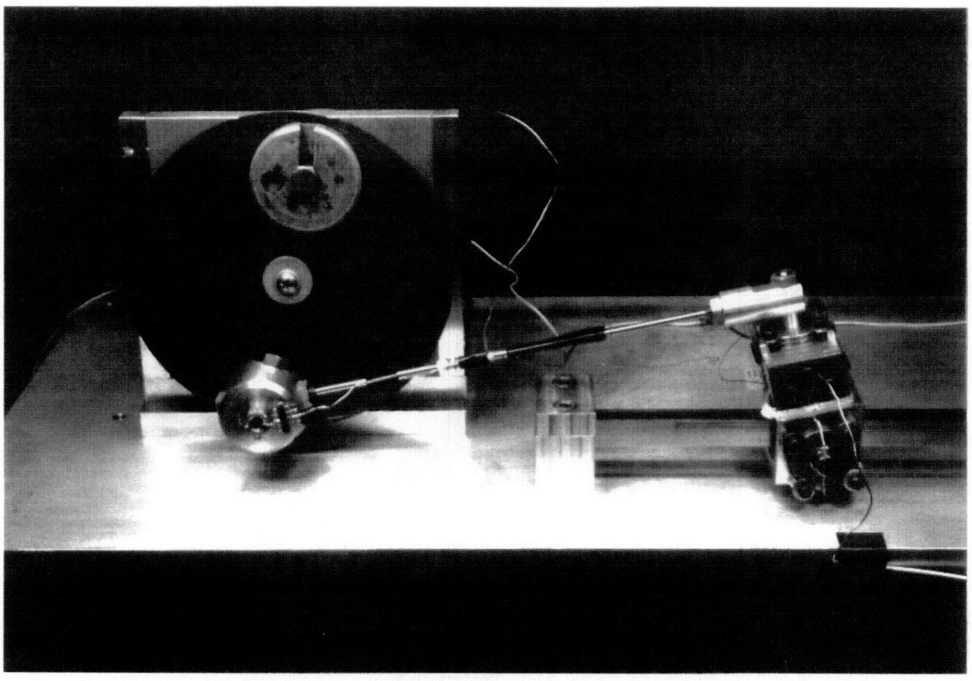

(b) Front view, 0° motor angle.

Figure 4.2 Experimental spatial slider crank mechanism [3].

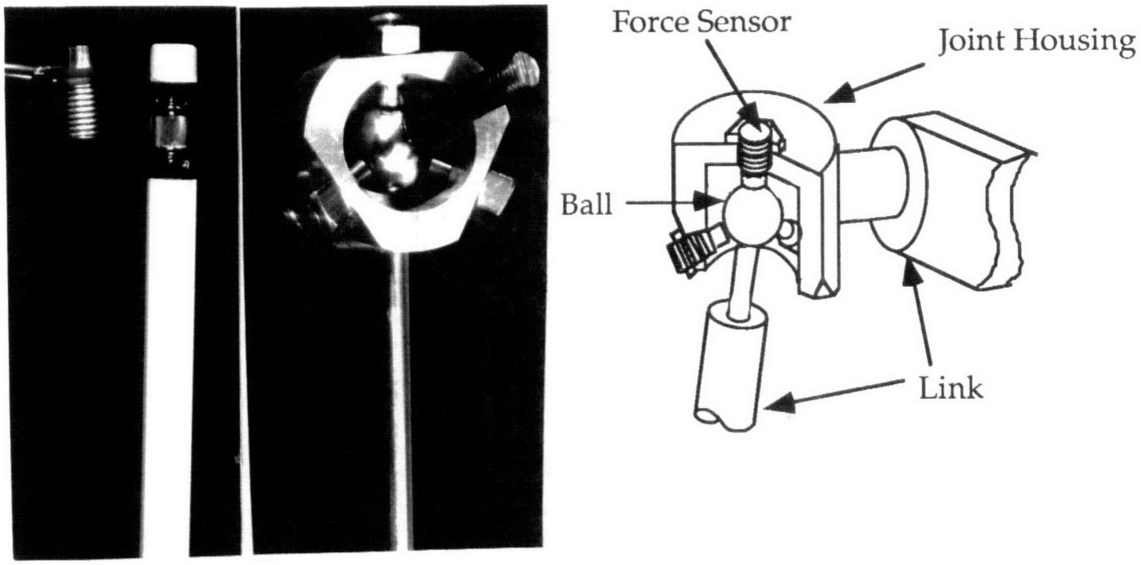

Figure 4.3 (a) Instrumented, adjustable clearance ball joint.

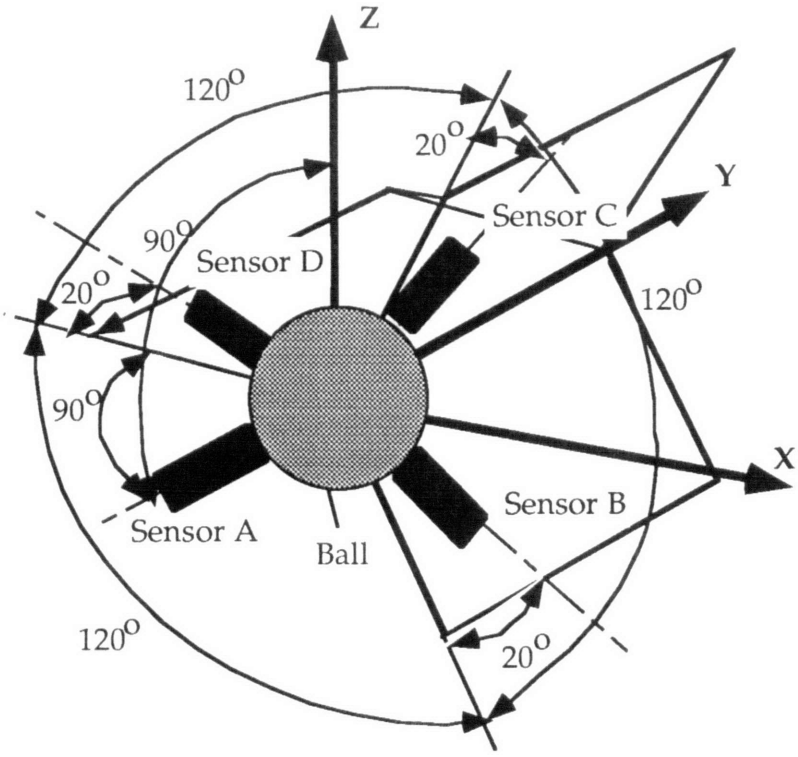

Figure 4.3 (b) Geometrical configuration of four force sensors inside ball joint.

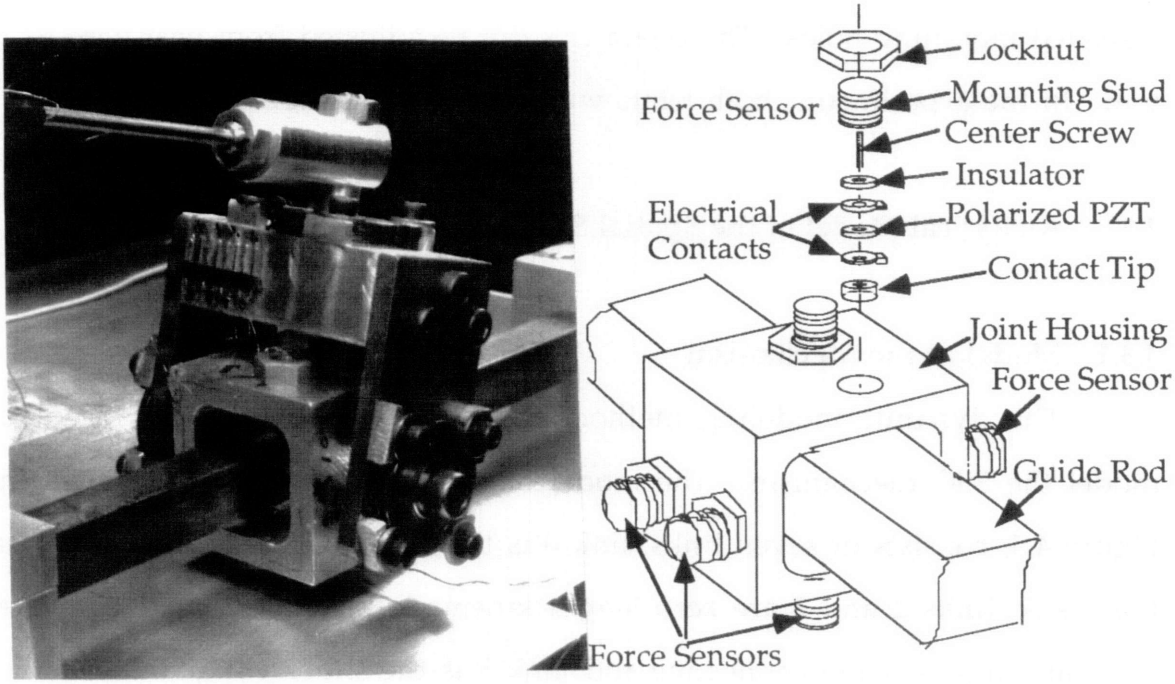

Figure 4.4 (a) Instrumented, adjustable clearance slider joint

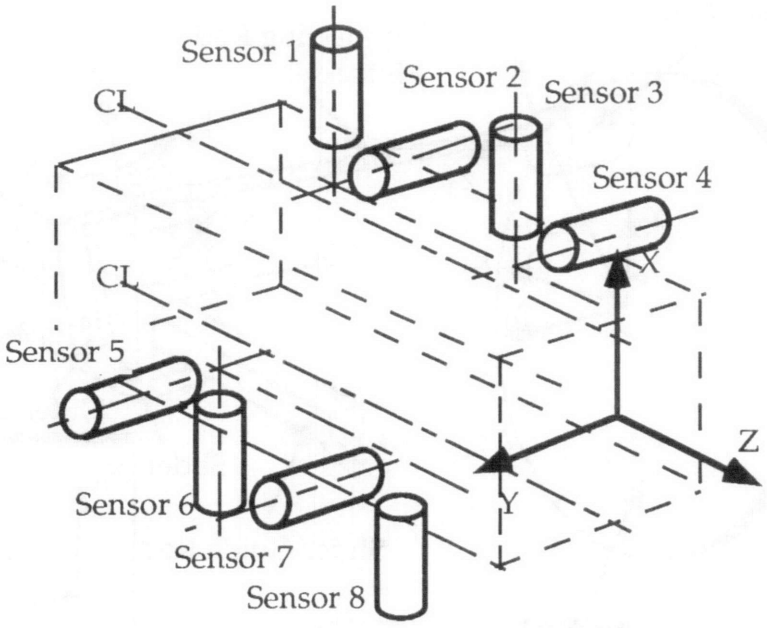

Figure 4.4 (b) Geometrical configuration of eight force sensors inside slider joint

The clearances in both joints are set by adjusting the sensors in their threaded mounting holes. The clearances can be adjusted from near zero to 1 mm. In the experiments, both joints were lubricated using light machine oil.

4.3 Analytical Model of the Spatial Slider Crank Mechanism

4.3.1 Model of the Mechanism

The dynamic modeling method presented in Section 2.2 is used to model the SSC mechanism. The model of the experimental SSC, shown in Figure 4.5, consists of seven links: link 0 is the base and the motor; link 1 is the crank; links 2 and 3 are zero length kinematic links associated with the ball joint; link 4 is the connecting rod; link 5 is the slider yoke; link 6 is the slider. The slider guide rod is modeled as part of link 0 because it is mounted on the base.

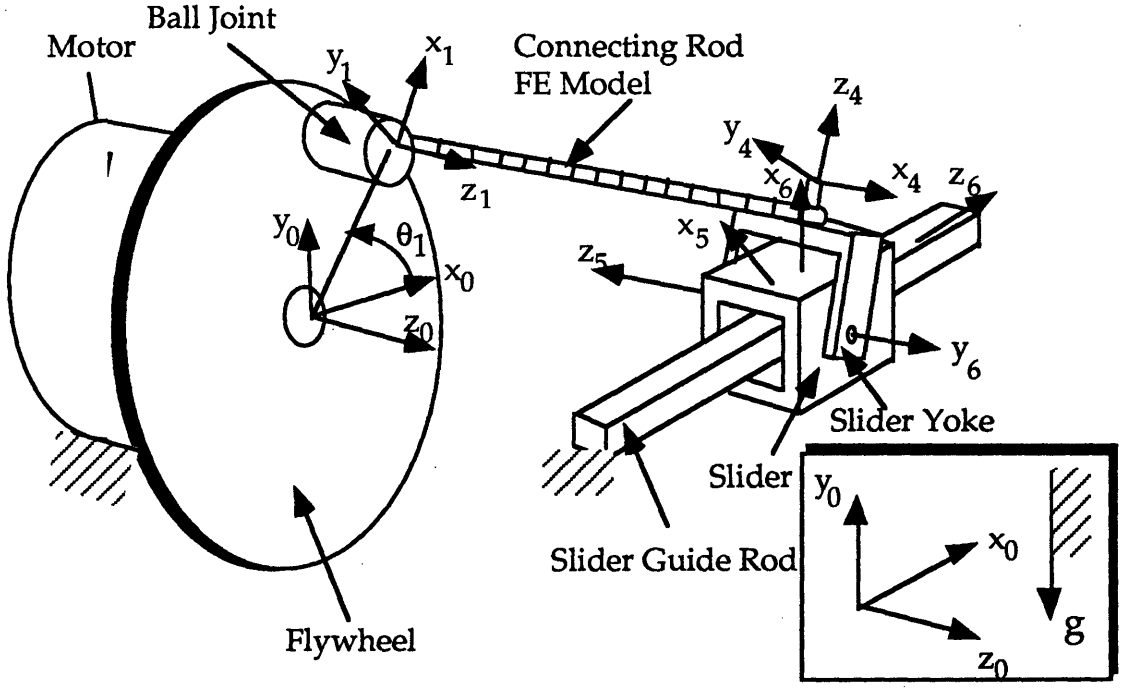

Figure 4.5 Numerical model of the SSC. Hartenberg-Denavit coordinate frames of links.

The Hartenberg-Denavit reference frames used in numerical simulations are attached to links in the model. The Hartenberg-Denavit parameters and the link types of seven links are listed in Table 4.1. The nominal motions of these seven links, $\theta_0(t)$ to $\theta_6(t)$, and their derivatives are provided by kinematic analysis of the mechanism.

Table 4.1 Hartenberg-Denavit parameters and link types of the SSC

Link	θ	L	H	α	Link Type
0	θ_0	0	0	0	Kinematic
1	θ_1	L_1	0	0°	Kinematic
2	θ_2	0	H_2	90°	Kinematic
3	θ_3	0	0	90°	Kinematic
4	θ_4	L_4	0	0°	FE Model Link
5	θ_5	0	H_5	90°	Rigid Link
6	θ_6	0	0	-90°	Rigid Link

In the model, the connecting rod, link 4, is modeled using finite elements. Other components such as the slider yoke, slider, and slider guide rod are assumed to be rigid.

4.3.2 Models of Clearance Connections

In this study, two models for the ball joint are used. One is the instrumented clearance ball joint model shown in Figure 4.3. The other is the spherical clearance model shown in Figure 4.6 [7]. In the spherical clearance model, one part is a hollow spherical shell, and the other part is a solid sphere that fits closely within the shell part. The depicted spherical

clearance model is exaggerated for illustrating the clearance. While the spherical clearance model is close to conventional ball joints, the instrumented clearance model is a representation of the ball joint used in the experimental SSC in this study.

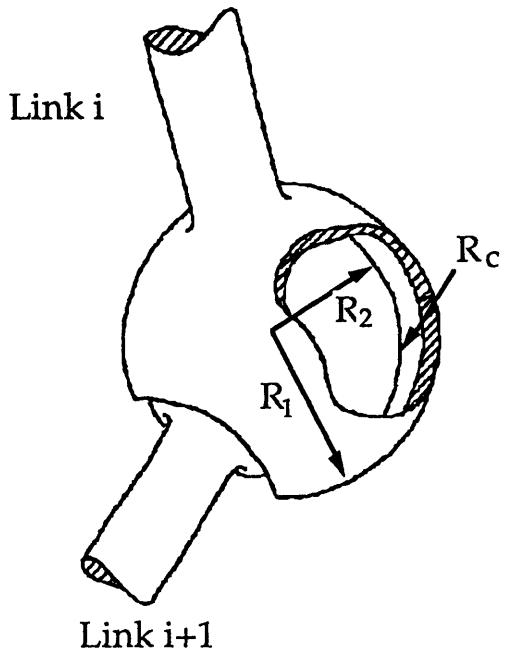

Figure 4.6 Spherical Clearance Connection Model [7].

There are two relative motion modes for clearance joints: contact and no contact. The contact mode is a point contact in both ball joint models. In the spherical clearance model, the point contact is between the ball and the shell. In the instrumented ball joint model, the contact is between the ball surface and the surfaces of the sensor tips, see Figure 4.3 (b) .

To represent the sliding prismatic joint, the instrumented prismatic joint model, illustrated in Figure 4.4, is used in this study. The contact mode

is either a point contact or a multi-point contact, which is between the hemispherical tips of the force sensors and the flat sides of the guide rod. The multi-point contact may involve simultaneous contacts with several sensors, representing a line contact.

When contact occurs in the joints, a contact force is calculated from the local deformations of the contact parts, which are determined by the kinematic interference of the contact parts at their contact location. The interference is calculated based on the geometrical configurations and the relative motions of the contact parts. The detailed computation procedure of the contact force can be found in Reference [3,7]. These forces are used in simulations to predict the contact forces.

4.4 Simulations of Dynamic Responses of the Mechanism

The dynamic responses of the SSC were simulated using the system model described in the previous section. In numerical simulations, impacts occurred in the clearance joints with certain clearance sizes and operating speeds. In the parameter regions where the impacts occurred, the SSC model was found to have chaotic behavior in some cases, and to have periodic behavior in other cases.

To provide general insights into the SSC, the motor angle was set to be zero degrees, i.e., the planar case of the mechanism was studied. Simulations were performed for two situations: (1) The ball joint was assumed to be a clearance joint while the slider joint was assumed to have zero clearance; (2) The slider joint was assumed to be a clearance joint while the ball joint was assumed to have zero clearance. The results are presented in Sections 4.4.1 and 4.4.2, respectively.

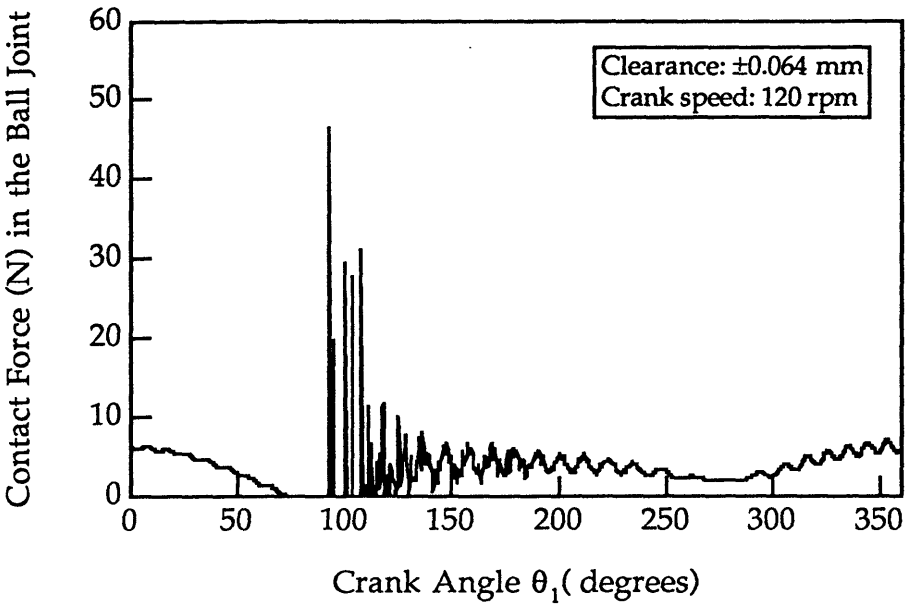

Figure 4.7 A simulation result. Contact force in ball joint. Spherical Clearance model.

4.4.1 Impact Responses in the Clearance Ball Joint

For simulation results presented in this section, the ball joint is modeled a clearance joint while the slider joint has zero clearance. For the ball joint, both the spherical clearance model and the instrumented clearance model are used. Results of the spherical clearance model are presented first, followed by results of the instrumented clearance model.

Spherical Clearance Model

To determine whether impacts occur in the clearance ball joint, the system model was simulated for different clearance sizes at different operating speeds. It was found that impacts occur usually at large clearances and low crank speeds, and that system responses could be chaotic only in the impact regions.

Figure 4.7 shows a sample response of the SSC in one revolution during which an impact occurs. In the figure, the contact force in the ball joint is plotted as a function of the crank rotation angle for ±0.0635 mm clearance and 120 rpm crank speed. A non-zero contact force corresponds to a contact between the ball and shell, and a zero contact force indicates the loss of contact between these two parts. Impacts occur when contact is resumed after the contact loss. As seen in the figure, the ball and shell are in contact at crank angles from 0° to 70°, out of contact afterwards, then in contact again at 95°. After bouncing for a while in the range from 95° to 130°, the ball and shell remain in contact for the rest of the cycle.

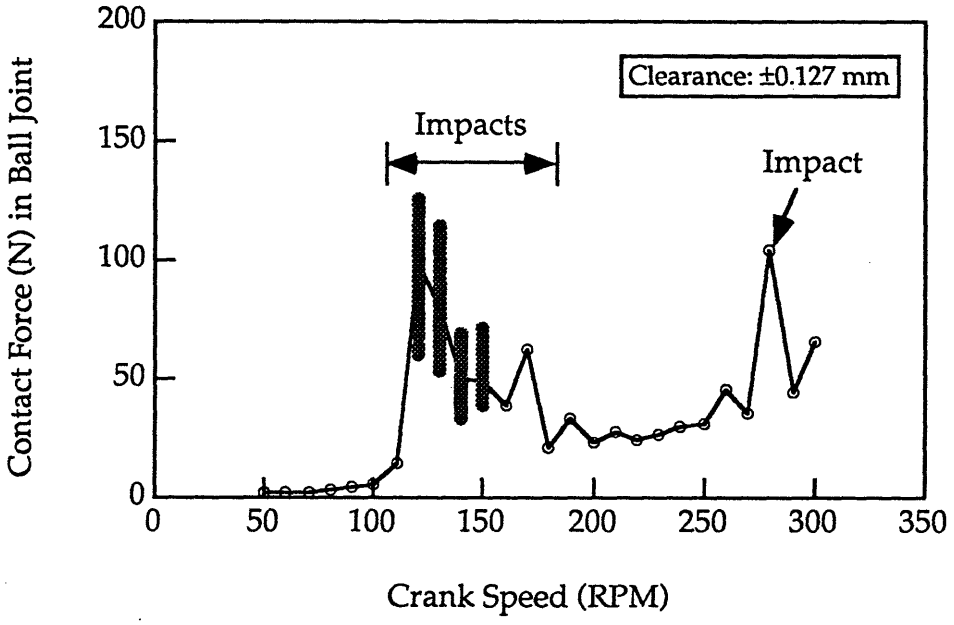

Figure 4.8 Simulation results. Peak impact forces as a function of the crank speed. Spherical clearance model.

Figure 4.8 shows different responses as the crank speed is varied, with ±0.127 mm clearance. In the figure, the peak contact forces of 50 operating cycles are plotted at each crank speed. A single point at a given crank speed

indicates a periodic response at that speed, since the peak values of 50 cycles are the same. A few discrete points indicate a subharmonic response. Densely distributed points indicate a chaotic response since the peak force varies from one operating cycle to another. As noted above, the examination of the contact force time history reveals whether the peak contact force is caused by impacts. Speed regions where the peak force is due to impacts are indicated on the figure. Impacts occur in the crank speed range from 110 rpm to 190 rpm and at 280 rpm. Chaotic responses are found to occur at 120 rpm, 130 rpm, and 140 rpm, which are in the region with impacts. Chaotic responses are observed only in crank speed regions with impacts.

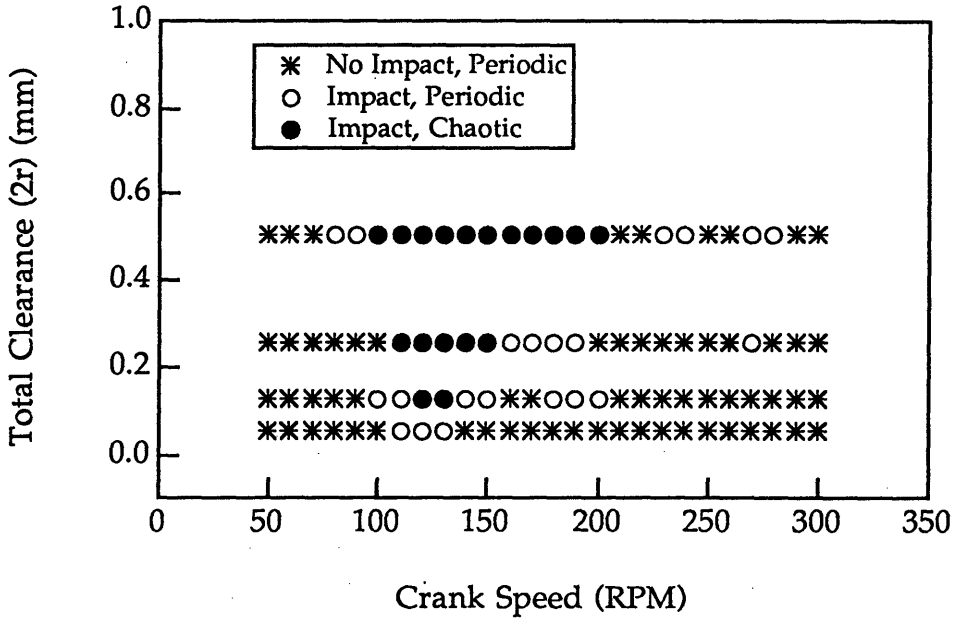

Figure 4.9 Simulation results. The nature of responses in *Crank speed-Clearance* space. Spherical clearance model.

To further examine the characteristics of responses in the *Crank speed-Clearance* space, the above analysis was repeated using different clearance sizes of the ball joint. Simulation results are plotted in Figure 4.9. The stars

represent responses without impacts. The black dots represent responses with impacts and chaotic behavior, while the open circles mark responses with impacts and periodic behavior. As seen in the figure, responses with impacts occur only in a small crank speed range (100 - 200 rpm) at typical sizes of clearances (< ±0.127 mm). For the clearance range considered here, there are no impacts at crank speeds above 300 rpm.

These dynamic behaviors are affected by the orientation of the mechanism. In the above cases, the mechanism operates in a plane which is parallel to the gravitation (see Figure 4.5). For a given clearance, whether impacts occur depends upon not only the magnitudes of the centrifugal force (proportional to the square of the crank speed) and the inertia force of the slider during a revolution, but also the magnitude and direction of the gravity forces acting on the mechanism (proportional to the mass of the mechanism). At crank speeds of less than 100 rpm, the gravity force and the inertia force of the slider keep the ball in contact with the shell. When the operating speed is higher than 300 rpm, centrifugal force keeps the ball in continuous contact with the shell. In between, depending upon the net effect of these three forces, contact between the ball and the shell may be lost and impact occurs when contact is resumed. If the mechanism operates in the plane which is perpendicular to gravity, centrifugal force and the inertia force of the slider keep the ball in continuous contact with the shell. In this case there are no contact loss or no impacts.

Instrumented Clearance Ball Joint Model

The simulated dynamic behavior of the SSC with the instrumented clearance model can be different from the behavior just discussed using the spherical clearance model. In the instrumented clearance model, an impact

can occur without a complete contact loss between the ball and four tetrahedrally distributed sensors around it. Whenever the ball strikes one of the sensors, an impact is recorded by the sensor no matter whether or not the ball is still in contact with other sensors.

Figure 4.10 shows the magnitude of the contact force vector in the joint as a function of the crank angle with ±0.127 mm clearance at 100 rpm crank speed. Two large impulsive forces occurring at 100° and 300° crank rotation angles indicate the impacts. Note that there is no contact loss, since the contact force is not zero before the impacts occur, particularly at the 300° crank angle. When an impact was recorded by one sensor at the 300° crank angle , the ball was in contact with one or more other sensors.

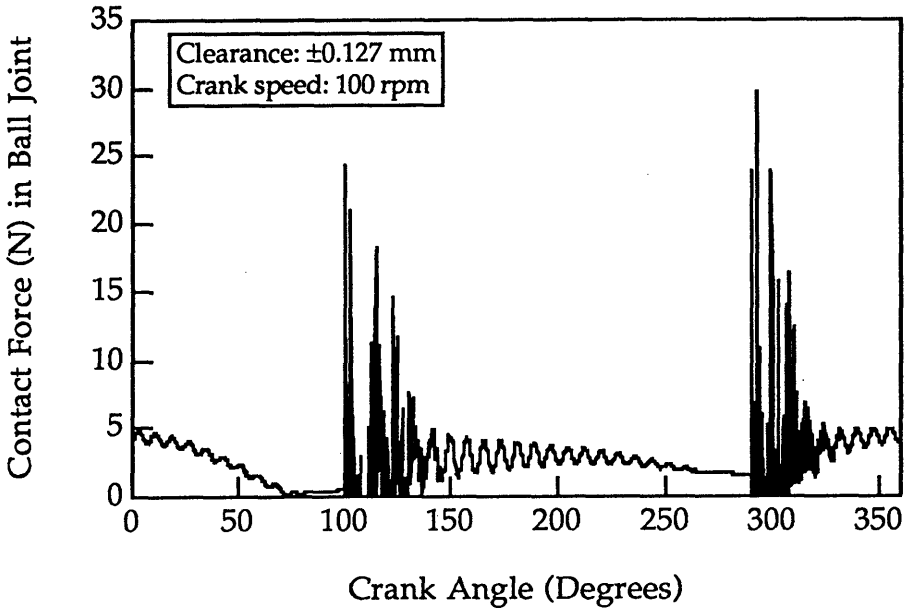

Figure 4.10 A simulation result. Contact force in instrumented clearance ball joint.

Although the instrumented clearance model can not predict the dynamic behavior of conventional ball joints, it provides good predictions of

the instrumented ball joint. The comparison between numerical and experimental results are given in Section 4.7.

4.4.2 Impact Response in the Clearance Slider Joint

For simulation results presented in this section, the slider joint is modeled as a clearance joint while the ball joint has zero clearance. The system response was found to be chaotic in some parameter regions and periodic in other cases.

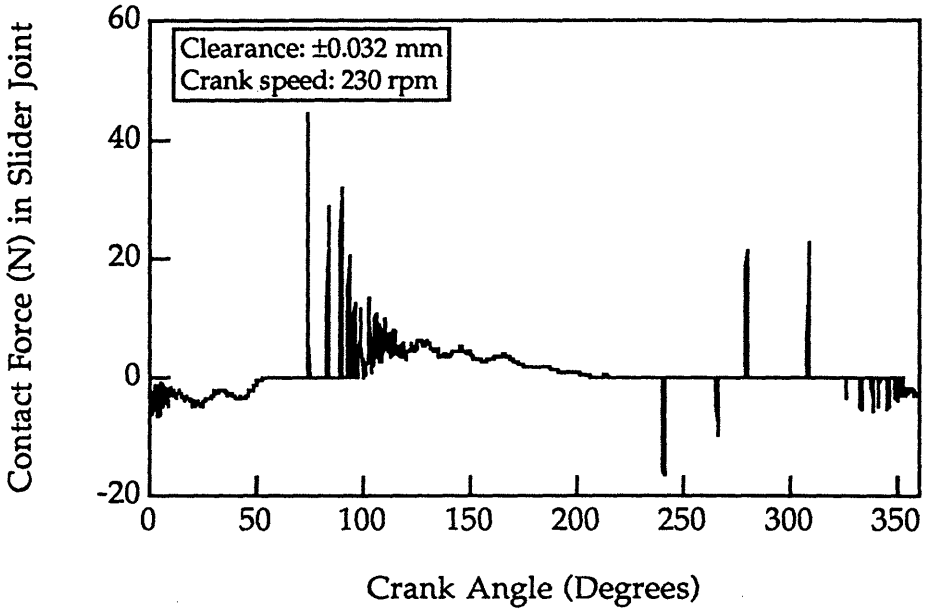

Figure 4.11 A simulation result. Contact force in instrumented clearance slider joint.

Figure 4.11 shows a sample response in one revolution during which an impact occurs. The figure shows the contact force in the instrumented slider joint as a function of the crank angle for ±0.032 mm clearance and 230 rpm crank speed. While positive values of the contact force indicate contacts of the upper sensors of the slider with the guide rod, negative values indicate

contacts of the lower sensors. A non-zero contact force corresponds to contact between the contact force sensors and the slider guide rod, and a zero contact force indicates contact loss. Impact occurs when contact is resumed after contact loss. The figure indicates that contact loss occurs at 55° crank angle, and contact is resumed at 75°, which is characterized by a large impact force.

Figure 4.12 shows the above response in time and phase domains for the slider motion perpendicular to the axis of the slider guide rod with ±0.032 mm clearance and 230 rpm crank speed. Figures 4.12 (a), (b), and (c) show the time history of the displacement, phase portrait and Poincaré Map of the slider vibration, respectively. The impact force in the slider joint is shown in Figure 4.12 (d). As seen in the figures, the displacement time history, phase portrait and Poincaré Map of the slider vibration show irregular variations and non-repeatability. The impact force varies from one operating cycle to another. Therefore, the response is chaotic.

Figure 4.13 shows the peak contact forces in the slider joint as a function of the crank speed for ±0.032 mm clearance. For each crank speed, the peak contact forces for 50 cycles of machine operation are recorded. Thus, at a given crank speed in the figure, a single point appears for a periodic response; a few discrete points appear for a subharmonic response; and distributed points appear for a chaotic response. Chaotic responses occur at a number of crank speeds (e.g., from 110 - 190 rpm) and periodic responses occur at other speeds (e.g., at 100 , 200 rpm).

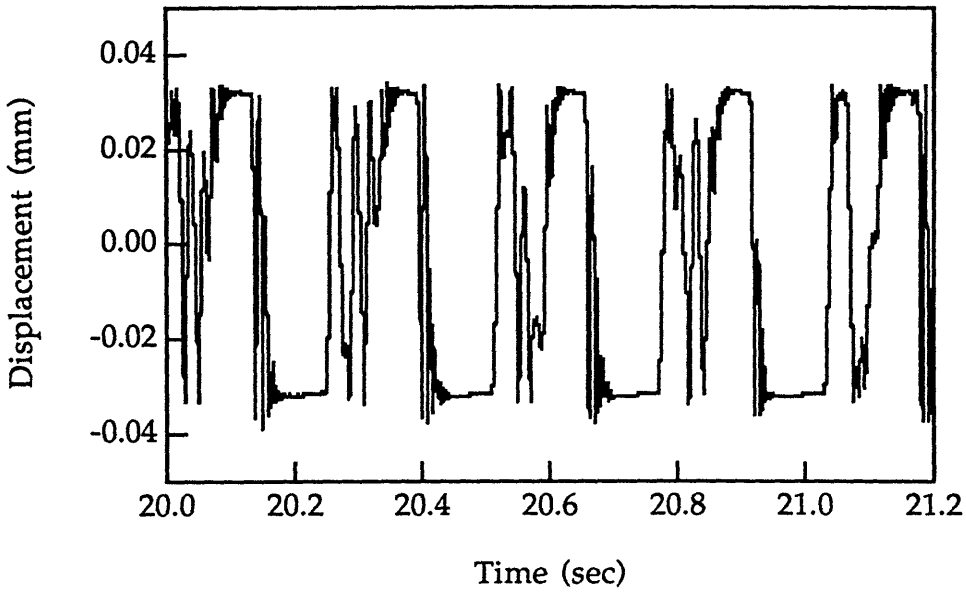

(a) Displacement of the slider vibration.

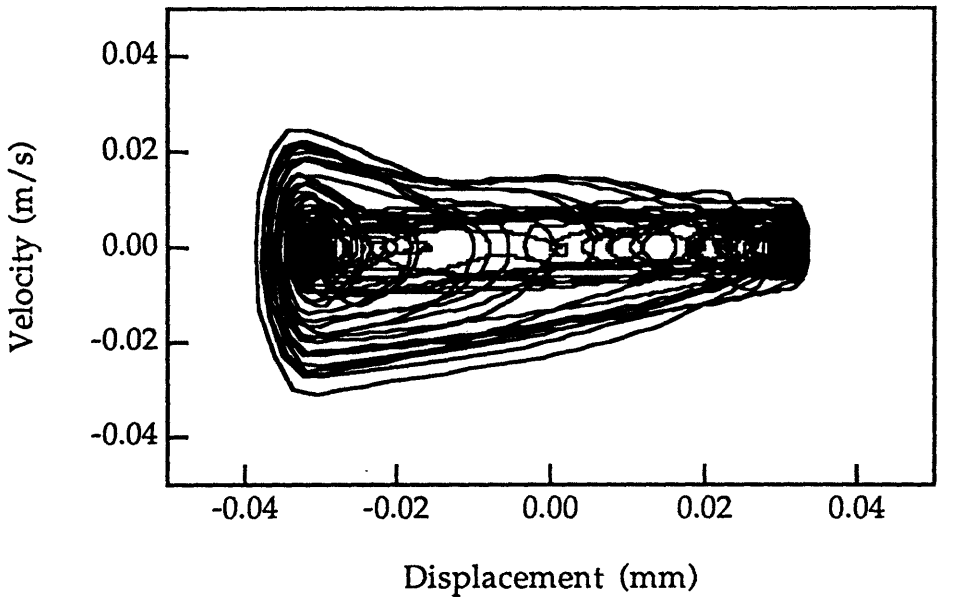

(b) Phase plane portrait of the slider vibration.

Figure 4.12 A simulation result. (a) Time history, (b) phase plane portrait, (c) Poincaré map of the of the slider vibration, and (d) time history of the impact force. ±0.032 mm clearance and 230 rpm crank speed. Instrumented clearance slider joint model.

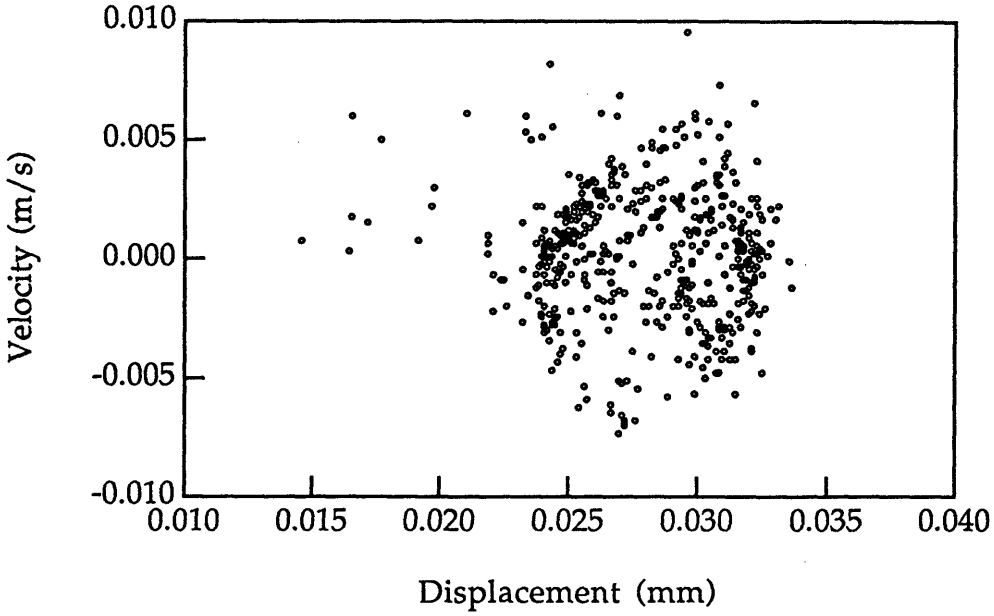

(c) Poincaré map of the slider vibration.

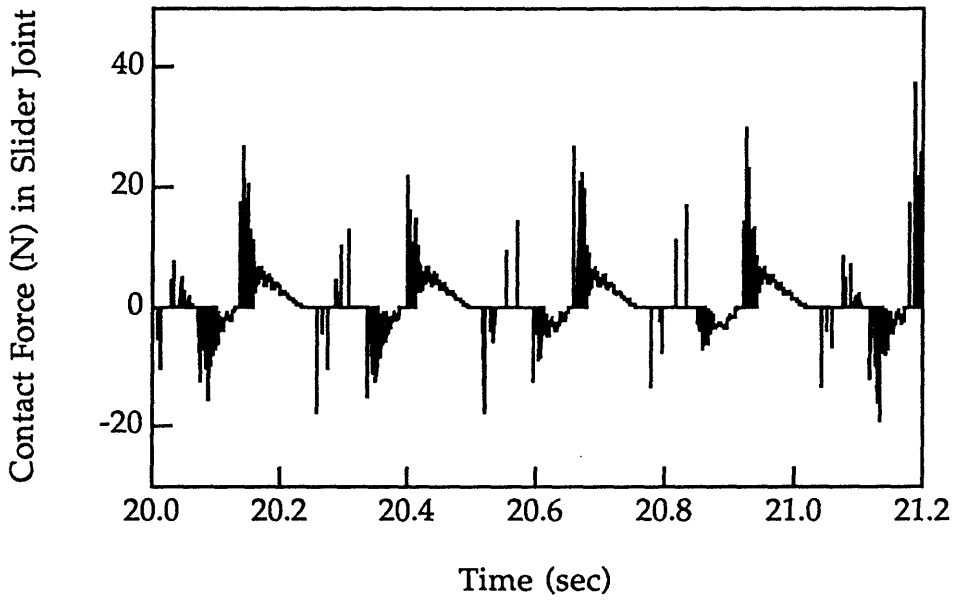

(d) Time history of the impact force in the slider joint.

Figure 4.12 (Continued).

Results shown in Figures 4.7, 4.10 and 4.11 indicate that the contact forces of the SSC follow a pattern similar to the one observed in the IBS: an initial large peak force, then a bouncing period, finally a contact period. Other similar characteristics between these two systems will be discussed in the following sections.

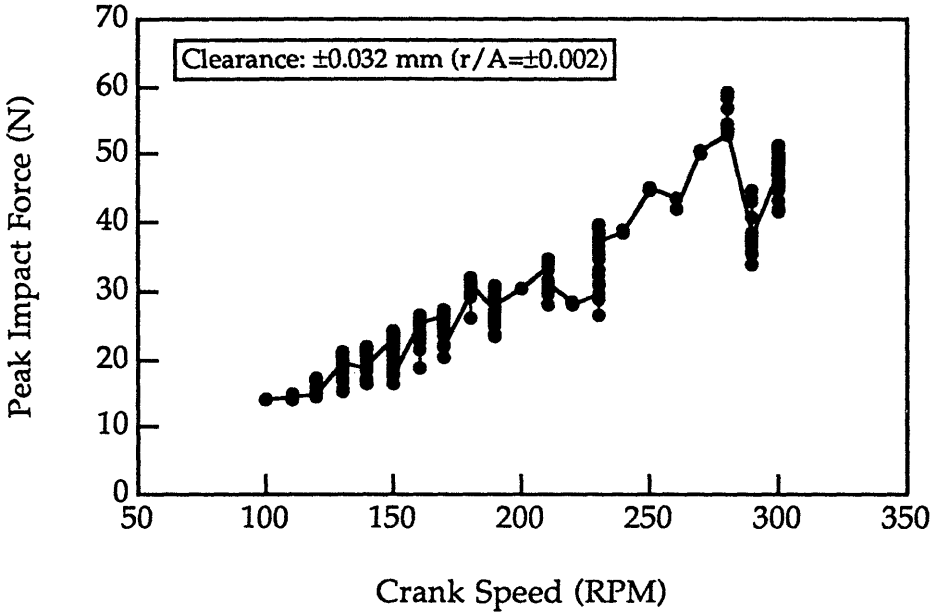

Figure 4.13 Simulation results. Peak impact force in slider joint as a function of crank speed. 6.35 mm diameter connecting rod.

4.5 Effects of System Parameters on the Dynamic Response

The clearance size, crank speed, joint friction, link dimension, contact damping, and component flexibility are the system parameters that strongly affect the contact force in the clearance joint. The effects of each of these parameters on the dynamic response of the SSC are discussed in this section. The results presented are for the slider joint with clearance and the ball joint with no clearance.

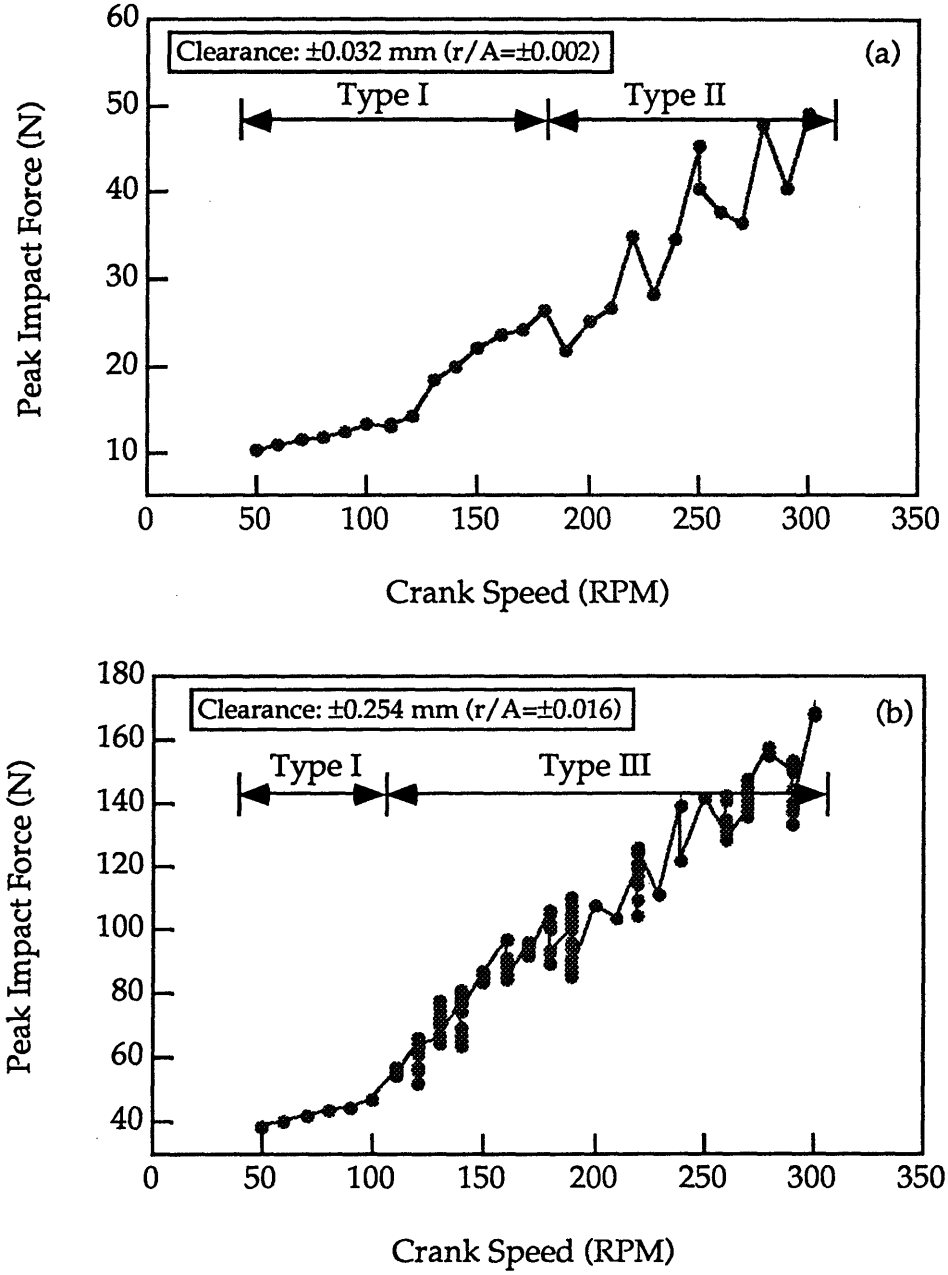

Figure 4.14 Simulation results. Peak impact force in slider joint as a function of crank speed for different clearances. (a) ±0.032 mm clearance. (b) ±0.254 mm clearance. Instrumented clearance slider joint model.

4.5.1 The Effect of Clearance and Crank Speed

To examine the effects of the slider clearance and crank speed on the dynamic behavior of the SSC, Figures 4.14 (a) and (b) present the peak impact force as a function of the crank speed for dimensionless clearances of ±0.002 (±0.032 mm clearance) and ±0.016 (±0.254 mm clearance). The dimensionless clearance is the actual clearance normalized by the magnitude of the slider vibration due to a force equal to the slider inertia force, applied perpendicular to the slider guide rod axis. In Figures 4.8 and 4.13, the peak forces from 50 cycles of operations are plotted for each crank speed, and the nature of the response - periodic, subharmonic or chaotic - is indicated by the distribution of dots. The responses are further classified into three characteristic types based on the trend of the peak impact force as the crank speed is varied.

Type I Response is periodic, and not sensitive to initial conditions or small parameter variations. The predicted impact force increases smoothly as the crank speed increases in the range of 100 - 180 rpm for ±0.032 mm clearance. This well-behaved response permits designers to predict trends.

Type II Response is periodic and not sensitive to initial conditions. However, it is sensitive to small parameter variations. This sensitivity is seen as the crank speed varies from 190 - 300 rpm for ±0.032 mm clearance. The peak impact force fluctuates significantly as the crank speed varies. For example, as the crank speed increases from 270 to 290 rpm, the peak impact force first increases from 35 to 48 N, a 40% increase, and then drops to 40 N, a 20% decrease. The hidden danger of the Type II Response is its periodicity. Designers may see periodic responses, and overlook the sensitivity to small variations of system parameters.

Type III Response is unpredictable, either chaotic or periodic as shown in Figure 4.14 (b). For a chaotic response, the predicted impact force, which is

characterized by the large variations in the peak impact force at a given crank speed, is sensitive to initial conditions. For example, at 190 rpm, the peak impact force varies between 85 and 110 N, depending on the initial displacements and velocities used in the simulation. The peak impact force also fluctuates considerably as the crank speed changes. For example, while the response is periodic with a peak impact force of 105 N at 210 rpm, it becomes chaotic with a peak impact force in the range of 110 to 130 N as the crank speed increases to 220 rpm. For the Type III Response, the variation range and statistical properties of the peak impact force may be obtained through sufficient cycles of simulation. These statistical properties may be sufficient for designers to perform the necessary design analysis. However, the uncertainty and sensitivity of the responses present ambiguities for a designer or analyst to use the predictions of computer-based simulations.

The above analysis was repeated for several more slider clearances. Figure 4.15 summarize the simulation results. The black dots represent chaotic responses, while the open circles mark periodic responses. The responses in this parameter space are classified into three types according to the definitions of the Type I, Type II, and Type III Responses. The corresponding regions of these three types of responses in the parameter space are suggested in the figure using three different shadings. This figure also shows that chaotic responses usually occur at large sizes of clearance and high operation speeds.

These three types of responses demonstrate that the dynamic behavior of the SSC has characteristics similar to those of the IBS .

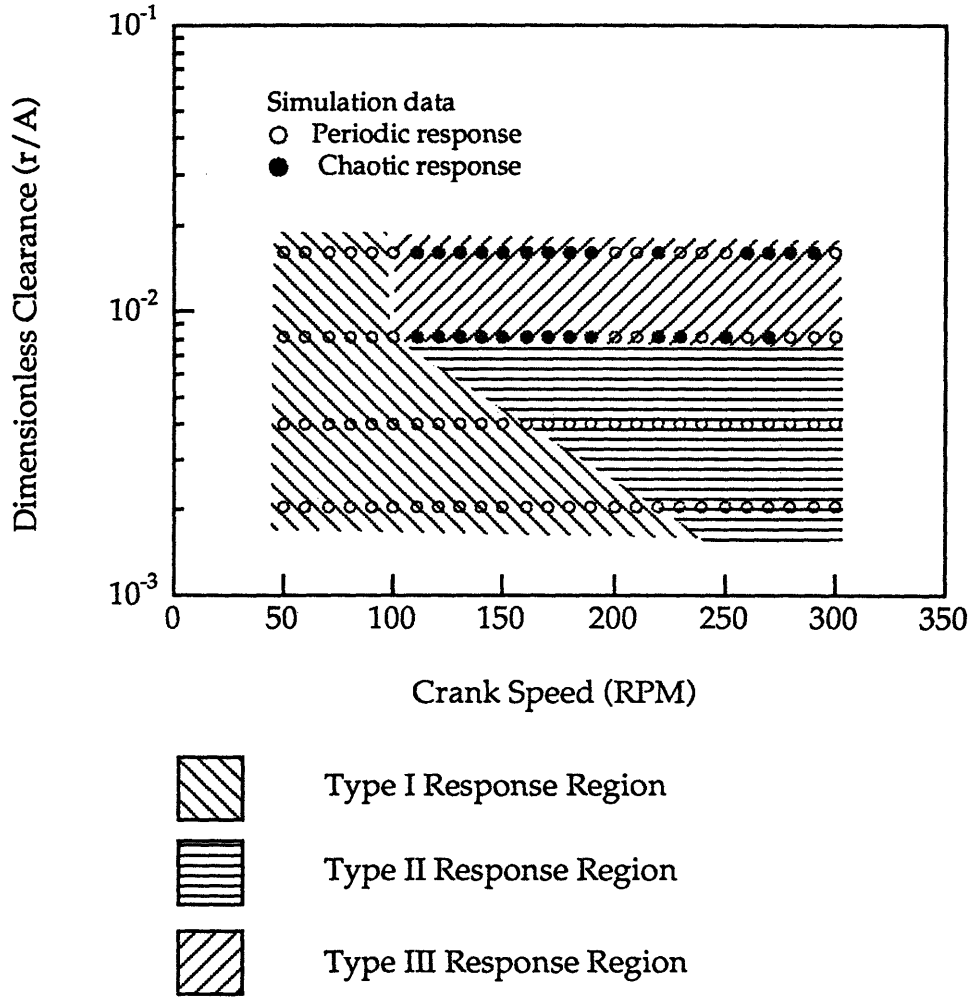

Figure 4.15 Simulation results. The nature of responses of the SSC in *Crank speed-Clearance* space. Instrumented clearance slider joint model.

4.5.2 The Effect of Link Dimensional Variation

The length of the connecting rod is one of the design parameters for the SSC, and was chosen to investigate the effect of dimensional variation on dynamic behavior.

Figure 4.16 shows the peak impact force as a function of the variation in connecting rod length for 250 rpm crank speed and ±0.032 mm clearance.

In this parameter region, the response is a Type III Response. The length of the connecting rod varies from 0.235 to 0.265 m. The figure shows that even a small variation in the length of the rod can change the nature of the response. For instance, as the rod length decreases from 0.2575 to 0.255 m, a decrease of approximately 1%, the response changes from periodic to chaotic, and peak impact force changes from 34 N to a range of 33 to 43 N, a 25% increase in the maximum values. The effect of dimensional variation on the dynamic behavior in the SSC is similar to that of the IBS.

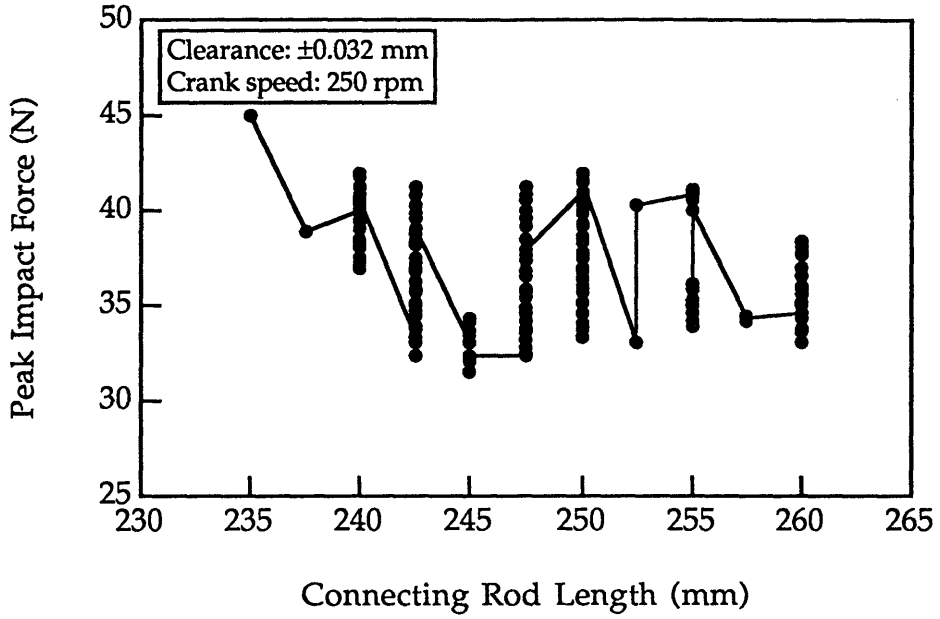

Figure 4.16 Simulation results. Peak impact force in slider joint as a function of length variation of the connecting rod.

4.5.3 The Effect of Friction in the Slider Joint

Friction was added to the numerical model of the slider joint to examine its effect on the dynamic responses. The Coulomb friction model was used to model friction in the slider joint. In the model, the magnitude of friction force is proportional to the normal contact force in the joint, and the

direction of the friction force opposes the nominal velocity of the slider. For the reciprocating motion of the slider, friction force calculated based on this model is discontinuous when the nominal velocity of the slider passes through zero. This discontinuity makes numerical integration difficult. To overcome this difficulty, a ramp function is used to modify the model so that the friction force changes continuously when the nominal velocity of the slider passes through zero [3].

Figures 4.17 (a) and (b) show the peak impact force as a function of the crank speed for ±0.032 mm clearance with and without friction in the slider joint. The friction coefficient μ was set to be 0.1 in Figure 4.17 (b). Here, a Type III Response is chosen as an example. Similar to Figure 4.13, the peak impact forces are recorded for 50 cycles of machine operations at each crank speed. The figure shows the effect that lubrication between the contact surfaces can have on the nature of the responses. For example, when Coulomb friction is added to model an non-lubricated joint, the response changes from periodic to chaotic at 230 rpm, but chaotic to periodic at 260 rpm.

The sensitivity of responses to friction suggests the difficulty of predicting the dynamic behavior of a machine when it is built, since it is difficult to get reliable estimations of friction conditions between contact surfaces in the machine.

4.5.4 The Effect of Contact Damping

In all the simulation results presented in this section, two contact damping ratios, 2.5% and 5%, were used. The results in Figure 4.17 (a) were obtained using a 2.5% contact damping ratio, while the results in Figure 4.14 (a) were obtained using a 5% contact damping ratio. Other parameters are the same for both figures. Comparing these figures indicates that all chaotic

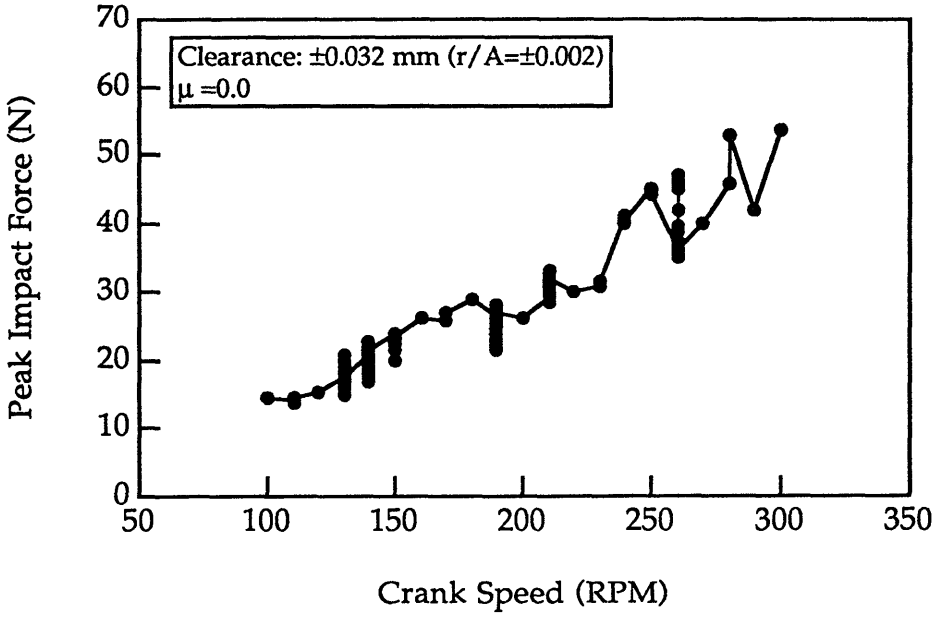

(a) Without friction

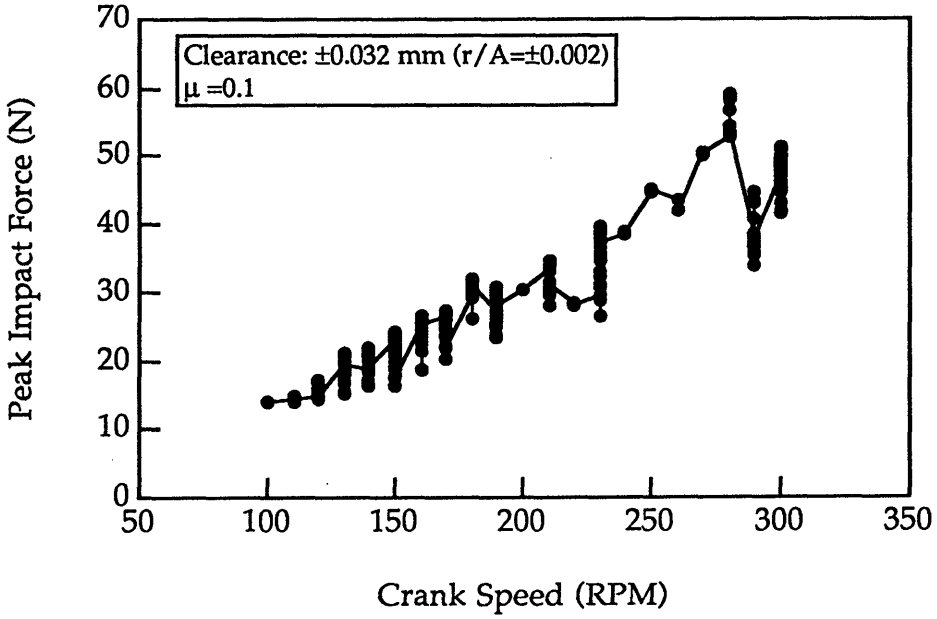

(b) With friction

Figure 4.17 Simulation results. Effect of friction in the slider joint on the dynamic behavior. (a) without friction. (b) with friction.

responses disappear when the damping ratio increases from 2.5% to 5%. As a result, the responses change from Type III to either Type I or Type II.

From this comparison, two points should be noted. First, increasing contact damping is an effective way of minimizing chaotic behavior. Second, the Type II Response can not be eliminated by increasing the contact damping. This conclusion is consistent with the characteristics of the Type II Response discussed in Section 3.5.

4.5.5 Effect of Component Flexibility

As seen in Chapter 3, the component flexibility strongly affects the characteristics of the dynamic behavior of the IBS, especially for the Type II Response. In addition to this similar effect, numerical simulations of the SSC reveal that superharmonic resonant responses occur at certain operating speeds due to the flexibility of the connecting rod.

Figure 4.18 shows the peak impact force as a function of the crank speed with ±0.127 mm clearance. The peak impact forces are recorded for 50 cycles of machine operations at each crank speed. The figure shows several resonant responses, occurring at 600 rpm (15 Hz), 1140 rpm (19 Hz), and 1500 rpm (25 Hz). The curve of the peak impact force has local maxima at 600, 1140 and 1500 rpm. These extrema are due to superharmonic resonances. They can be either periodic or chaotic. The resonant responses are found to be independent of the clearance size, and they occur even for zero clearance.

These superharmonic responses are excited by inertia force in the SSC. In contrast to the IBS, where the excitation force is a pure sinusoidal, the inertia force of the slider in the SSC is periodic with different harmonic components due to the nonlinear kinematic motion of the mechanism. The high order harmonic terms of the inertia forces excite the resonances when

their frequencies coincide with the natural frequencies of the systems. Eigenvalue analysis of the system at the zero crank angle position (see Figure 4.5) shows the first natural frequency of the system to be 75.6 Hz. The mode shape at this frequency is bending of the connecting rod with the ball joint housing mass at its one end and the slider yoke mass at its other end. This mode is excited when the crank speed is at 15, 19 and 25 Hz. Hence, the resonant responses at 15, 19, and 25 Hz are the 5th-order, 4th-order, and 3rd-order superharmonic resonant responses.

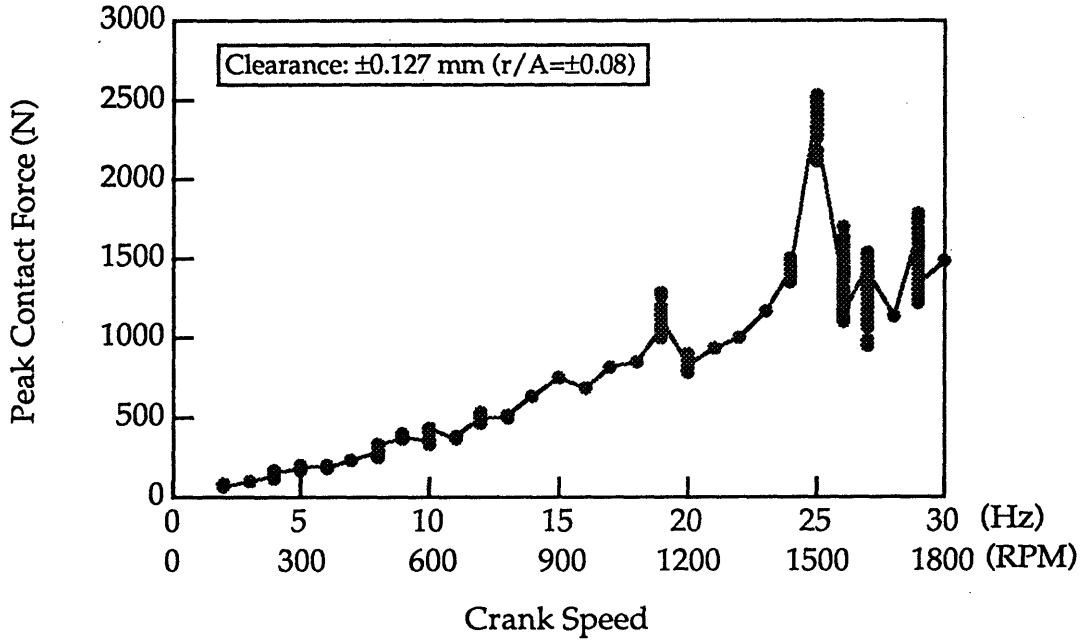

Figure 4.18 Simulation results. Peak impact force in slider joint as a function of crank speed. Showing superharmonic resonant responses at 15, 19, and 25 Hz.

In general, the natural frequencies of a mechanism with nonlinear kinematic motion are configuration dependent. However, it is found that the first natural frequency of the SSC varies only slightly, from 75.6 to 76.8 Hz as the mechanism configuration changes in operation.

The superharmonic resonant responses are dangerous since they induce much larger impact forces than non-resonant responses. As shown in Figure 4.18, the peak impact force of the 3rd order superharmonic resonant response at 1500 rpm is up to 2500 N. The corresponding vibration of the connecting rod violates the small perturbation assumption of the model. In reality, this indicates a likely failure of a machine. One suggestion for avoiding superharmonic resonances is to choose a material with high stiffness and light mass for the connecting rod in order to maintain high operating speeds.

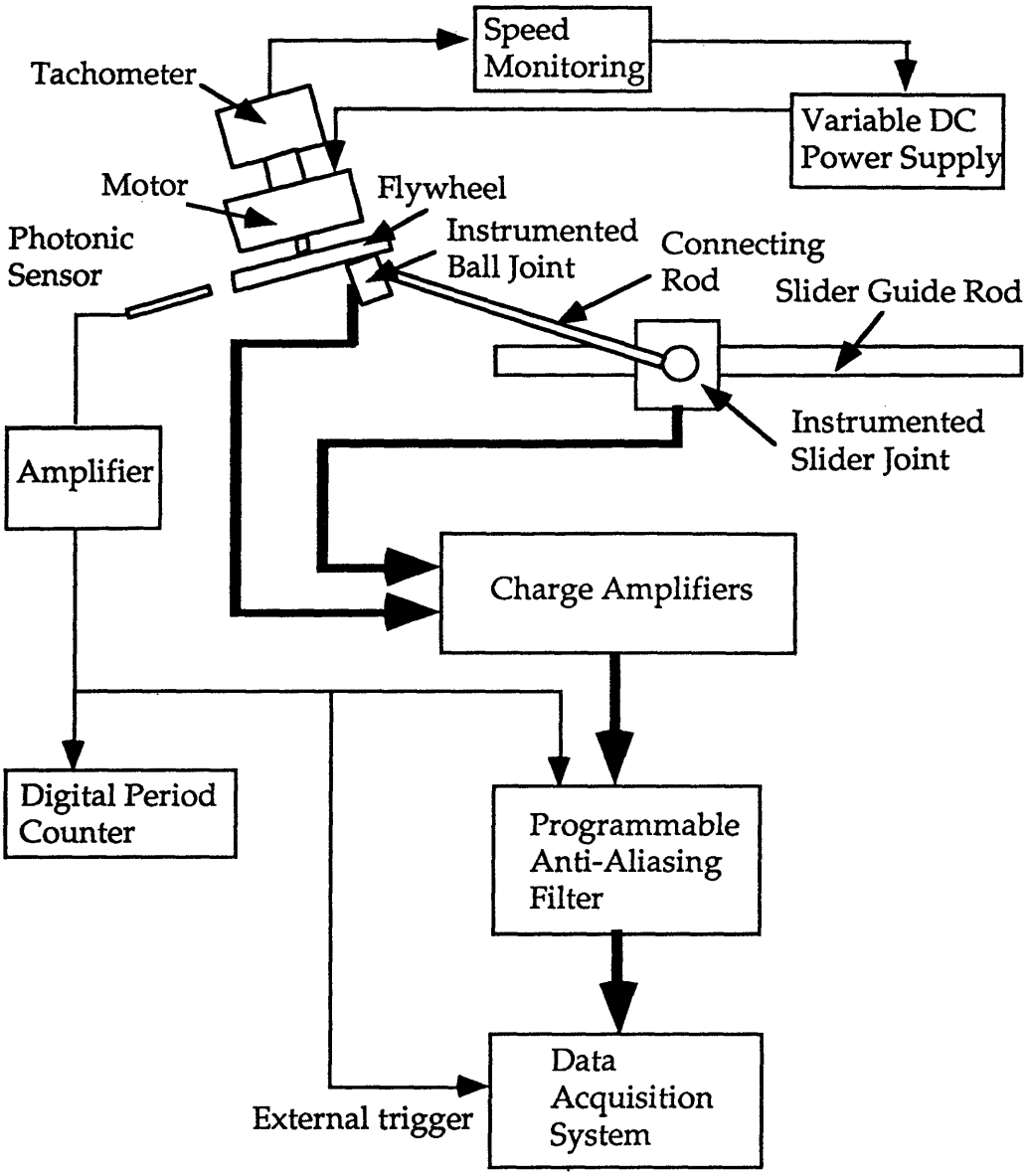

Figure 4.19 Schematic diagram of the SSC measurement.

4.6 Experimental Responses of the Mechanism

A schematic diagram of the experimental measurement for the SSC is shown in Figure 4.19. A Hewlett-Packard variable regulated DC power supply drives the motor. The output of the motor's tachometer is fed back to a control loop to stabilize the motor speed. A photonic sensor reads an optical mark on the flywheel to provide a synchronizing pulse per revolution at 0°

crank angle. The pulse signal is sent to a digital period counter to precisely monitor cycle period. This pulse is also used as an trigger signal to acquire signals from the force sensors. The outputs of the force sensors in the instrumented clearance joints are amplified by charge amplifiers and sent to the data acquisition system. A Frequency Device 9016 multichannel programmable analog filter provides anti-aliasing filtering for the signals before they enter the A/D converter of the data acquisition system. The data are collected by a Concurrent 6000 computer with laboratory data acquisition hardware and software called Laboratory Workbench [2].

Extensive experiments were performed for different crank speeds and clearances for the SSC with 0° motor angle. In the experiments, two connecting rods, of 6.35 mm and 3.18 mm diameter, were used. Results presented here are for the 6.35 mm rod unless noted.

Contact Force in the Ball Joint

Figure 4.20 (a) shows the measured outputs of the four contact force sensors in the ball joint as functions of the crank angle for 100 rpm crank speed and ±0.127 mm clearance. The position of each sensor in the joint is shown in Figure 4.2 (b). Note that the ball is always in contact with at least one sensor. There is no real contact loss in the joint. The occurrence of impacts with large forces in the outputs is due to the fact that the ball contacts each sensor sequentially, causing an impact to be recorded even when the ball is still in contact with another sensor. The recorded forces of the four sensors can be summed vectorially to obtain the resultant contact force in the ball joint. Figure 4.20 (b) depicts the magnitude of the contact force as a function of the crank angle.

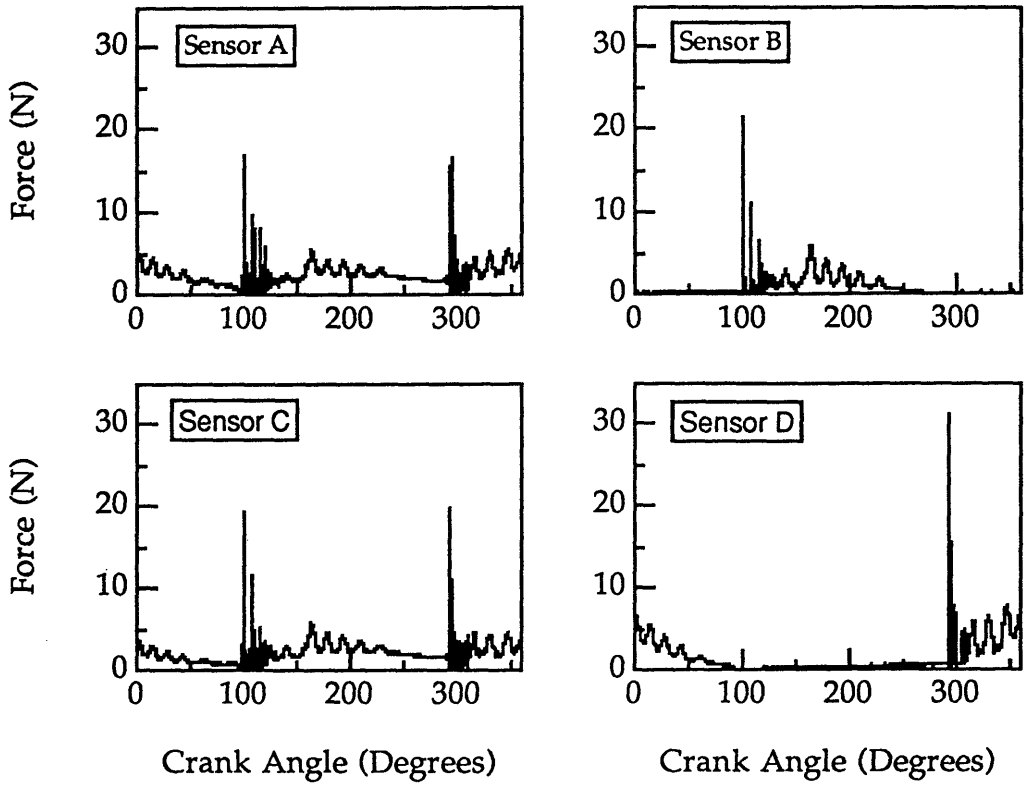

Figure 4.20 (a) Measured contact forces of four sensors in instrumented ball joint. ±0.127 mm clearance and 100 rpm crank speed.

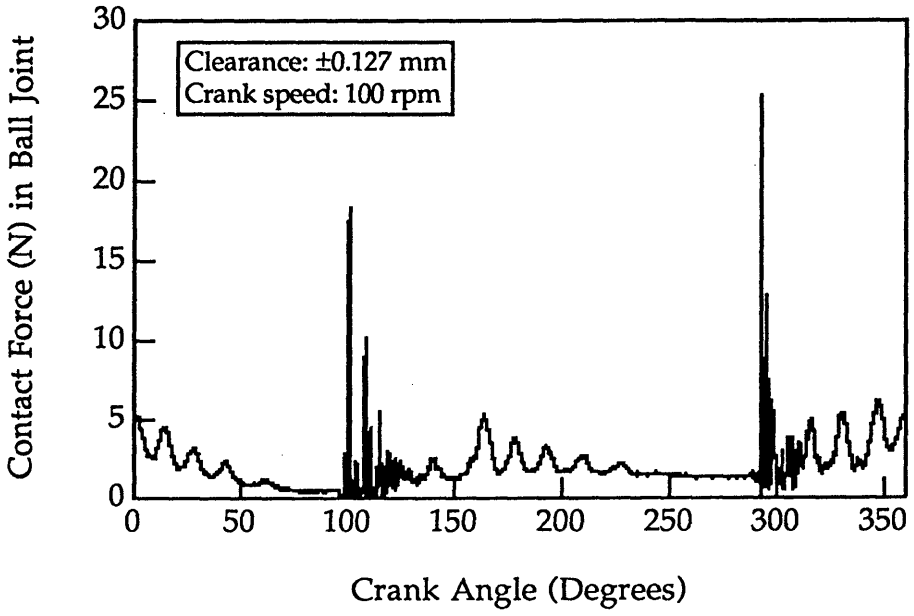

Figure 4.20 (b) Resultant force in instrumented ball joint.

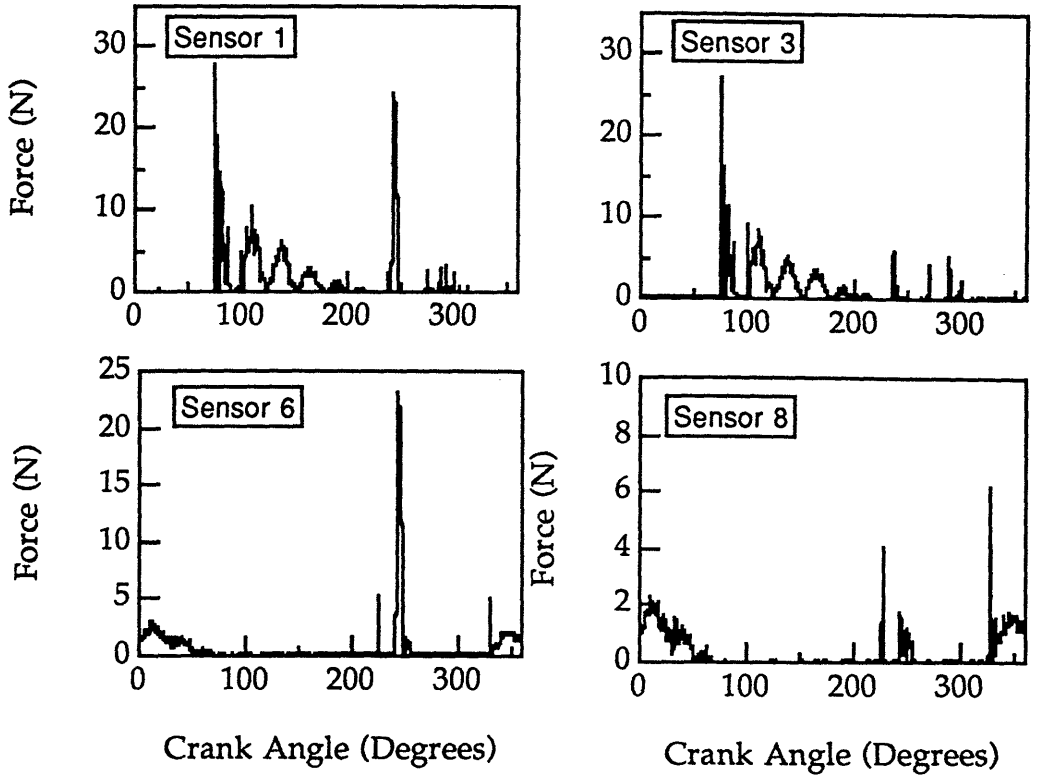

Figure 4.21 (a) Measured contact forces of four sensors in instrumented slider joint. ±0.032 mm clearance and 230 rpm crank speed.

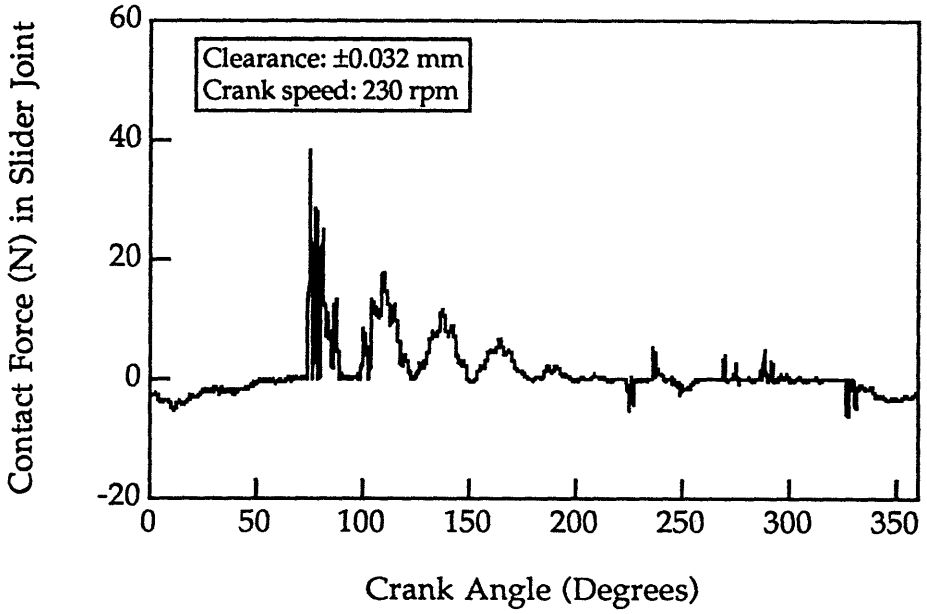

Figure 4.21 (b) Resultant force in instrumented slider joint.

Contact Force in the Slider Joint

Figure 4.21 (a) shows the measured outputs of the four vertical contact force sensors in the slider joint as functions of the crank angle for 230 rpm crank speed and ±0.032 mm clearance. The position of each sensor in the joint is shown in Figure 4.4 (b). This figure shows that impacts occur at each of the vertical sensors. The outputs of the four sensors are summed according to the orientation of each sensor to obtain the resultant contact force in the joint. Figure 4.21 (b) shows the resultant force in the joint as a function of the crank angle. The resultant force in this figure reveals impacts due to contact loss.

Characteristics of Measured Responses: Periodic and Chaotic

The nature of the response can be characterized based on the time history and phase plane portrait of the slider vibration, and the variation of the peak impact force in response to the periodic operation. The dynamic responses of the SSC are found to be chaotic for certain crank speeds and clearances, and to be periodic in other cases.

Figure 4.22 shows the measured peak impact force as a function of the crank speed for ±0.032 mm slider joint clearance and near zero ball joint clearance. This figure is constructed for 20 cycles of machine operation at each crank speed. For each cycle of machine operation, the peak value of the resultant contact force is calculated from outputs of four force sensors and depicted in the figure as a point.

In principle, a periodic response has zero variation in 20 cycles of machine operation and should produce a single point at a given crank speed on this figure. The non-repeatability of the force sensors and other uncertainties in the measurement produce a small variation in the measured

values for a periodic response. On the other hand, a chaotic response produces highly irregular peak impacts from one operating cycle to another, leading to a large variation in the peak impact force, shown by distributed points in the figure at a given crank speed.

The non-repeatable error of the force sensors was found to be approximately ±3 N. This value is used as the maximum amount of the variation of the peak impact force in a response classified as periodic. As shown in Figure 4.22, the responses are periodic at crank speeds of 100, 110, 120, 180, 200, 240 rpm and chaotic at other speeds. The response in the studied crank speed range(100 - 250 rpm) is Type III since whether it will be periodic or chaotic is unpredictable. The response at 130 rpm was seen to be a likely period three subharmonic response during the experiments since the pattern of the contact force repeats every three revolutions.

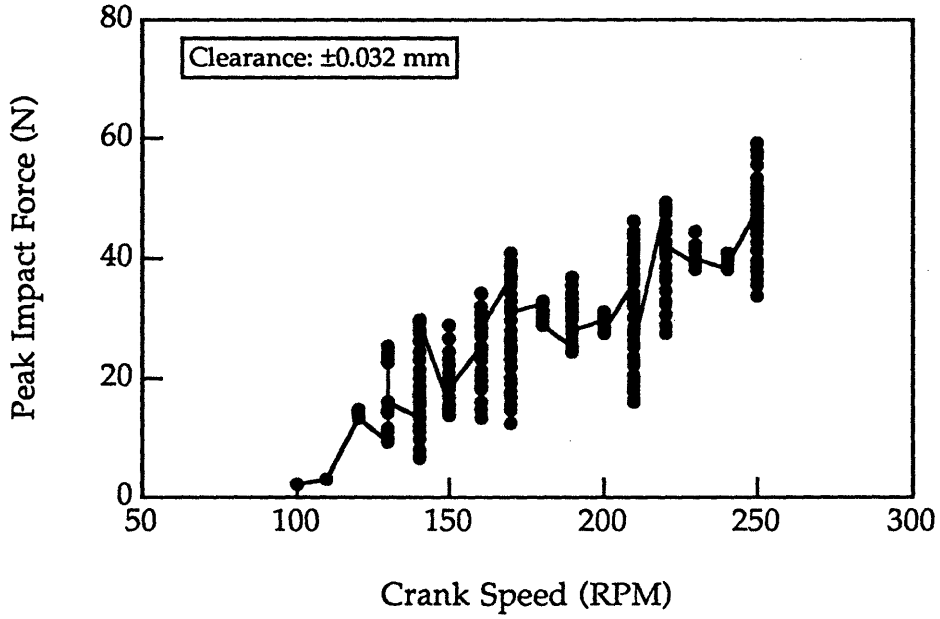

Figure 4.22 Measured peak impact force in instrumented slider joint as a function of crank speed.

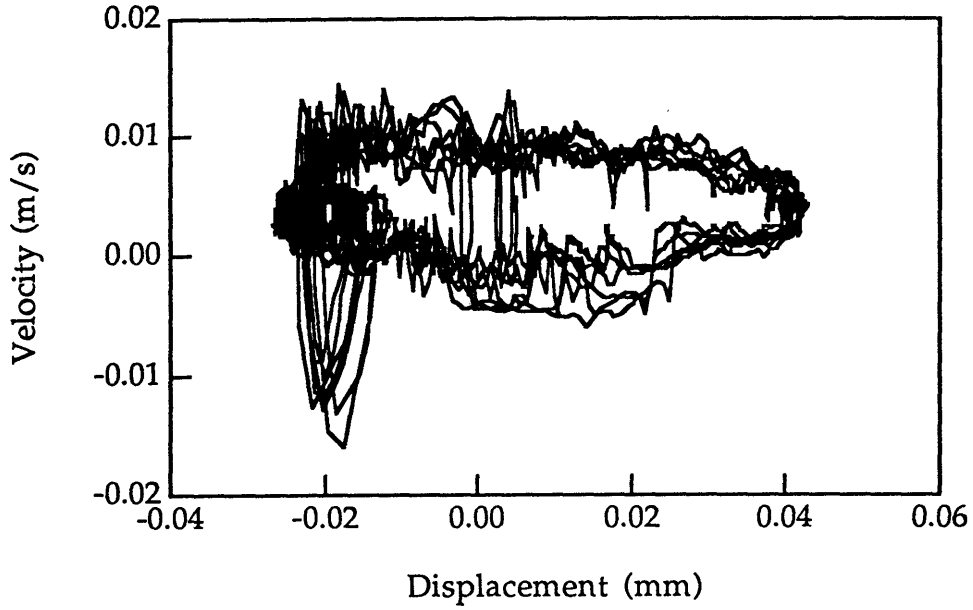

Figure 4.23 (a) An experimental result. Phase plane portrait of slider vibration. ±0.032 mm clearance and 210 rpm crank speed.

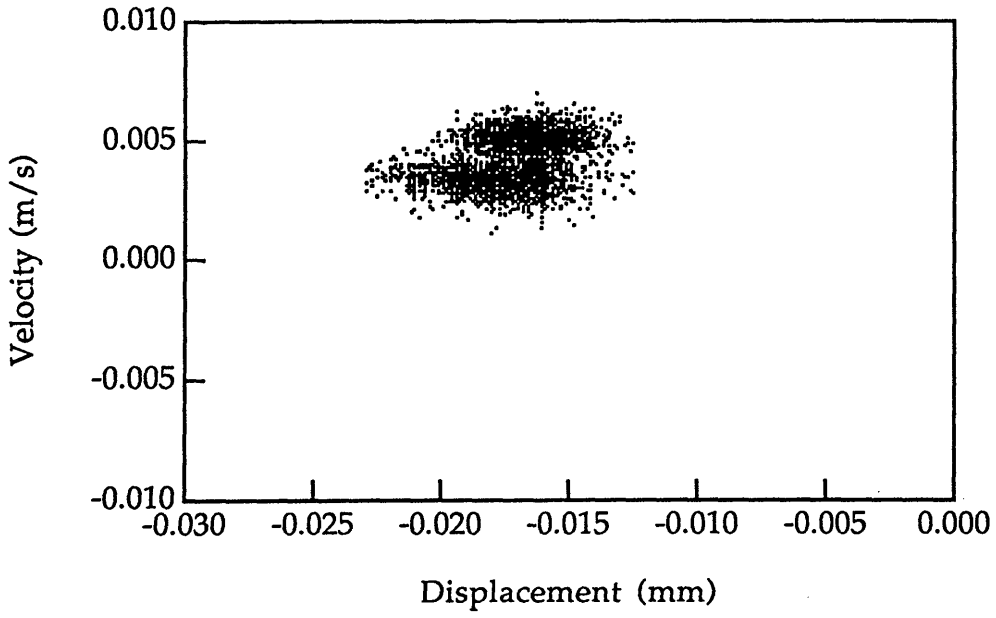

Figure 4.23 (b) An experimental result. Poincaré map of slider vibration. ±0.032 mm clearance and 210 rpm crank speed.

The phase plane portrait and Poincaré map of the slider vibration are used to confirm the chaotic behavior shown in Figure 4.22. The slider vibration perpendicular to the axis of the slider guide rod is measured by an accelerometer attached to the slider. As an example, at 210 rpm crank speed, the measured phase plane portrait and Poincaré map are shown in Figures 4.23 (a) and (b), respectively. These figures show the characteristics of chaotic responses. The phase trajectory of the slider vibration does not close for each revolution, and the Poincaré map shows a fuzzy collection of points with no visible pattern.

In the experiments, the variation of the peak impact force was found to be slightly reduced when the accelerometer was attached to the slider. This is because the accelerometer's cable adds constraint to the slider. However, the phase plane portrait still shows the irregular vibration of the slider.

The Effect of the Length Variation of the Connecting Rod

To investigate the sensitivity of the dynamic response to the length variation of the connecting rod, experiments are performed for two different connecting rod lengths of 0.235 m and 0.240 m (about 2% variation). The diameter of the connecting rod is 3.18 mm. Figures 4.24 (a) and (b) show the peak impact force as a function of the crank speed for connecting rod lengths of 0.235 m and 0.240 m, respectively. These two figures are constructed in the same way as Figure 4.23. The responses in the measured region are Type III. It is seen that the responses change from chaotic to periodic or vice versa when there is even a small variation in the length of the connecting rod. For instance, as the rod length increases by 5 mm, the response changes from chaotic to periodic at crank speeds of 210 and 220 rpm, and from periodic to chaotic at 180 rpm.

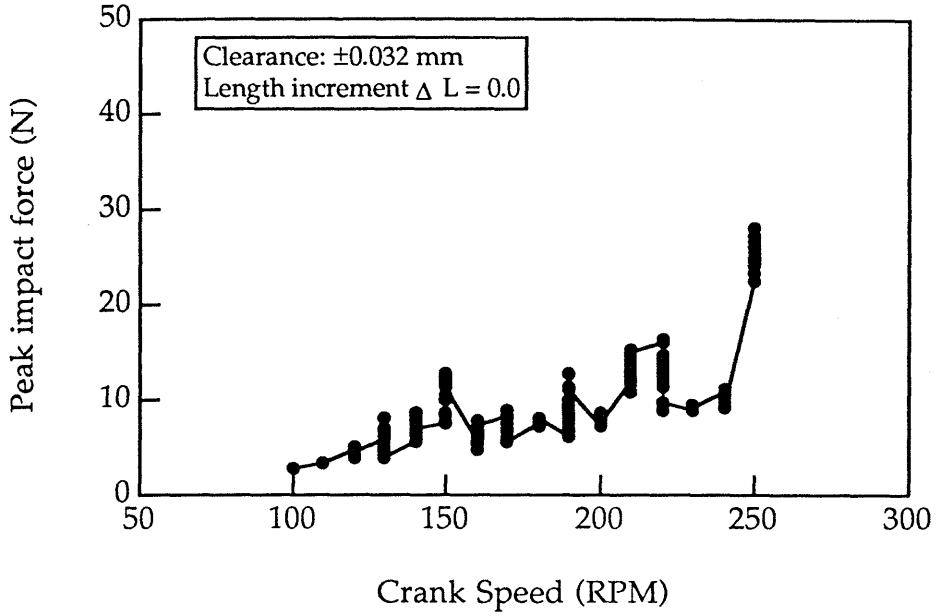

Figure 4.24 (a) Experimental results. Peak impact force in instrumented slider joint as a function of crank speed. Original rod length. 3.18 mm diameter connecting rod.

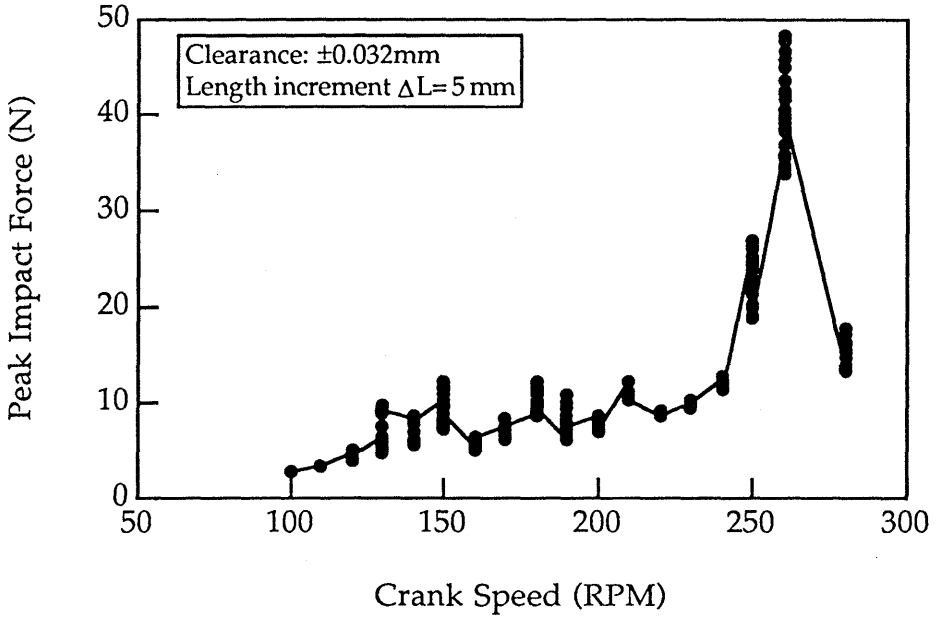

Figure 4.24 (b) Experimental results. Peak impact force in instrumented slider joint as a function of crank speed. Length increment of the connecting rod is 5 mm. 3.18 mm diameter connecting rod.

The sensitivity of the dynamic behavior of the SSC to the dimensional variation of the connecting rod is experimentally demonstrated.

The Effect of the Flexibility of the Connecting Rod

In Figure 4.24 (b), there is a tremendous increase of peak impact force around 260 rpm. This is due to superharmonic resonance. From the fluctuation interval (the ripples) of the measured contact force, it is found that the first natural frequency of the system is about 18 Hz, which corresponds to 1080 rpm. Therefore, the resonant response at 260 rpm is a 4th-order superharmonic resonant response or near a 4th-order superharmonic resonant response. In the experiment, the connecting rod broke when the mechanism operated at 260 rpm.

The experimental results presented in this section confirm experimentally, *for the first time,* the existence of chaotic vibrations in a realistic mechanism with nonlinear kinematic motions, in this case, a spatial slider crank.

4.7 Comparison of Experimental and Numerical Results

This section compares results from the numerical model with experimental measurements. The instrumented clearance ball joint model and instrumented clearance slider joint model are used in the numerical model. The predictions and measurements are found to be in close agreement for some sets of parameters, and qualitatively consistent for the whole parameter space.

Figures 4.25 (a) and (b) present a comparison between experimental and numerical results of the contact force in the ball joint, for a 3.175 mm

diameter connecting rod, 200 rpm crank speed, and ± 0.127 mm clearance. The figures show a close agreement between the numerical results and experimental data in two aspects: the contact forces have similar patterns, and the contact forces agree in order of magnitudes. This consistency can also be seen by comparing Figure 4.19 with Figure 4.9 for the ball joint and Figure 4.20 with Figure 4.10 for the slider joint with the connecting rod of 6.35 mm in diameter.

Detailed profiles of the contact forces show small discrepancies between the numerical and experimental results. The frequencies of the fluctuations of the contact forces occurring after each impact are different. As shown in the above figures, the frequency of the fluctuation of the predicted contact force is higher than that of the fluctuation of the measured contact force. Since the fluctuation of the contact force represent the impulse vibration of a system, the frequency of the fluctuation is the first natural frequency of the system. The high frequency fluctuation shown in the numerical results indicates that the numerical model is stiffer than the real system. One reason for this is the approximation in modeling the moment of inertia of the slider yoke. The moment of inertia of the slider yoke affects the first natural frequency of the system. Since the slider yoke consists of many components, the calculation of the moment of inertia may not be accurate. An underestimation of the moment of the inertia in the model can result in a high first natural frequency of the system.

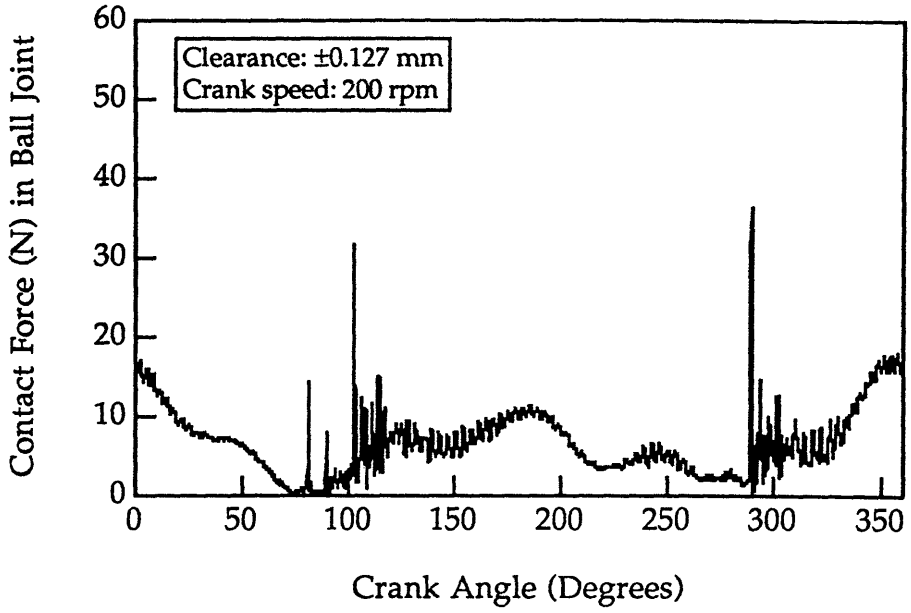

(a) Experimental result.

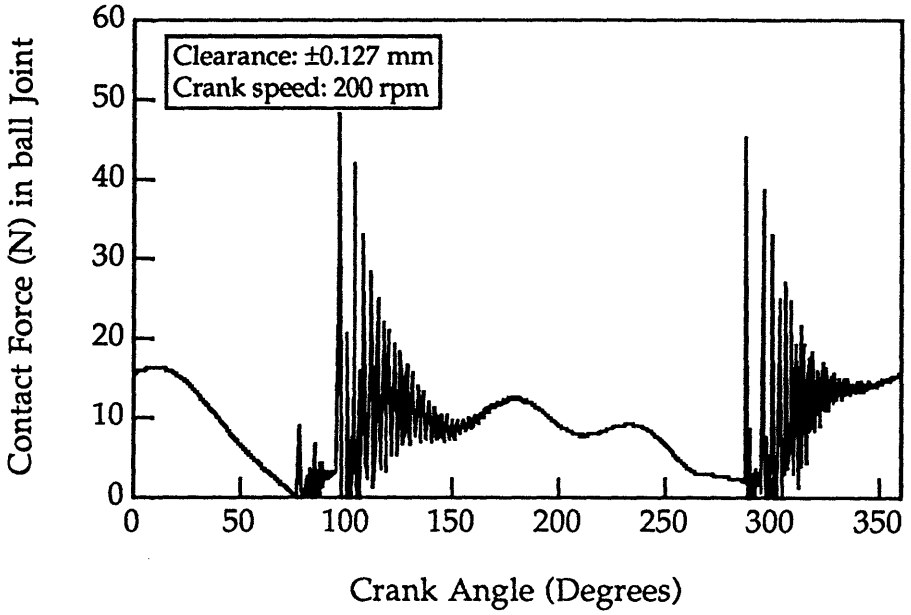

(b) Numerical result.

Figure 4.25 Comparison between experimental and numerical results. 3.18 mm diameter connecting rod. Instrumented clearance ball joint model.

The close agreement between numerical and experimental results shown above was found only for some sets of parameters. For the whole parameter space in this study, the numerical predictions are found to be qualitatively consistent with the experimental measurements. This can be seen by comparing Figure 4.22 and Figure 4.13 over a range of the crank speeds from 100 to 300 rpm for the slider joint with ±0.032 mm clearance. The results show that simulation and experimental results are qualitatively consistent in three aspects: (1) responses are sensitive to the crank speed; (2) chaotic responses are prevalent over this crank speed range; and (3) the responses are Type III, i.e. irregularly periodic or chaotic. Although there is no one-to-one corresponding relationship, the qualitative similarity of the numerical results and experimental data indicate that the numerical model captures much of the qualitative dynamic behavior of the SSC.

4.8 Summary

Numerical simulations and experimental measurements of the SSC have yielded the following important results, which are quite similar to those of the IBS:

- Chaotic vibration exists in the SSC.
- Chaotic responses are associated with large clearances, high crank speeds, and low values of the contact damping.
- Dynamic responses of the SSC can be classified into three characteristic types:

Type I Response is periodic, not sensitive to initial conditions or small variations of system parameters, such as clearance size, crank speed, component dimension, joint friction, and contact damping.

Type II Response is also periodic, not sensitive to initial conditions, but it is sensitive to small variations of system parameters.

Type III Response is unpredictable, either periodic or chaotic, sensitive to both initial conditions and small variations of system parameters.

Chapter 5
Design Methodology for Machine Systems with Chaotic Vibration

5.1 Introduction

The sensitivity of the dynamic behavior of a machine system to small variations of system parameters makes it difficult to use computer-based predictions of its dynamic behavior for reliable design analysis at the design stage. Yet, neglecting the effect of the sensitivity at the design stage could result in premature failure of the system, because the dynamic behavior of the system could be quite different from its model predictions due to small, inadequate variations of the parameters. In order to provide reliable design analysis, this chapter details a design methodology that effectively uses the predictions of machine models at the design stage.

As discussed in Chapters 3 and 4, the sensitivity is due to both the existence of chaotic behavior and the existence of clearance connections and component flexibility in machine systems. Therefore, Section 5.2 describes two methods called the Two-Step Test method and the Matrix Update Test method for testing chaotic vibration in machine models. Empirical predictive criteria are discussed in Section 5.3 for the values of design parameters that cause chaotic vibrations. In section 5.4, design guidelines are presented for the evaluations of the fatigue life and the reliability of a machine. For design purposes, an approach that classifies the responses into Type I, Type II or Type III is described in Section 5.5. Finally, a design methodology is proposed in Section 5.6.

5.2 Methods for Testing Chaotic Vibration

Based on the characteristics of the dynamic behavior of machines with clearance connections and component flexibility, the Two-Step Test Method (TST) and the Matrix Update Test method (MUT) for detecting chaotic vibrations in machine models are described in this section.

5.2.1 Two-Step Test Method

The Two-Step Test analyzes the nature of dynamic responses of a machine's model using three conventional tools: (a) Time history, (b) Poincaré map, and (c) Frequency spectrum. The first two are graphic methods that provide qualitative evidence for chaotic behavior. With current graphic software, these two methods can be easily applied to the results of machine system simulations. The frequency spectrum can give a quantitative measure of chaotic responses. Detailed descriptions of these tools have been given in Chapter 2.

The Two-Step Test has two steps. Step I determines whether the system response is periodic or non-periodic. Step II determines whether a non-periodic response is chaotic or quasiperiodic.

Step I

To test whether the response is periodic or non-periodic, the machine model needs to be simulated for many cycles of machine operations at a given set of system parameters. The time histories of the response parameters from the output of the numerical simulation, e.g. the peak impact force, are then plotted and observed. If the output of a particular parameter converges to one value or varies among a few values, the response is periodic or periodic

subharmonics. If the output exhibits irregular variations or non-repeatability, the response is non-periodic. In this case, the second test is applied.

Step II

Non-periodicity of the time history of a response is a necessary condition for chaotic response, but the Poincaré map and frequency spectrum must be generated to distinguish between a quasiperiodic response and a true chaotic response of the system. If the Poincaré map has the pattern of a closed orbit, the response is quasiperiodic, consisting of two incommensurate frequencies. If the Poincaré map shows a fractal structure, the response is chaotic. The appearance of the fractal structure in the Poincaré map is a strong indicator of the chaotic response.

A frequency spectrum needs to be generated for the following two cases. One case is a quasiperiodic response which consists of three or more dominant incommensurate frequencies, the other case is a chaotic response of a multiple DOF (>3) system. For multiple DOF (> 3) systems, the fractal nature of the Poincaré map might not be evident, since the Poincaré map is a projection of a multiple DOF phase space on a particular plane. For these two cases, the Poincaré map always appears as a fuzzy collection of points, and hence the frequency spectrum must be calculated to determine whether the response is quasiperiodic or chaotic. The frequency spectrum has a few well-pronounced peaks for a quasiperiodic response, but has a broad spectrum of frequency components for a chaotic response.

5.2.2 Matrix Update Test Method

The Matrix Update Test method is an effective means to test whether chaotic vibration exists in a machine model by examining characteristics of chaotic systems. This method directly tests whether the response is sensitive

to initial conditions, a necessary and sufficient condition for chaotic responses. A variation in initial conditions can be introduced by varying the time interval of matrix updates in the numerical simulation. In this section, a description of the Matrix Update Test method is given first, followed by a demonstration of its application.

The global dynamic equations of the machine system are given by Eq. (2.4) and repeated here:

$$\overline{\mathrm{M}}(\underline{\theta},\underline{\dot{\theta}},\underline{\ddot{\theta}})\underline{\ddot{q}}+\overline{G}(\underline{\theta},\underline{\dot{\theta}},\underline{\ddot{\theta}})\underline{\dot{q}}+\overline{K}(\underline{\theta},\underline{\dot{\theta}},\underline{\ddot{\theta}})\underline{q}=\underline{Q}\,, \tag{5.1}$$

where $\overline{M}$, $\overline{G}$ and $\overline{K}$ are the mass, damping and stiffness matrices of the system, respectively. Their elements are functions of the position vector $\underline{\theta}$, the velocity vector $\underline{\dot{\theta}}$ and the acceleration vector $\underline{\ddot{\theta}}$ of the components' nominal motion, as well as the physical properties of the components such as mass and stiffness.

Repeated calculations of these time varying matrices in numerical simulation can be computationally expensive for large systems. To improve simulation efficiency, Eq. (5.1) is implemented using piecewise constant values of the $\overline{M}$, $\overline{G}$, and $\overline{K}$ in the simulation. The $\overline{M}$, $\overline{G}$, and $\overline{K}$ matrices are updated at a time interval ΔT, which can be much larger than the integration time step, Δt. The update interval ΔT is chosen such that the change in physical configuration of the system is small between matrix updates. However, each matrix update results in a small step change of system parameters, and the dynamic equilibrium state of the system is disturbed. This disturbance amounts to a variation of initial conditions and therefore tests for the nature of the system's response.

To implement the method, the system dynamic equations are simulated twice, with different matrix update time intervals. The second

time interval differs only slightly from the first. If the outcomes of these two simulations agree at each observation, the response is periodic; if the outcomes of these two simulations are different at each observation, the response is chaotic.

To demonstrate the Matrix Update Test method, the SSC is used as an example. Two cases are selected here: case one is from Figure 4.14 (a) with 270 rpm crank speed, and case two is from Figure 4.14 (b), with 190 rpm crank speed. In both cases, the matrix update time interval is described by the crank rotation angle instead of time.

Case One: Figure 5.1 shows the peak impact force of each operation cycle as a function of crank rotation cycles for matrix-update intervals of 5° and 10° of crank angle. The response is periodic, and the two results converge after the initial transient response which lasts about 6 cycles. The initial transient response will be discussed in Section 5.2.3.

Case Two: Figure 5.2 shows the peak impact force of each operation cycle as a function of crank rotation cycles for matrix update intervals of 5° and 6° of crank angle. The two outcomes diverge from each other as simulation continues. For example, at the 62nd crank rotation cycle, the peak impact forces are 85 N for the 5°-update simulation and 105 N for the 6°-update simulation.

The outcomes of two chaotic responses with different update intervals (different initial conditions) are different at each observation. According to theory of chaotic dynamics, their statistical parameters should remain the same because the trajectories in both cases are traveling on the same strange attractor. This is illustrated in Figure 5.3 which shows the means and standard deviations (STD) of the peak impact forces as functions of different

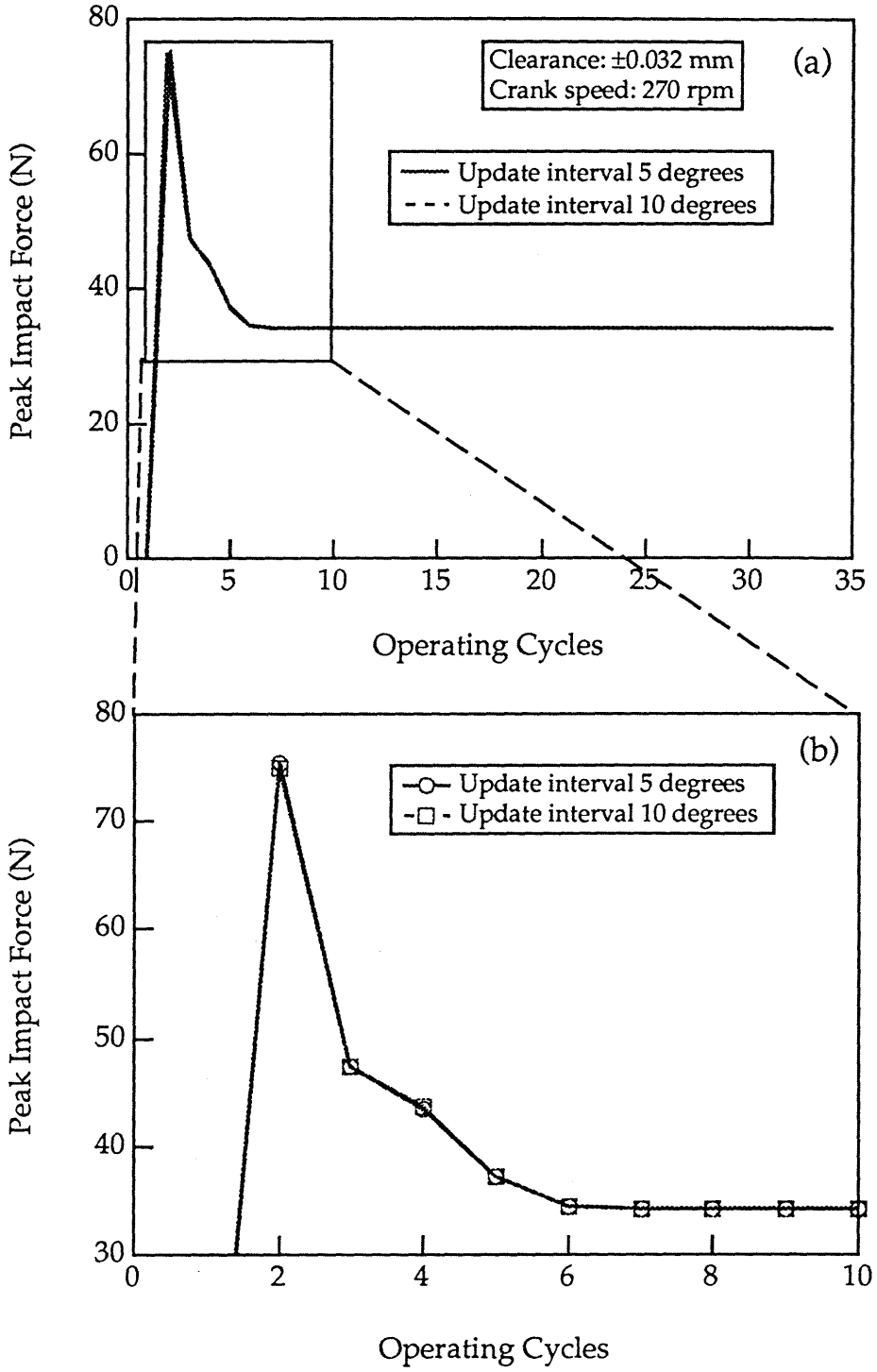

Figure 5.1 Simulation Results of the SSC. Peak Impact Force in the slider joint as a function of operating cycle. (a) 35 Cycles. (b) Enlargement of figure in (a) within 10 cycles.

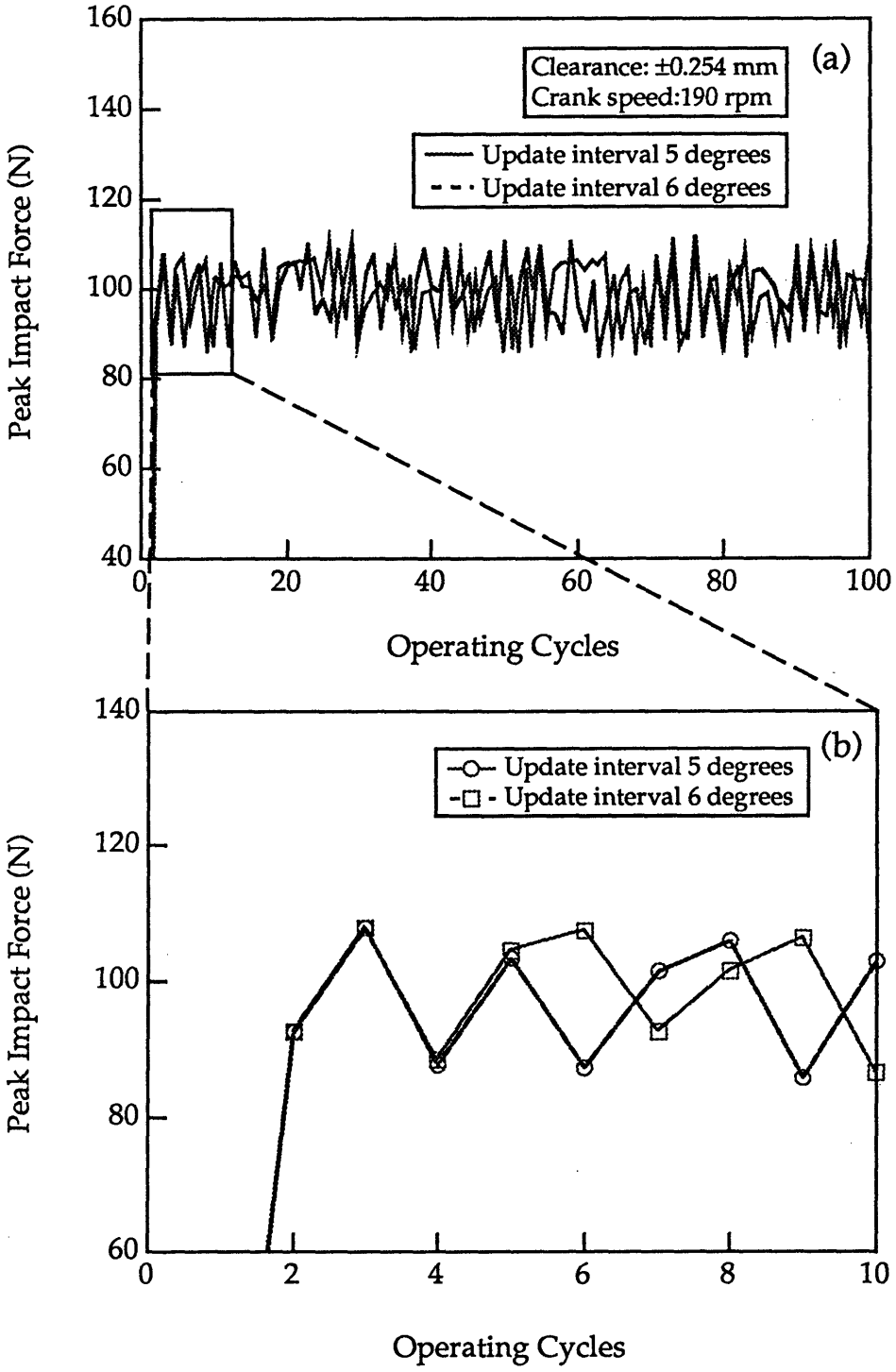

Figure 5.2 Simulation Results of the SSC. Peak impact force in the slider joint as a function of operating cycle. (a) 100 Cycles. (b) Enlargement of figure in (a) within 10 cycles.

update intervals. Variations of the statistical parameters for different update intervals are very small.

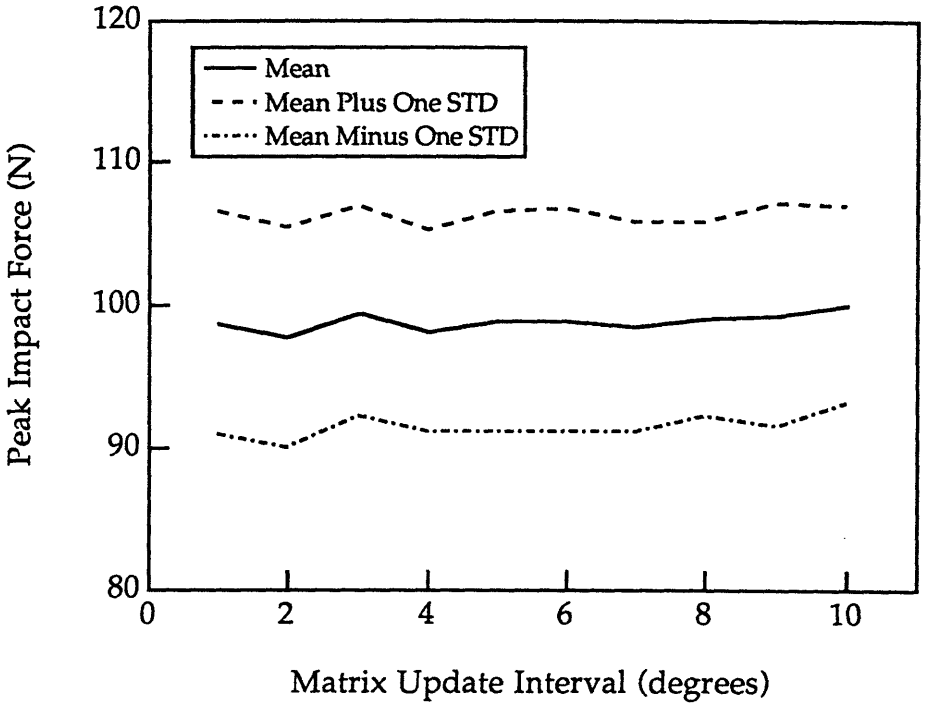

Figure 5.3 Simulation Results of the SSC. The mean and one standard deviation of the chaotic response as functions of matrix update interval. . ±0.254 mm clearance and 190 rpm crank speed.

5.2.3 Discussion

In applying the Two-Step Test and the Matrix Update Test method to the design analyses, designers should be aware of the initial transient responses of the machine model. Usually, a designer arbitrarily selects initial conditions for a simulation. This leads to an initial transient response, which could last a few operating cycles or a few hundred operating cycles. The initial transient response always exhibits non-periodicity, which may result in an incorrect conclusion that the response is non-periodic. In the numerical analyses, the simulation should run long enough to guarantee that the

response reaches the steady state (either periodic or chaotic). However, the computer time must be manageable. These are competing constraints, although more powerful computers are steadily relaxing the latter. The simulation periods specific to the IBS and SSC are discussed here.

For the numerical models of the IBS and SSC, the transient decay time was found to be inversely proportional to the number of DOF in the machine model. More DOF resulted in quick decay of the transient response. For an IBS model with 5 DOF, the response converged to its steady state after about 50 excitation cycles. When simplified to a single DOF model, up to 150 cycles were required before the response became steady. For a 9 DOF model of the SSC, the response reached its steady state after 10 operating cycles. These observations suggest that the response of a machine model with more than 5 DOF is non-periodic if the response continuously shows non-periodic patterns after 50 cycles.

Transient chaos is another phenomenon to be noted. Transient chaos is a chaotic response which appears when some parameters are changed, but eventually settles into a periodic or quasiperiodic motion after a certain period [16,36,61]. Transient chaos lasts much longer, well beyond what would be typically considered as an initial transient response just mentioned. Transient chaos was observed in the simulations. As an example, Figure 5.4 (a) shows a transient chaotic response for the IBS with ±0.127 mm clearance, excited by a force of 8.9 N at 30 Hz. In the figure, the peak impact force is plotted as a function of the excitation cycle. The transient chaotic response lasts about 350 cycles before it settles into a period-four subharmonic response eventually. For the same system, when the structural damping ratio slightly decreases by 0.001 (from 0.011 to 0.01), the simulated response is chaotic up to 4000 cycles, as shown in Figure 5.4 (b). Transient chaos is sensitive to small

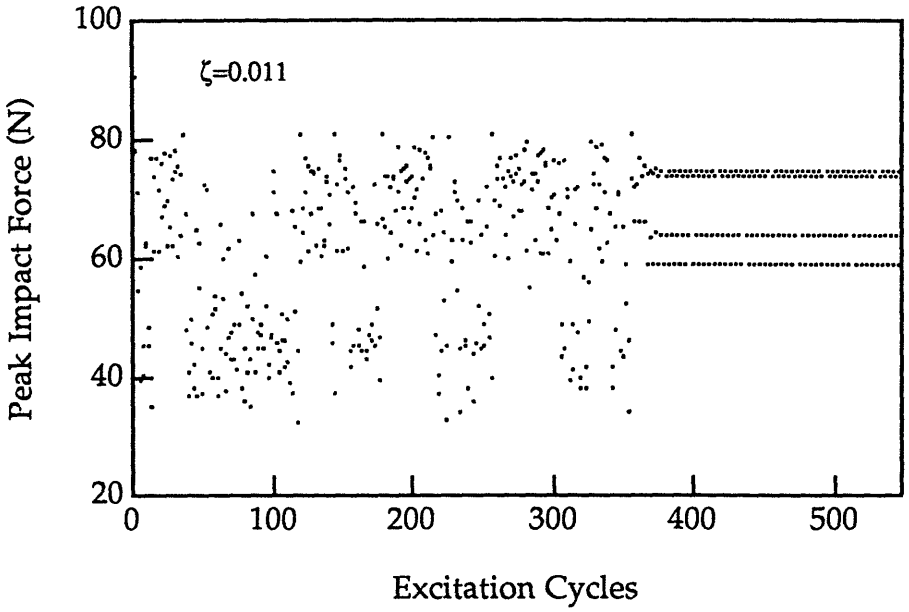

Figure 5.4 (a) A simulation result of the IBS. A transient chaotic response. ±0.127 mm clearance, 30 Hz excitation frequency, and structural damping ratio ζ=0.011.

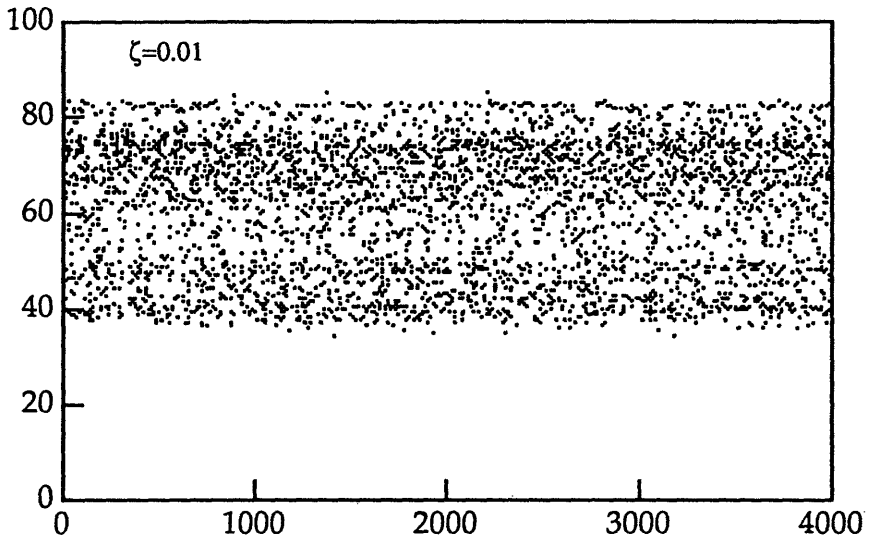

Figure 5.4 (b) A simulation result of the IBS. A chaotic response. ±0.127 mm clearance, 30 Hz excitation frequency, and structural damping ratio ζ=0.01.

parameter variations and is usually a precursor to steady state chaos [16,36,61]. The Two-Step Test method and the Matrix Update Test method classify transient chaos as a chaotic response.

It should be pointed out that the Matrix Update Test method is limited to systems whose $\overline{M}$, $\overline{G}$ and $\overline{K}$ matrices are functions of system configurations. For systems such as the IBS whose matrices are constant, the Two-Step Test is more suitable. The application of these two methods for determining the dynamic nature of a machine system is shown by a flow chart in Figure 5.5.

5.3 Predictive Criteria for Chaotic Vibration

From a design point of view, it would be useful to have criteria that could predict whether chaotic behavior would result from a given set of system parameters and operating conditions. In this section predictive criteria for the values of the clearance size, operating speed, and damping that cause chaotic vibrations are discussed based on studies of the IBS and the SSC. A discussion of a precursor of chaotic vibrations in the machine model is also provided.

5.3.1 Predictive Criteria

To classify the specific parameter regions for the IBS and SSC (i.e., to obtain predictive criteria for chaotic response), some important results presented in Chapters 3 and 4 are reviewed here. From these studies, chaotic response in the IBS and the SSC has been found to be associated with large clearances, high operating speeds, and low values of damping.

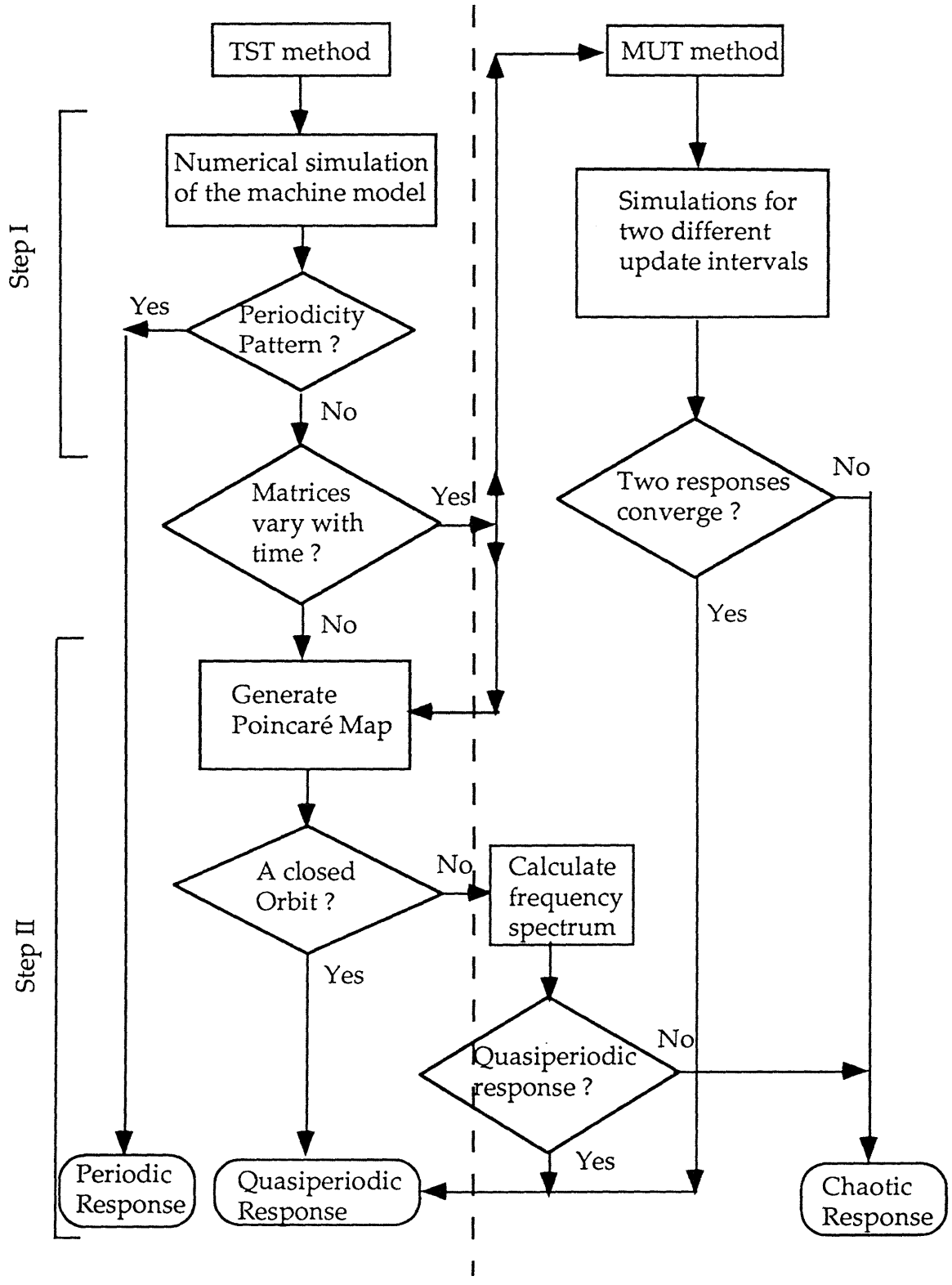

Figure 5.5 Flow chart of testing chaotic vibrations for computer-based simulations of machine models.

For the IBS, Figure 3.18 indicates that chaotic vibrations occur when the dimensionless clearance is larger than ±0.02 (i.e., ±0.064 mm clearance) and the excitation frequency is higher than 16 Hz. The structural damping ratio of the beam used for these results is 1%. When the structural damping ratio of the beam increases, the minimum clearance value causing chaotic vibration shifts upwards. As shown in Figure 3.13, chaotic vibrations do not occur even at a larger dimensionless clearance of ±0.04 (i.e., ±0.127 mm clearance), as the damping ratio increases from 1% to 8%.

For the SSC, Figure 4.15 shows that chaotic vibrations occur when the dimensionless clearance is larger than ±0.004 (i.e., ±0.064 mm clearance) and the crank speed is higher than 100 rpm. The contact damping ratio used for these results is 5%. When the contact damping ratio decreases, the minimum clearance value causing chaotic vibration shifts downwards. For example, as discussed in Section 4.5.4, chaotic vibrations occur even at a smaller dimensionless clearance of ±0.002 (i.e., ±0.032 mm clearance), as the damping ratio decreases from 5% to 2.5%.

Damping plays an important role in determining the nature of dynamic responses. If larger damping is introduced, it is possible to suppress chaotic vibrations in all of the studied parameter regions.

These observations provide the predictive criteria for the regions in a parameter space where chaotic vibrations are possible for the IBS and the SSC. However, the search for predictive criteria that indicate under what set of parameters and operating conditions a machine will exhibit chaotic tends to be *ad hoc*. Therefore, the strategy for designers is to find predictive criteria for specific machine models with basic features in more general or complex machines, and then use these models as paradigms to infer when the more general or complex machine systems exhibit chaotic vibrations.

5.3.2 Precursors of Chaotic Behavior

In addition to the above predictive criteria for the IBS and the SSC, observations from simulations indicate three precursors of chaotic vibrations.

The period-doubling scenario, one of the routes to chaos described in Section 2.3.2, is one precursor: period-doubling bifurcation in the simulations of the IBS and SSC. Another precursor is the occurrence of a subharmonic motion of order 3 [33,69]. The numerical simulations of the IBS and the SSC showed that subharmonic responses of order 3 are followed and/or preceded by chaotic responses.

Besides the above precursors observed previously, another precursor was directly observed in the course of this study. This precursor can be seen from the pattern of the time history of the impact force. Consider the IBS as an example. During each half-cycle of operation, an impact event begins with an initial, large impact force as the beam hits one of the two sensors. The impact is followed by a period of bouncing in and out of contact. The bouncing period can be as short as a small fraction of the half-cycle or last for the rest of the half-cycle. In the former case, the bouncing period is followed by a continuous contact. If the bouncing period does not end before the end of the half-cycle, the chance of having chaotic vibration is greater. This is because the long bouncing period provides many sequential impacts. These impacts are sensitive to small disturbances that exist in a system, such as high frequency residual vibrations [3] and noise in experiments or numerical round-off errors in simulations [64]. During the bouncing period, the motion of the beam is influenced by these small disturbances. At the moment when the beam hits another sensor, the velocity of the beam could vary from cycle to cycle, if the system is sensitive to the disturbances. Hence, the long bouncing period is a necessary condition for chaotic vibrations.

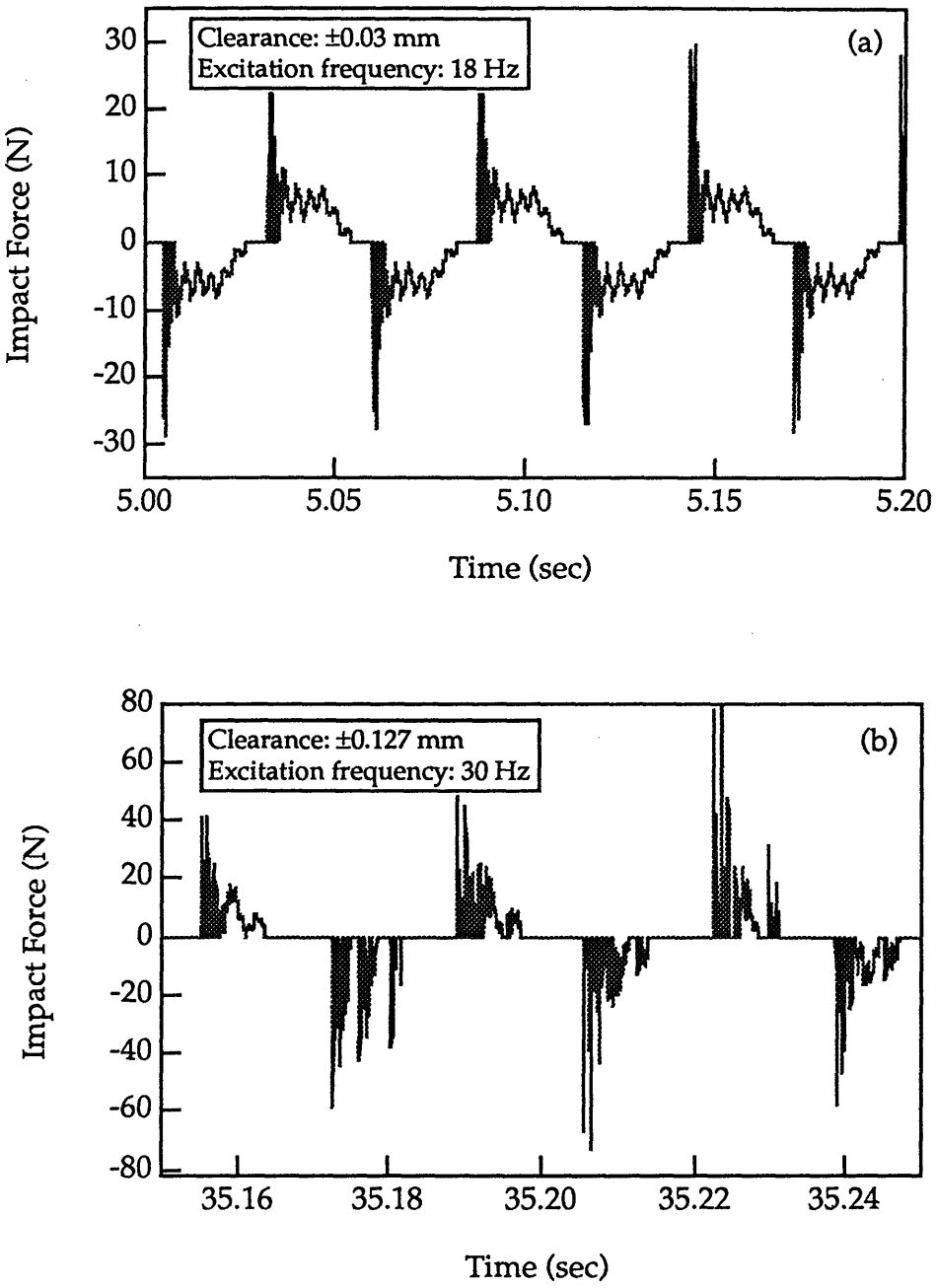

Figure 5.6 A simulation result of the IBS. Time history of impact force. (a) ±0.03 mm clearance and 18 Hz excitation frequency. (b) ±0.127 mm clearance and 30 Hz excitation frequency.

This idea is consistent with the following facts: 1) the bouncing of the impact lasts long for small damping, but has little time to be damped out for high excitation frequency, and 2) small damping or high excitation frequency corresponds to a large possibility of chaotic vibrations.

To illustrate this idea, Figure 5.6 shows two time histories of impact forces for periodic and chaotic responses, respectively. For the periodic response as shown in Figure 5.6 (a), the bouncing period lasts only one seventh of each half excitation cycle. For the chaotic response as shown in Figure 5.6 (b), the bouncing periods for some of the cycles last until the end of the half-cycle.

5.4 Design for Machines with Chaotic Response

One fundamental characteristic of a machine's chaotic vibrations is that the values of response parameters, such as the impact force, change irregularly from one operating cycle to another. This characteristic creates a difficult problem for designers: a single value of each response parameter, preferred for classical design, is not available in the case of chaotic response. Using the statistical properties of these parameters becomes an essential approach for design. In this section, the statistical characteristics of the peak impact force of chaotic responses in the IBS and SSC are studied first, then guidelines for estimations of fatigue life and reliability are developed by combining the statistical characteristics of the peak impact force with the probabilistic design method.

5.4.1 Characteristics of Impact Force

Impact Force and its Variation

Results presented in Chapters 3 and 4 indicate that a chaotic response induces larger peak impact forces as well as a large variation range of the forces in comparison with a periodic response. This conclusion may be explained as follows. According to the theory of chaotic dynamics, a chaotic attractor in the phase space of a response is an ensemble of unstable periodic orbits, i.e., a chaotic attractor occurs when all possible periodic orbits become unstable [16,61]. The large variation range of the force is a result of the trajectory moving from one unstable periodic orbit to another. The large impact force induced by the chaotic response is due to the transient motions of the trajectory as it moves from one unstable periodic orbit to another. The transient motions can make the trajectory reach some of the unstable periodic orbits associated with large impact forces.

Histogram of Peak Impact Force

As discussed in the following, the peak impact force for the chaotic response of a machine is bounded. Individual impact forces vary irregularly, but the ensemble characteristics over many impacts is a multi-peak statistical distribution that is time invariant.

There are two methods often used to obtain the statistical properties of chaotic responses. One is a time average method, carrying out a large number of simulations in order to provide a sufficiently large number of observations to calculate the statistical properties. The assumption of ergodicity for a chaotic response is used in this method [31]. The other method is called the state space averaging method using the Cell-to-Cell Mapping technique developed by Hsu [23].

In this study, the time averaging method is chosen to calculate the statistical properties of the peak impact force. During a simulation or experiment, the peak impact force of each operation cycle is recorded. The data for many cycles are collected to generate the distribution of the peak impact force. To show the basic features of the peak impact force distribution, the histograms of peak impact forces for different systems, with different parameters and operating conditions, are plotted. Figures 5.7 (a), (b), and (c) show such histograms from the simulations of the IBS with the ±0.127 mm clearance and an excitation force of 8.9 N at frequencies of 22 Hz, 25 Hz, and 30 Hz, respectively. Figures 5.8 (a), (b), and (c) show the experimental histograms of peak impact forces in the slider joint of the SSC with 250 rpm crank speed and clearances of ±0.032 mm, ±0.064 mm, and ±0.127 mm, respectively. Figure 5.9 shows the numerical histogram of peak impact forces in the slider joint of the SSC at a crank speed of 190 rpm and ±0.254 mm clearance.

These histograms suggest two features specific to impact forces for chaotic vibrations.

First, the impact force is bounded because of the bounded motion of the beam. With regard to the chaotic response of dissipative systems after transients have decayed, the response is always "attracted" to a strange attractor which occupies a finite bounded space.

Second, the peak impact force distribution is mainly characterized by a multiple-peak distribution function. That is, for most cases the distributions of the peak impact force have more than one peak. Typical random processes obey a Gaussian Distribution which has only one peak. Since the chaotic attractor is an ensemble of unstable periodic orbits [16,61], a multi-peak distribution appears when the trajectory moves among these unstable periodic orbits in a random fashion but visits some more than others.

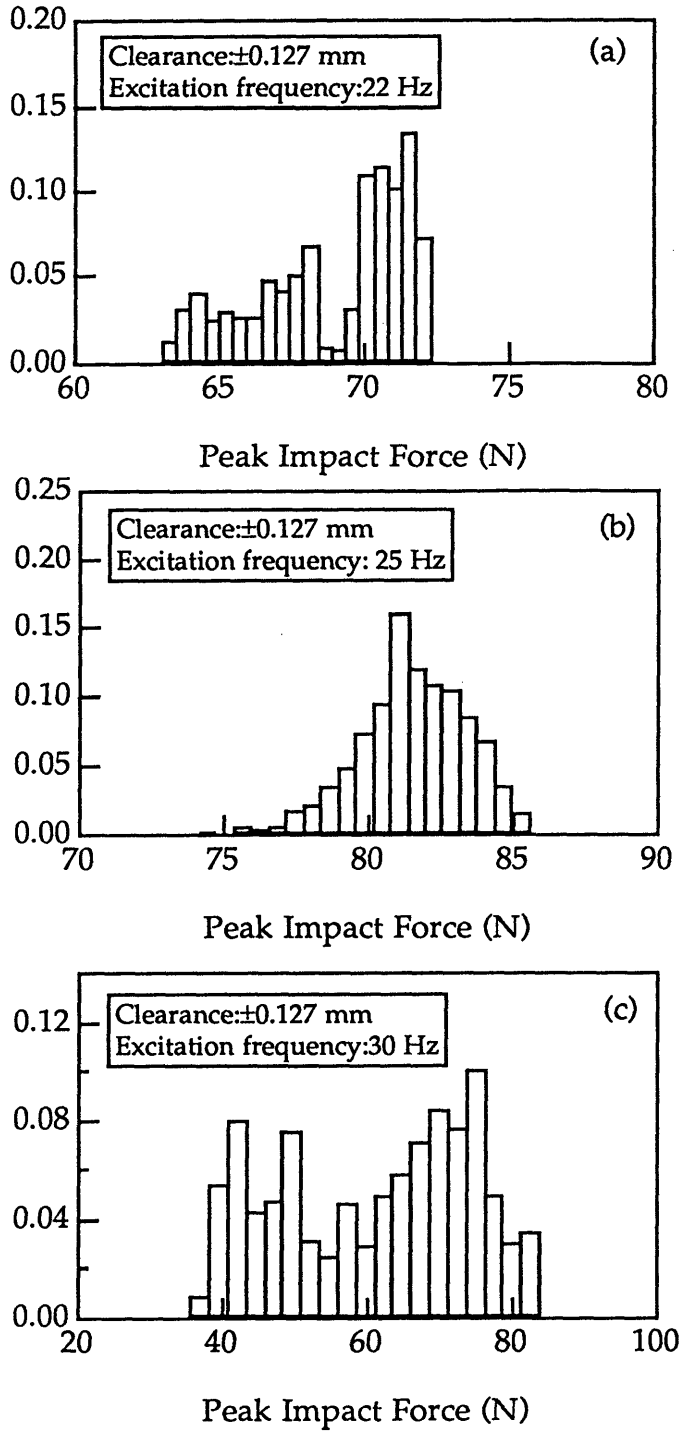

Figure 5.7 Simulation results of the IBS. Histograms of the peak impact force.

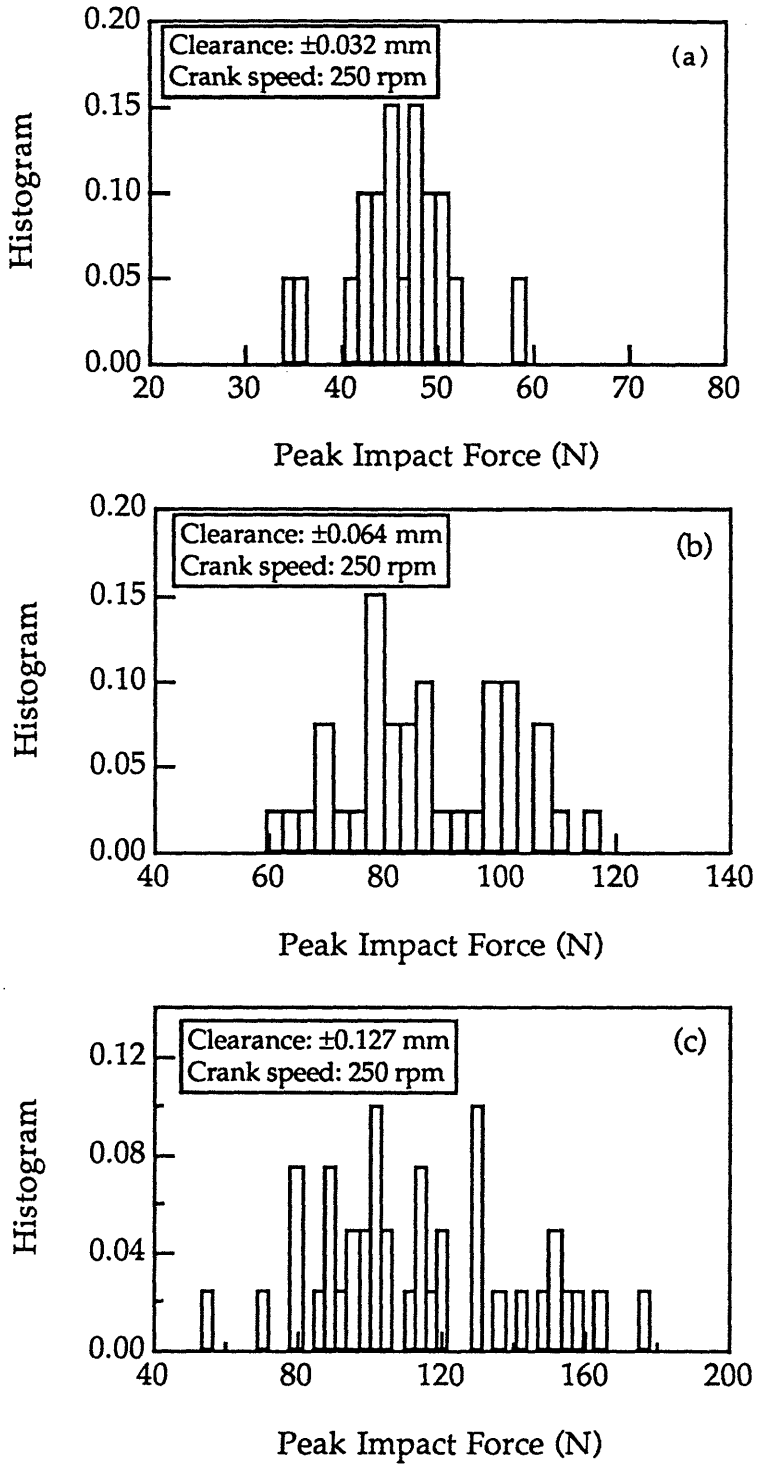

Figure 5.8 Experiment results of the SSC. Histograms of peak impact forces in instrumented slider joint.

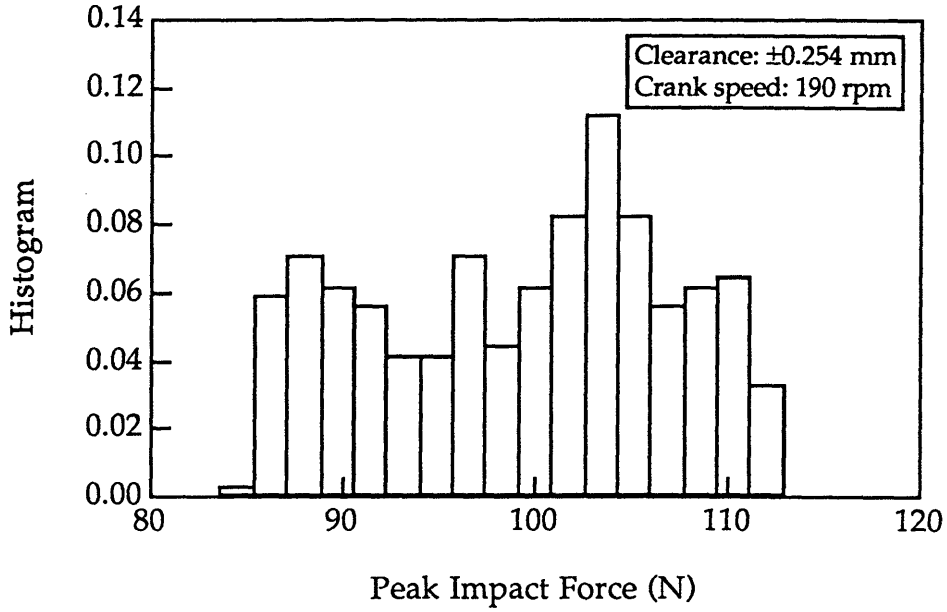

Figure 5.9 A simulation result of the SSC. Histogram of peak impact forces in slider joint. Instrumented clearance slider joint model.

Peak Impact Diagram

The Peak Impact Diagram is a figure which shows the magnitude and the location of the peak impact force on the bearing surface for each operating cycle. While one point corresponds to a periodic response, many points spread on the diagram correspond to a chaotic response. Unlike the case of a periodic response, in which the impact is localized on one spot of the bearing surface, the impacts in a chaotic response act on different locations of the bearing surface for different operating cycles. Because of these distributed impacts on the bearing surface, the fatigue life of the bearing surface might be improved.

Figures 5.10 and 5.11 show the Peak Impact Diagrams of the SSC for the ball joint and slider joint, respectively. Figures 5.10 (a) and (b) are plotted for 120 rpm crank speed with ±0.064 mm clearance and for 110 rpm crank speed

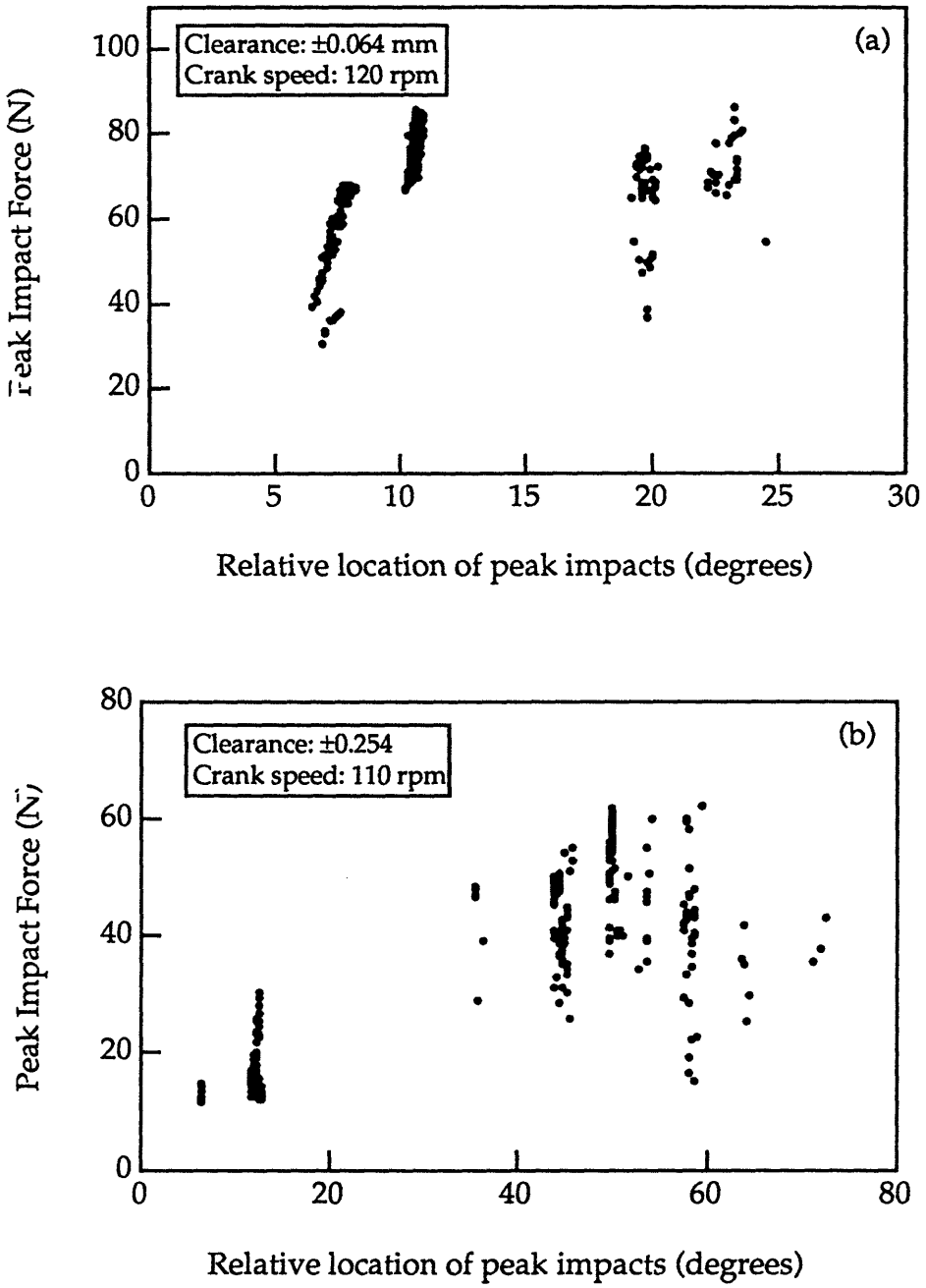

Figure 5.10 Simulation results of the SSC. Peak Impact Diagrams of peak impact forces in ball joint. Spherical clearance model.

with ±0.245 mm clearance, respectively. In these figures, the location of each peak impact on the bearing surface is represented by a relative polar angle. For ±0.064 mm clearance, the peak impacts are spread on only one sixth of the half bearing surface, while for ±0.245 mm clearance the peak impacts are spread over almost half of the bearing surface . In Figure 5.11, the Peak Impact Diagram is plotted for 190 rpm crank speed with ±0.127 mm clearance. The location of each peak impact on the bearing surface is represented by the relative distance along the slider guide rod. The peak impacts distribute over a region of about 6 mm in length, which is about 6% of the bearing length.

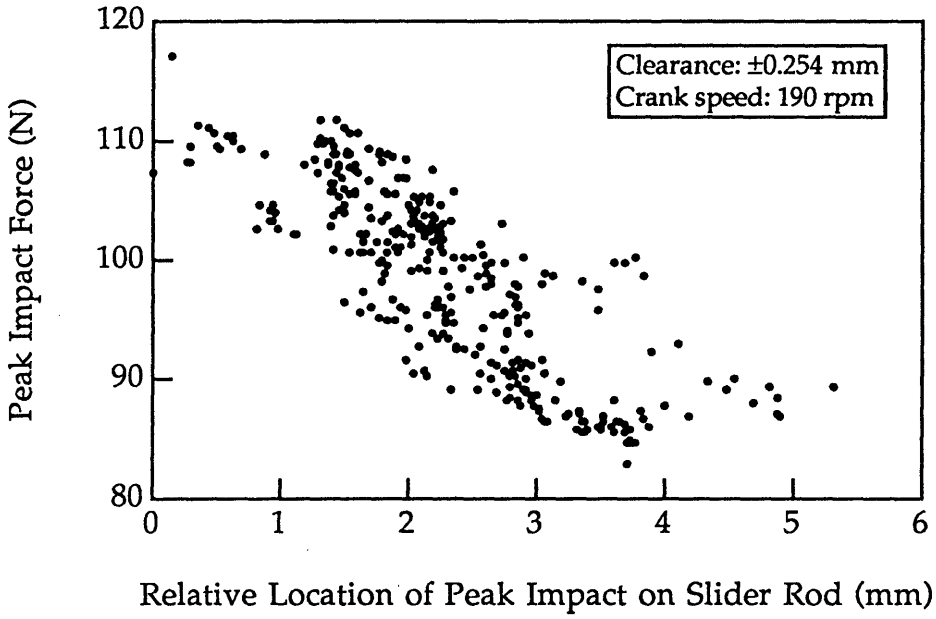

Figure 5.11 A simulation result of the SSC. Peak Impact Diagram of peak impact forces in slider joint. Instrumented clearance slider joint model.

A large clearance gives a large distributed region of impacts. The distributed impacts may moderately improve the fatigue life of the bearing. However, the large clearance results in large impact forces which strongly

reduce the fatigue life. Therefore, there is a trade off between minimizing the peak impact force and maximizing the distributed region of impacts in choosing an optimal clearance size for potential chaotic vibrations.

5.4.2 Estimations of Fatigue Life and Reliability

In this section, guidelines for designs by integrating the statistical properties of the chaotic vibration into the probabilistic design method are proposed. Two examples, i.e. fatigue life estimation and reliability evaluation, are descried here.

Fatigue Life Estimation

Take a simple rolling contact bearing as an example. The general formula for the fatigue life of the rolling contact is given by[19]

$$L = \left(\frac{C}{F}\right)^{P}, \tag{5.2}$$

where p=10/3. L is the life in millions of revolutions, C is the basic dynamic load rating of the bearing, and F is the bearing load acting under the conditions applicable to the basic dynamic load rating.

When a designer selects a bearing which meets the requirements of a particular design, he is usually interested in finding the value of C so that he can enter the table in a bearing catalog and pick up a bearing for a desired fatigue life. For convenience, we rewrite Eq. (5.2) as

$$C = F(L)^{\frac{1}{P}} \tag{5.3}$$

In the current design approach, Eqs. (5.2) and (5.3) are used to predict the bearing life or to find a suitable bearing based on the dynamic simulation of a machine model. If the machine model exhibits periodic responses in the designed operation conditions, the bearing life can be estimated based on the

prediction of impact force magnitudes given in Eq. (5.2). Similarly, the required dynamic load rating C for a desired fatigue life can be calculated using Eq. (5.3).

However, this approach needs to be modified if the model exhibits chaotic responses. For a chaotic response, there is a large variation of peak impact forces from one operating cycle to another. Since the simulated peak impact forces are different for different simulation cycles, the estimated values for the fatigue life are different, i.e. the information for design is ambiguous. Moreover, since the fatigue life is inversely proportional to the power of the force magnitude, even a small difference in peak impact forces can result in a large difference in the fatigue life.

For example, the relative fatigue life calculated based on the experimental data of Figure 4.16 is shown in Figure 5.12. The fatigue life for different crank speeds is normalized by the fatigue life at 100 rpm crank speed. The fatigue life is assumed to be inversely proportional to the third power of the peak impact force. This figure reveals two points. First, when the response is chaotic, a few cycles of measurement are not enough to get a complete picture of fatigue life. The arbitrary selection of the measured peak force could result in a few orders of difference in the estimation of the fatigue life, e.g., the relative fatigue life varies from 10^{-3} to 10^{-1} at 140 rpm crank speed. Secondly, if the crank speed has a small variation the fatigue life could change dramatically, e.g., the relative fatigue life varies from about 10^{-3} at 200 rpm to a range of 10^{-2}-10^{-4} at 210 rpm crank speed.

Hence, in the case of chaotic responses, sufficient simulation is necessary in order to obtain a complete picture of the impact force and therefore reliable design parameters. Here two approaches are suggested for estimating fatigue life and dynamic load rating. The first is a conservative

design approach which applies the maximum value of the varying peak impact force from numerical simulation into Eqs. (5.2) and (5.3).

The second approach is to combine the statistical distribution of the peak impact force with the Palmgren-Miner cycle-ratio summation theory, which is widely used at the present time to explain cumulative fatigue damage [56]. The magnitudes of the peak impact forces in a chaotic response are assumed to consist of n levels. The life estimation for chaotic response is given by

$$\frac{1}{L} = \sum_{i=1}^{n} \frac{p_i}{L_i}, \tag{5.4}$$

where p_i is the occurrence probability of the i^{th} impact force with a magnitude of F_i, and $L_i = \left(\frac{C}{F_i}\right)^p$ is the fatigue life corresponding to the i^{th} impact force F_i. Substituting $L_i = \left(\frac{C}{F_i}\right)^p$ into Eq. (5.4) and rearranging the terms, we obtain the equation for dynamic load rating:

$$C = \left[L\left(\sum_{i}^{n} p_i F_i^p\right) \right]^{\frac{1}{p}}. \tag{5.5}$$

The estimations of the fatigue life using Eq. (5.5) for the data presented in Figure 5.12 are also shown in the same figure with a solid line. Use of the cumulative damage theory with the distribution of the peak impact forces gives a reasonable estimation of the fatigue life. This approach is consistent with the idea of probabilistic design which will be addressed shortly.

In comparison with the second approach which uses statistical estimation, the first approach is too conservative to be economical. To justify the validity of the statistical estimation for the fatigue life, one has to check whether the impact induced stress meets the specified Hertzian endurance

strength of the materials. Hence, the reliability of the component should be estimated.

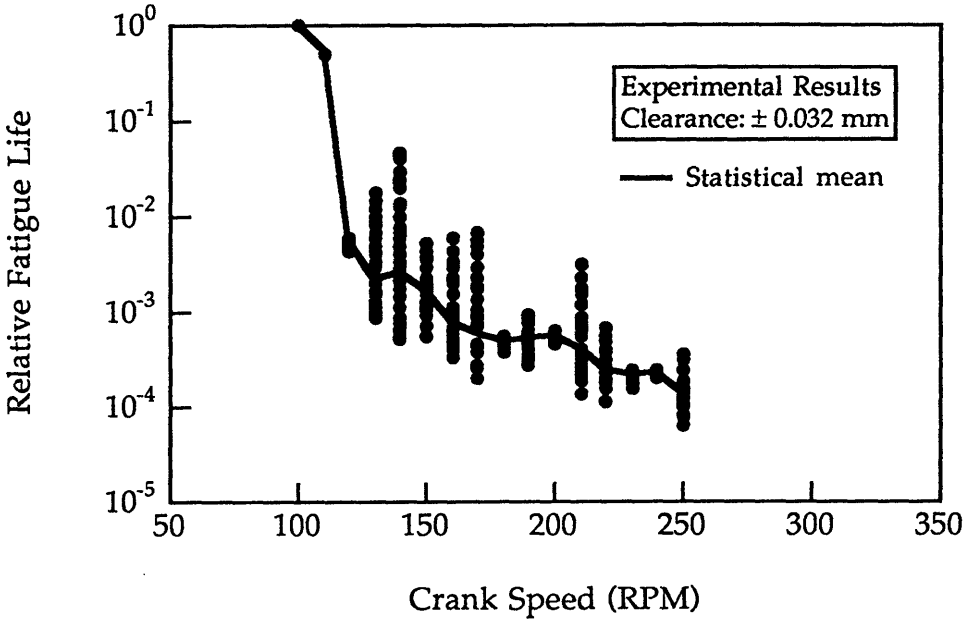

Figure 5.12 Experimental results of the SSC. Estimated relative fatigue life of slider joint as a function of crank speed. The solid line represents the statistical mean life calculated based on Eq. (5.4).

Component Reliability Estimation

In the classic design for a component, the accepted criterion is set such that the impact induced stress is always less than the specified Hertzian endurance strength of the materials. For an adequate strength-limited design, the criterion is stated as:

$$S_e = (SF) \cdot K_f \cdot s, \tag{5.6}$$

where S_e denotes the component Hertzian endurance limit, K_f is the fatigue factor, SF denotes the safety factor and s denotes applied stress. If the prediction of applied stress based on the dynamic simulation of the machine model meets the condition (5.6), then the design of the component is

finished. Otherwise the design of the component needs to be modified until the criterion is satisfied.

When uncertainties of loading, geometry and material properties encountered in engineering design exist, the single-value condition in Eq. (5.6) is no long available. To deal with this situation, the probabilistic design method was developed [20]. In this method, the allowed stress (S) and applied stress(s) are modeled by distribution function with some statistical parameters. The accepted design criterion for this situation is that the probability which the strength of the material exceeds the applied stress equals or exceeds a stated probability. This probability is called reliability of the component.

When the machine model exhibits a chaotic response, a further complexity is introduced due to the large variation of the impact force and the behavior which is sensitive to the parameter variations. Considering the similarity of the force variations in chaotic responses and the load uncertainty in real environments(?), we propose to use the modified probabilistic method. Instead of using the loading distribution caused by random events, the distributions of impact forces of the chaotic responses are used in the estimation of the component reliability.

Suppose a component's endurance limit S_e, is described by a probability density function $f(S_e)$, selected at random from a population of nominally identical components. The component is subjected to a chaotic loading, which induces impact stress s described by probability density function $f(s)$. Then, by definition,

$$\text{Re}liability = R = P(S_e > s). \tag{5.7}$$

where $P(S_e > s)$ indicates the probability of S_e greater than s.

When distributions of S_e and s are known, the reliability of the component is given by [20]:

$$R = \int dR = \int_{-\infty}^{\infty} f(s) \cdot \left[\int_{s}^{\infty} f(S) dS \right] ds, \tag{5.8}$$

where

$$\int_{-\infty}^{\infty} f(S) dS = 1: \quad \int_{-\infty}^{\infty} f(s) ds = 1.$$

As an example, for the Normal distributions of S_e and s, the Reliability, R, is given by [20]:

$$R = \frac{1}{\sqrt{2\pi}} \int_{\frac{\mu_S - \mu_s}{\sqrt{\sigma_S^2 + \sigma_s^2}}}^{\infty} e^{-z^2/2} dz \tag{5.9}$$

where μ_s, μ_S are the means, and σ_s, σ_S are the standard deviations of the normal distributions of stress and strength, respectively. The random variable z is a standard normal variable. Hence for given μ_s, σ_s, μ_S, and σ_S the reliability can be found by referring to the Normal tables. Equation(5.9) can also be utilized to estimate the effects of design parameters such as clearance size, if μ_s and σ_s are functions explicitly or implicitly containing the design parameters when R is specified.

In most cases of chaotic responses, the distributions of the peak impact forces are not the Normal distribution, but the multi-peak distribution as described in Section 5.4.1. To calculate the reliability for such cases, numerical integration for evaluating Eq. (5.8) must be used. For a rough estimation, we may use the normal distribution to approximate the distributions of the peak impact forces. The normal distribution model ignores the details of the real distributions of peak impact forces of chaotic response, but retains the main features of the distributions such as the variation ranges and mean values.

Also note that larger stresses in the components can be induced in the chaotic response than in the periodic responses. The design of machine systems which might exhibit chaotic response should be relatively

conservative in terms of operating conditions. Design reliability should be high to provide a design tolerance for the system.

5.4.3 Calculation of Statistical Parameters

In estimations of fatigue life and component reliability using the above approaches, the length of the simulation period becomes an important issue. It should be not only long enough to obtain the complete statistical properties of chaotic responses, but also short enough to have an efficient computation. To obtain the statistical properties of the impact force, the simulation should run until the chaotic trajectory has visited most regions of the attractor. To verify this (i.e. to determine the minimum number of the simulation cycles), there are two tests. One test is to examine the Peak Impact Diagram, as shown in Figure 5.8. Testing the Peak Impact Diagram involves observing when the Peak Impact Diagram takes shape and when the peak impact forces fill in the different sections of the Diagram. Shown in Figure 5.13 is an example to demonstrate this test for the SSC for 190 rpm crank speed and ±0.127 mm clearance. In the figure, three Peak Impact Diagrams are shown for operating cycles of 40, 60, and 80, respectively. When these three figures are compared with Figure 5.11, it is clearly shown that after 80 cycles the Peak Impact Diagram takes shape. Therefore, at least 80 cycles are needed for calculation of the statistical parameters for this specific case.

To avoid *subjective judgment* in deciding whether the peak impact forces have filled in the different sections of the Diagram, a second test is developed. Running values of the mean and the standard deviation of the ensemble of the peak impact forces are calculated as the simulation runs. The necessary number of simulation cycles is obtained when the calculated mean and standard deviation converge to steady values. This method is more

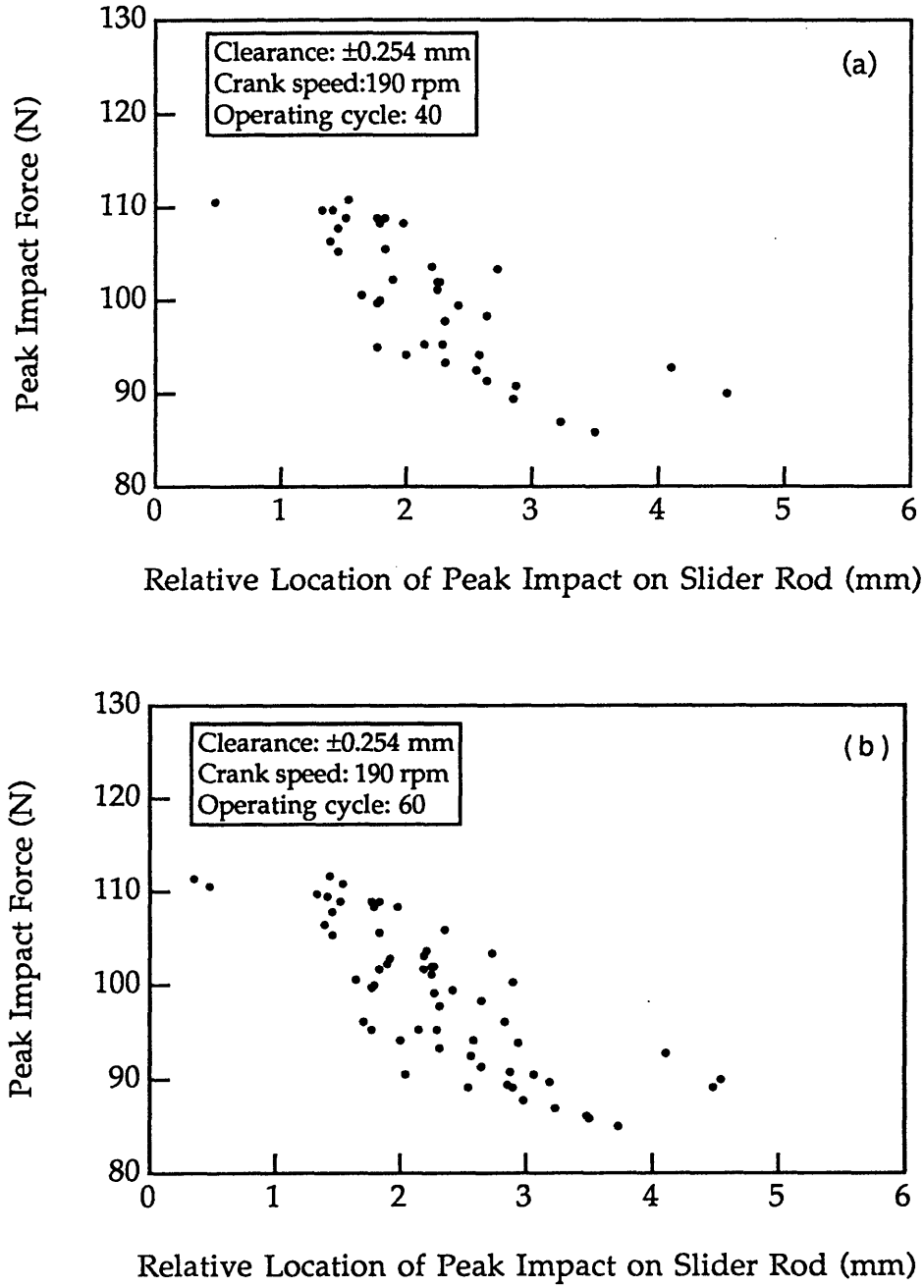

Figure 5.13 A simulation result of the SSC. Peak Impact Diagrams of slider joint. The diagrams are constructed using different lengths of the data. (a) 40 operating cycles. (b) 60 operating cycles. (c) 80 operating cycles.

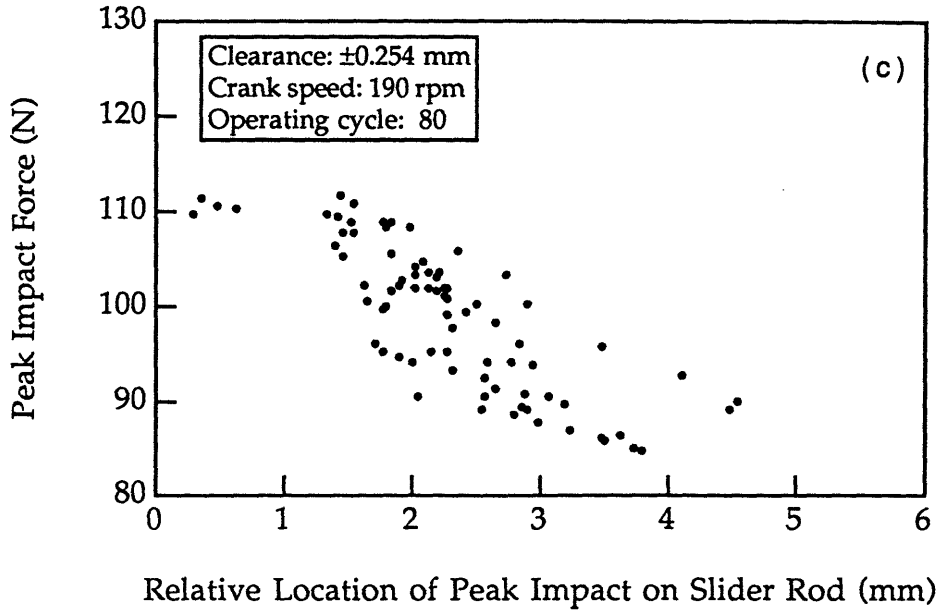

Figure 5.13 (Continued).

convenient and reliable. For the same case shown in Figure 5.13, Figure 5.14 shows the mean and standard deviation of the peak impact forces as functions of the number of operating cycles. The mean and standard deviation of the ensemble converge after 80 cycles, as is expected to be consistent with the first test.

5.5 The Classification of Type I, Type II, and Type III Responses

5.5.1 The Approach

As described in Chapters 3 and 4, classifying responses into Type I, Type II, and Type III is very important at the design stage. Type I Response is periodic and not sensitive to small variations of system parameters or initial conditions. Type II Response is also periodic and not sensitive to initial

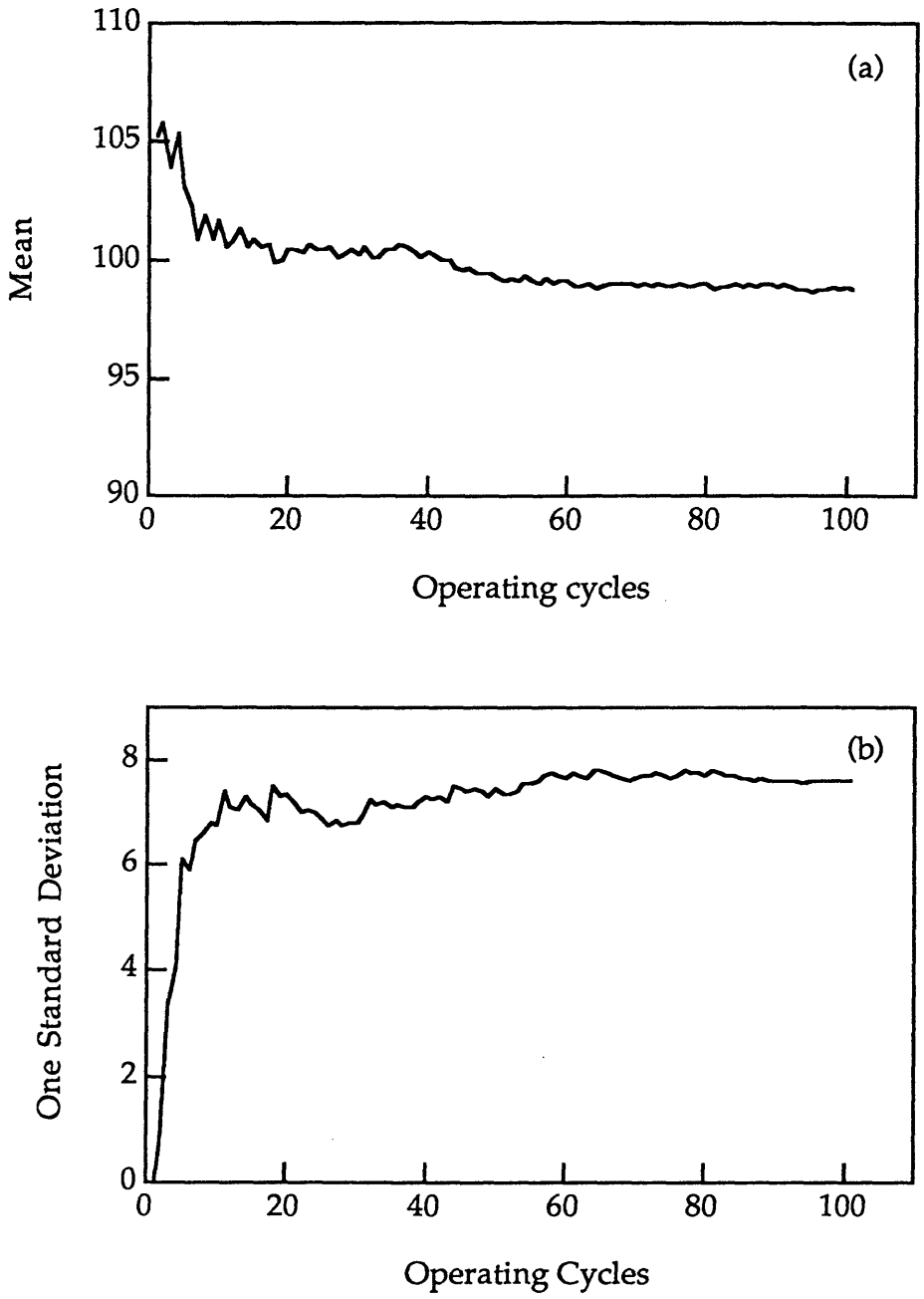

Figure 5.14 A simulation result for the SSC. Statistical parameters of peak impact forces of a chaotic response as functions of the number of simulation cycles. (a) Mean value as a function of the number of cycles, and (b) One standard deviation as a function of the number of cycles. ±0.254 clearance and 190 rpm crank speed.

conditions, but it is sensitive to small variations of system parameters. Type III Response is unpredictable, either periodic or chaotic, and sensitive to small variations of system parameters and initial conditions. If a system response is Type II or Type III Response, the machine behavior might be quite different from the prediction due to variations in parameters caused by manufacturing processes and to uncertainties in parameters chosen for the simulation. Unexpected behavior could substantially reduce the machine's performance. Hence, designers need to identify the regions in parameter space that result in Type I, Type II, and Type III Responses.

In classification, a designer first evaluates each system's response at each point in parameter space (i.e., for each given set of system parameters), over a selected region with densely-spaced trials. Each response can be characterized as periodic, quasiperiodic, or chaotic by using the Two-Step Test method and the Matrix Update Test method. Then, the designer classifies the responses into Type I, Type II, or Type III Responses. The selected region may consist of one, two or three response types. All possible situations are summarized in the following three cases

Case I If all the responses over the selected region are periodic, three possible outcomes must be distinguished. (1) If all responses are well-behaved as the parameters vary within the whole region, the responses are Type I. (2) If all responses change irregularly as the parameters vary within the whole region, the responses are Type II. (3) If in a subset of the region, a group of responses is well-behaved as the parameters vary within the subset, this group of responses is Type I, and the rest of the responses are Type II.

Case II If chaotic responses occur in a subset of the selected region, they are Type III. The rest of the periodic responses are further classified into

Type I, or Type II, or Type I and Type II, following the procedure described in Case I.

Case III If periodic and chaotic responses distribute irregularly in the selected region, the responses are Type III.

5.5.2 Discussion

In applying the above approach to classify the Type I, Type II, and Type III Responses, several issues are discussed here.

The Quasiperiodic Response

If a response is quasiperiodic, it is classified as Type III. Note that the quasiperiodic response is non-periodic, and, of course, does not belong to Type I or Type II. From a design point of view, a quasiperiodic response exhibits a problem which is similar to the problem of a chaotic response. That is, a large amount of simulation is required to obtain the variation range of the response for each input parameter set. In this thesis study, no quasiperiodic response has yet been observed. Therefore, more detailed discussion of the quasiperiodic responses would be beyond the scope of this study.

The Selection of Variation Region of Parameters

The variation region of the parameters used to classify the response types is selected according to the possible variations of the parameters introduced in the manufacturing and assembly processes. The design tolerances of geometrical dimensions and the empirical data ranges of important parameters are the basic references. The selected parameter region can be chosen as one tolerance of the parameter or double of the tolerance if

necessary. For example, if the nominal clearance of a journal bearing of a shaft of X mm in diameter is Y mm and the tolerance of the clearance is Z mm, the selected variation region for the clearance in the analysis is from Y-Z to Y+Z. If consequences of the bearing wear are considered, the clearance size will increases in the service. Thus, the selected variation region may be from Y-2Z to Y+2Z.

The Criterion for Sensitivity to Small Variations of Parameters

The classification of the Type I and Type II Responses is based on the criterion of whether the responses are sensitive to small variations of the parameters. When a parameter changes by a small amount, whether the change of the response is *well-behaved* or significantly *irregular* depends on the relevant engineering significance. Take a bearing system as an example. Suppose that a decrease of the bearing fatigue life within 25% is acceptable. This 25% decrease corresponds to a 10% increase of the impact force in the bearing, assuming that the fatigue life is inversely proportional to the third power of the force magnitude. This 10% increase of the force is used as a criterion for determining the degree of the response sensitivity to parameter variations. If any small parameter variation causes a less than 10% increase of the impact force (e.g., operating speed drifts by 10 rpm), the responses in that parameter variation region are classified as Type I. Otherwise, the responses are classified as Type II. Hence, from the design point of view, less than a 10% increase of the impact force is not significant, and the responses are well-behaved as the parameter varies. On the other hand, more than a 10% increase of the impact force is significant, and the responses change irregularly as the parameter varies.

5.6 The Proposed Design Methodology

Every engineering design is subject to: (1) dimensional variations when the design is manufactured, (2) uncertainties in values chosen for model parameters such as damping coefficients, Young's Modules, etc., and (3) inconsistencies between assumed and actual boundary conditions. Chapters 3 and 4 show the significant effects of parameter variations on the dynamic behavior of machines. These issues have not yet been considered in current design approaches. Here, a systematic methodology is proposed for designing such machines with clearance connections and component flexibility. The flow chart of this methodology is presented in Figure 5.15.

The basic idea of the methodology is to effectively use the predictions of the machine models at the design stage. The methodology consists of seven phases: machine modeling, parameter selection, numerical simulation, test of response nature, classification of dynamic responses, and design analysis. The methods and guidelines presented in the previous four sections are used in the implementation of these phases.

Phase I. The methodology begins with the dynamic modeling of a machine, using the modeling techniques such as one presented in Section 2.1. The machine model is described by the major system parameters, such as the values of the clearances, operating speed, component dimensions, and damping. The dynamic response of the machine model is characterized by response parameters such as the impact force. All these parameters are called design parameters.

Phase II. To analyze the effects of the variations of the system parameters on the dynamic behavior, the variation region for each parameter

is selected according to its possible variation in the manufacturing and assembly processes. The selection procedure is described in Section 5.4.2.

Phase III. The simulation is performed over the selected parameter regions with densely-spaced trials. The designer should run the simulation long enough to let the response reach steady state after the initial transient response decays. The determination of the transient decay time is discussed in Section 5.2.3.

Phase IV. When the machine model is simulated for each combination of parameters in their variation ranges, the nature of each response is tested using the flow chart given in Figure 5.5, which combines the Two-Step Test and the Matrix Update Test. The characteristics of the response are recorded for each specific parameter set. If the response is chaotic, further simulation needs to be done. Following the guidelines given in Section 5.4, the designer first determines the required length of simulation necessary for obtaining a complete statistical picture, then calculates the statistical values of the response parameters, such as the mean and standard derivation.

Phase V. After simulating all the possible combinations of parameters in the selected region, the designer can classify the dynamic responses into Type I, Type II and Type III Responses, following the approach described in Section 5.5. Thus, the major parameter region for each response type is defined.

Phase VI. Once the response types are determined in the parameter space, the machine's performance, such as fatigue life and reliability of the component for given design criteria, can be evaluated using different approaches for different response types.

For Type I Response, the designer can use the predicted trend of the machine behavior to evaluate the machine's performance.

For Type II Response, the designer should use the worst case (e.g. the maximum peak impact force) found in the Type II parameter region to evaluate the machine's performance.

For Type III Response, the designer should use statistical parameters of the response to evaluate the machine's performance using the modified probabilistic design method described in Section 5.4.

Phase VII. If the evaluation results indicate that the designed machine system meets the design criteria, the system is moved into the prototype stage. Otherwise, the system needs to be modified and again analyzed through Phase I to Phase VI. This process is repeated until the designed machine meets the design criteria.

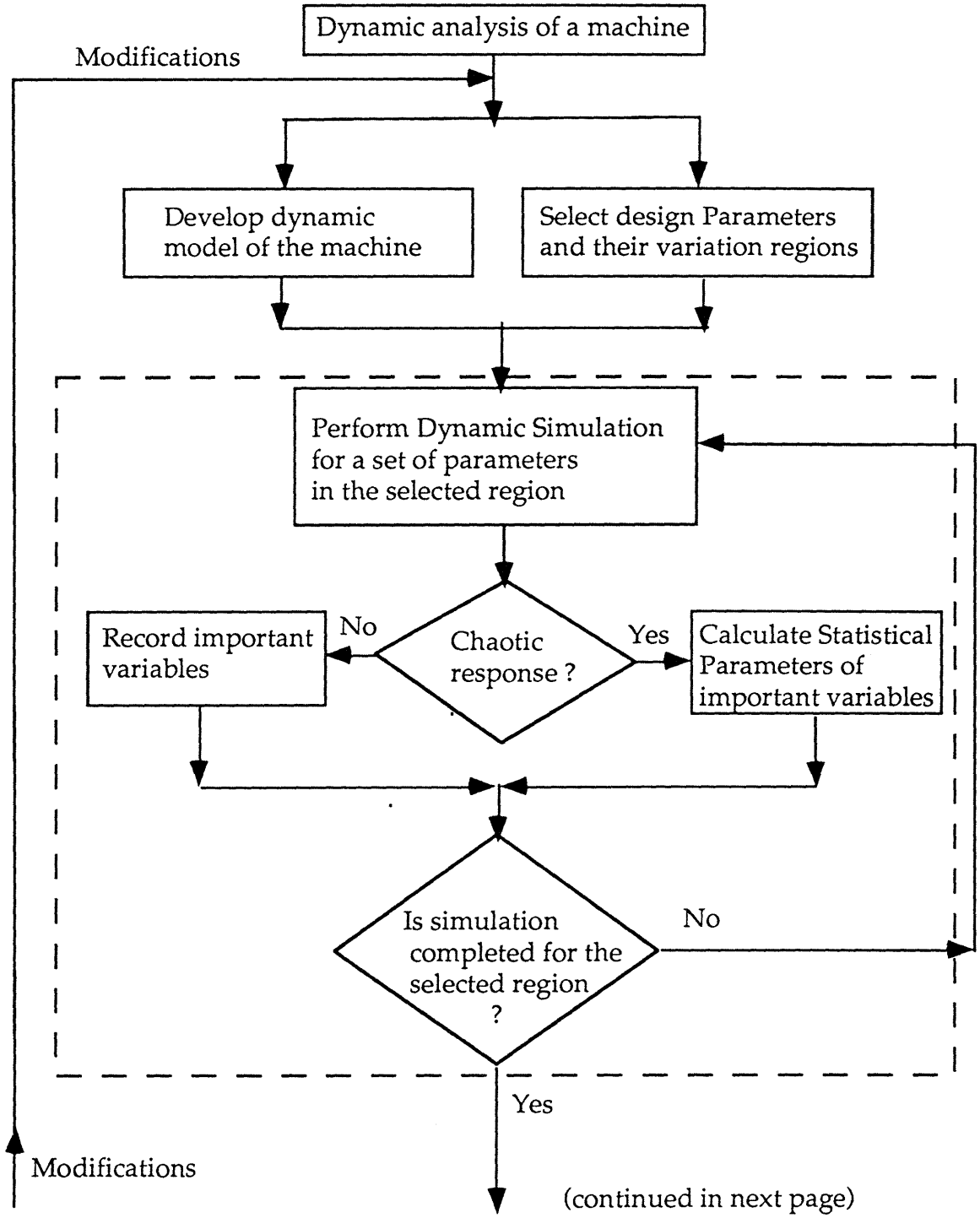

Figure 5.15 Flow chart of the proposed design methodology.

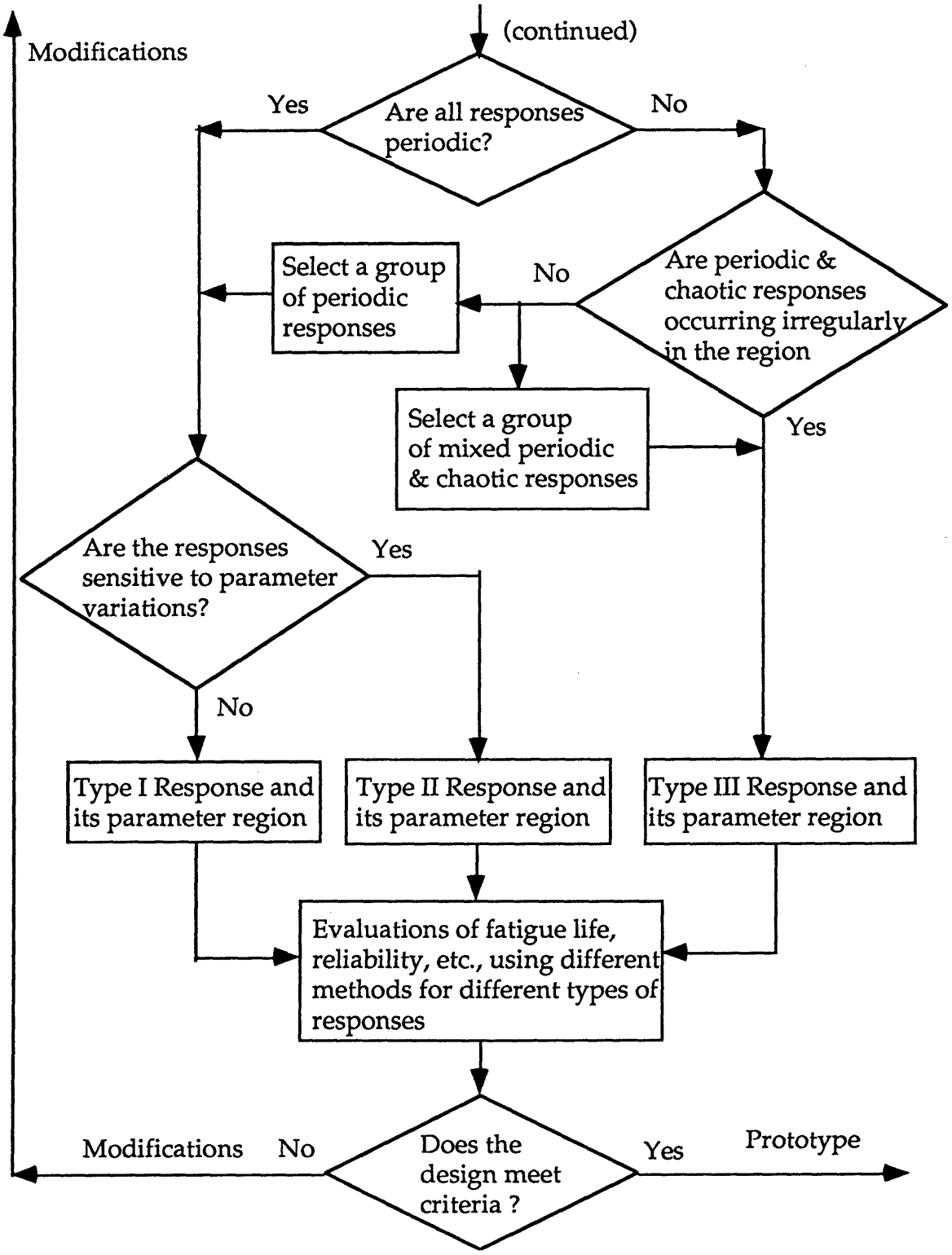

Figure 5.15 Flow chart of the proposed design methodology (continued).

5.7 Summary

This chapter discusses a major design issue for a machine that exhibits chaotic vibrations due to clearance connections and component flexibility. The following contributions have been achieved:

- The Two-Step Test method and Matrix Update Test method are developed for testing chaotic vibrations of the machine models and for classifying Type I, Type II, and Type III Responses at the design stage.
- Empirical predictive criteria are presented for the regions of system parameters that result in chaotic vibrations.
- Design guidelines are developed for evaluations of fatigue life and reliability of the components.
- A design methodology is developed to effectively use the predictions of the machine models at the design stage.

Chapter 6
Conclusions

6.1 Conclusions

The subject of this research is the design implications of chaotic vibrations in machine systems with clearance connections and component flexibility. In order to provide physical insights into the chaotic behavior of this class of machine systems, an Impact Beam System (IBS) and a Spatial Slider Crank (SSC) are investigated both numerically and experimentally. The major conclusions of this research are summarized as follows:

- The existence of chaotic vibrations in these two systems is confirmed both numerically and experimentally. The comparison between numerical and experimental results indicates that the numerical models capture much of the qualitative dynamic behaviors of the physical systems.

- Empirical predictive criteria are presented for the regions of system parameters that result in chaotic vibrations in the systems. Chaotic vibrations are found to be associated with large clearances, high operating speeds, and low values of damping.

- The sensitivity of the dynamic behaviors of the systems to small variations of the system parameters, such as clearance, component dimension, operating speed, and damping, is studied both numerically and experimentally. The sensitivities exhibited by both the physical systems and the numerical models limit the usefulness of predictions from computer-

based simulations for design. New approaches need to be developed in order to effectively use the predictions of machine models at the design stage.

- Based on the characteristics of the dynamic behaviors of the systems, the dynamic responses are classified into three characteristic types:

Type I Response is periodic, and is not sensitive to initial conditions and small variations of system parameters.

Type II Response is also periodic, and is not sensitive to initial conditions, but it is sensitive to small variations of system parameters.

Type III Response is unpredictable, either periodic or chaotic, and is sensitive to both initial conditions and small variations of system parameters.

- These classifications are useful guidelines for design. While the Type I Response is well-behaved, the Type II and Type III Responses are very sensitive to small variations of the parameters, presenting important design problems. If the system parameters are in the regions resulting in these two types of responses, the dynamic behavior of a machine system could be quite different from the predictions of its model, due to small dimension variations and uncertainties in the values chosen for model parameters. In particular, the periodicity of the Type II Response may lead designers to overlook the sensitivity of the dynamic behavior. The sensitivity of the Type II Response to the small variations of the parameters is due to the existence of clearance connections and component flexibility. If there is no component flexibility, other than bearing compliance, there will be no the Type II Response.

- To test the chaotic behavior of machine models at the design stage, the Two-Step Test method and the Matrix Update Test method are developed. Guidelines are developed for classifying three types of responses and for evaluating the fatigue life and reliability of machine systems. A design methodology, which implements these methods and guidelines, is developed to most effectively use the predictions of machine models at the design stage.

References

[1] Aidanpää, J. O. and Gupta, R. B., "Periodic and Chaotic Behavior of a Threshold-limited Two-degree-of-Freedom System," *J. of Sound and Vibration*, Vol. 165, No. 2, pp.305-327, 1993.

[2] Concurrent Computer Corporation, *Laboratory Workbench User's Guide*, 1989.

[3] Deck, J. F., *The Dynamics of Spatial Elastic Mechanisms with Clearances and Support Structures*, Ph.D Thesis, Dept. of Mechanical Engineering, MIT, 1992.

[4] Deck, J. F. and Dubowsky, S., "On the Limitations of Predictions of the Dynamic Response of Machines with Clearance Connections," To appear in *J. of Mechanical Design*.

[5] Dubowsky, S., and Freudenstein, F., "Dynamic Analysis of Mechanical Systems with Clearances - Pt. I: Formation of Dynamic Model; Pt. II: Dynamic Response," *J. of Engineering for Industry*, Vol. 93, Series B, No. 1, pp. 305-316, 1971.

[6] Dubowsky, S., and Gardner, T. N., "Dynamic Interactions of Link Elasticity and Clearance Connections in Planar Mechanical Systems," *J. of Engineering for Industry*, Vol. 97, No. 2, pp. 652-661, May 1975.

[7] Dubowsky, S., Deck, J.F., and Costello, H.M., "The Dynamic Modeling of Flexible Spatial Machine Systems with Clearance Connections," *J. of Mechanisms, Transmissions and Automation in Design*, Vol. 109, No. 1, pp. 87-94, Mar. 1987.

[8] Dubowsky, S., Gu, P.-Y., and Deck, J. F., "The Dynamic Analysis of Flexibility in Mobile Robotic Manipulator Systems," *Proc. of the Eighth World Congress on the Theory of Machines and Mechanisms*, Vol. 1, pp. 9-12, Prague, Czechoslovakia, 1991.

[9] Earles, S. W. E., and Seniviratne, L. D., "Some Kinetic Effects of Clearances in Revolute Joints of Linkage Mechanisms," *7th World Congress, Theory of Machines and Mechanisms*, Sevilla, pp. 523-528, 1987.

[10] Earles, S. W. E. and Wu, C. L. S., "A Design Criterion for Maintaining Contact at Plain Bearings," *Proceedings of the Institute of Mechanical Engineers*, 194. pp. 249-258, 1980.

[11] Farahanchi, F., and Shaw, S. W., "Chaotic and Periodic Dynamics of a Slider Crank Mechanism with Slider Clearance," To appear in *J. of Sound and Vibration*.

[12] Goodman, T.P., "Dynamic Effects of Backlash," *Machine Design*, May 23 pp. 150-157, 1963.

[13] Grant, S. J. and Fawcett, J. N., "Control of Clearance Effects in Mechanisms," *J. of Mechanical Design*, Vol. 100, pp. 728-731, 1978.

[14] Grant, S. J. and Fawcett, J. N., "Effects of Clearance at the Coupler-Rocker Bearing of a 4-Bar Linkage," *Mechanism and Machine Theory*, Vol. 14, pp. 99-110, 1979.

[15] Grebogi, C., Ott, E., and Yorke, J. A., "Crises, Sudden Changes in Chaotic attractors and Transient Chaos," *Physica*, 7D, pp. 181-200, 1983.

[16] Guckenheimer, J. and Holmes, P., *Nonlinear Oscillations, Dynamical Systems and Bifurcations of Vector Fields*, New York, Springer-Verlag.

[17] Haines, R. S., "An Experimental Investigation into the Dynamic Behavior of Revolute Joints with Varying Degrees of Clearance," *Mechanism and Machine Theory*, Vol. 20, No. 3, pp. 221-231, 1985.

[18] Haines, R. S., "Survey: Two Dimensional Motion and Impact at Revolute Joints," *Mechanism and Machine Theory*, Vol. 15, pp. 361-370, 1980.

[19] Harris, T. A., *Rolling Bearing Analysis*, Third Edition, John Wiley & Sons, INC., 1991.

[20] Haugen, E. B., *Probabilistic Mechanical Design*, John Wiley & Sons, 1980.

[21] Heiman, M. S., Bajaj, A. K. and Sherman, P. J., "Periodic Motions and Bifurcations in Dynamics of an Inclined Impact Pair," *J. of Sound and Vibration*, Vol. 124, No.1, pp. 55-78, 1988.

[22] Hendrikes, F. "Bounce and Chaotic Motion in Print Hammers," *IBM J. Res. Dev.*, Vol. 27, No. 3, pp. 273-280, 1983.

[23] Hsu, C. S., *Cell to Cell Mapping*, Springer-Verlag.

[24] Hurty, K. H., "Dynamic Analysis of Structural Systems using Component modes," *AIAA Journal*, Vol. 3, No. 4, pp. 678-685, 1965.

[25] Imam, I., Skreiner, M., and Sadler, J. P., "A New Solution to Coulomb Friction in Mechanism Bearings: Theory and Application," *J. of Mechanical Design*, Vol. 103, pp. 764-775, Oct. 1981.

[26] Isomaki, H. M., von Boehm, J., and Raty, R., "Devil's Attractors and Chaos of a Driven Impact Oscillator," *Phys. Lett.* Vol. 107A, No. 8, pp. 343-346, 1985.

[27] Johnson, R. C., "Impact Force in Mechanisms," *Machine Design*, v. 35, pp. 150-157, 1963.

[28] Khulief, Y. A., and Shabana, A. A., "Impact Responses of Multi-Body Systems with Consistent and Lumped Masses," *J. of Sound and Vibration*, Vol. 104, No. 2, pp. 187-207, 1986.

[29] Kleczka, M., Kreuzer, E. and Schiehlen, W., "Local and Global Stability of A Piecewise Linear Oscillator," *Phil. Trans. R. Soc. Lond.* A, Vol. 338, pp. 533-546, 1992.

[30] Li, G. X., Rand, R. H., and Moon, F. C., "Bifurcations and Chaos in a Forced Zero-Stiffness Impact Oscillator," *Int. J. of Non-linear Mechanics*, Vol. 25, No.4, pp.417-432, 1990.

[31] Lichtenberg, A. J. and Lieberman, M. A., *Regular and Stochastic Motion*, Springer-Verlag, New York, 1983.

[32] Lin, R. M. and Ewins, D. J., "Chaotic Vibration of Mechanical Systems with Backlash," *Mechanical Systems and Signal Processing*, pp. 257-272, 1993.

[33] Mahfouz, I. A., and Badrakhan, F. "Chaotic Behavior of Some Piecewise-linear Systems, Part 1, 2", *J. of Sound and Vibration*, Vol. 143, No. 2, pp. 255-328, 1990.

[34] Mansour, W. M. and Townsend, M. A., "Impact Spectra and Intensities for High-Speed Mechanisms," *J. of Engineering for Industry*, Vol. 97, pp. 347-353, 1975.

[35] Mevel, B and Guyader, J. L., "Routes to Chaos in Ball Bearing," *J. of Sound and Vibration*, Vol. 162, No.3, pp. 471-487, 1993.

[36] Moon, F. C., *Chaotic Vibration*, John Wiley & Sons, New York, 1987.

[37] Moon, F. C. and Li, G., "Experimental Study of Chaotic Vibration in a Pin-Joint Space Truss Structure," *AIAA Journal*, Vol. 28, No. 5, pp. 915-921, 1990.

[38] Moon, F. C. and Shaw, S.W., "Chaotic Vibrations of a Beam with Non-linear Boundary Conditions," *Int. J. Non-linear Mechanics*, Vol. 18, No.6, pp. 465-477, 1983.

[39] Moore, D. B. and Shaw, S. W., "The Experimental Response of Impact Pendulum System," *Int. J. of Non-linear Mechanics*, Vol. 25, No. 1, pp. 1-16, 1990.

[40] Nguyen, D. T., Noah, S. T. and Kettleborough, C. F., "Impact Behavior of an Oscillator with Limiting Stops, part 1,2," *J. of Sound and Vibration*, Vol. 109, No. pp. 293-325, 1986.

[41] O'Connell, E., *Dynamic Response of a Spatial Slider Crank Mechanism with Clearances and Link Elasticity*, MS Thesis, MIT, Department of Mechanical Engineering, Cambridge, MA, August, 1990.

[42] Oppenheimer, C. H., *Impact-Induced Noise and vibration in Machine Systems for Design*, Ph.D. Thesis, MIT, Department of Mechanical Engineering, Cambridge, MA, Sept. 1992.

[43] Païdoussis, M. P. and Li, G. X., "Cross-flow-induced Chaotic Vibrations of Heat-exchanger Tubes Impacting on Loose Supports," *J. of Sound and Vibration*, Vol. 152, No. 2, pp. 305-326, 1992.

[44] Peterka, F. and Vacík, J., "Transition to Chaotic Motion in Mechanical Systems with Impacts," *J. of Sound and Vibration*, Vol. 154, No.1, pp. 95-115, 1992.

[45] Peurach, J. and Tongue, B. H., "Chaotic Response of a Slider Crank Mechanism," *J. of Vibration and Acoustics*, Vol. 113, pp. 69-73, 1991.

[46] Seneviratne, L. D. and Earles, S. W. E., "Chaotic Behavior Exhibited during Contact Loss in a Clearance Joint of a Four-bar Mechanism," *Mechanism and Machine Theory*, Vol. 27, No. 3, pp. 307-321, 1992.

[47] Seneviratne, L. D. and Earles, S. W. E., "Correlation between Contact Loss and Chaotic Behavior in a Four Bar Mechanism with a Clearance Joint," *Proc. of the Eighth World Congress on the Theory of Machines and Mechanisms*, Prague, Czechoslovakia, pp. 217-220, 1991.

[48] Sharif-Bakhtiar, M. and Shaw, S. W., "The Dynamic Response of a Centreifugal Pendulum Vibration Absorber with Motion-limiting Stops," *J. of Sound and Vibration*, Vol. 126, pp. 221-235, 1988.

[49] Shaw, Jinsiang and Shaw, S. W., "The Onset of Chaos in a Two-degree-Freedom Impact System," *J. of Applied Mechanics*, Vol. 56, pp. 168-174, 1989.

[50] Shaw, S. W., "The Dynamics of a Harmonically Excited System Having Rigid Amplitude Constraints, Part1,2," *J. of Applied Mechanics*, Vol. 52, No.2, pp. 453-464, 1985.

[51] Shaw, S. W., "Forced Vibration of a Beam with One-sided Amplitude Constraint: Theory and Experiment," *J. of Sound and Vibration*, Vol. 99, No.2, pp. 199-212, 1985.

[52] Shaw, S. and Holmes, P. J., "Periodically Forced Linear Oscillator with Impacts: Chaos and Long Period Motions," *Physical Review Letters*, Vol. 51, No. 8, pp. 623-626, 1983.

[53] Shaw, S. and Holmes, P. J., "A Periodically Forced Impact Oscillator with Large Dissipation," *J. of Applied Mechanics*, Vol. 50, pp. 849-851, 1983.

[54] Shaw, S. and Holmes, P. J., "A Periodically Forced Piecewise Linear Oscillator," *J. of Sound and Vibration*, Vol. 90, No.1, pp. 129-155, 1983.

[55] Shaw, S., and Rand, R. H., "The Transition to Chaos in a Simple Mechanical System," *Int. J. of Non-Linear Mechanics*, Vol. 24, No.1, pp. 41-56, 1989.

[56] Shigley, J. E. and Mischke, C. R., *Mechanical Engineering Design*, Fifth Edition, McGraw-Hill Inc., 1989.

[57] Soong, K., and Thompson, B. S., "A Theoretical and Experimental Investigation of the Dynamic Response of a Slider-Crank Mechanism with Radial Clearance in the Gudgeon-Pin Joint," *J. of Mechanical Design*, Vol. 112, pp. 183-189, 1990.

[58] Sunada, W. H., and Dubowsky, S., "The Application of Finite Element Methods to the Dynamic Analysis of Flexible Spatial and Co-planar Linkage Systems," *J. of Mechanical Design*, Vol. 103, No. 3, pp. 643-651, 1981.

[59] Sunada, W.H., and Dubowsky, S., "The Application of Finite Element Methods to the Dynamic Analysis of Flexible Spatial and Co-planar

Linkage Systems," *J. of Mechanical Design*, Vol. 103, No. 3, pp. 643-651, July 1981.

[60] Thompson, J. M. T., "Complex Dynamics of Compliant Off-shore Structures," *Proc. R. Soc. Lond.* A 387, pp. 407-427, 1983.

[61] Thompson, J. M. T. and Stewart, H. B., *Nonlinear Dynamics and Chaos*, Wiley, Chichester.

[62] Thompson, J.M. T. and Ghaffari, R., "Chaos after Period-Doubling Bifurcations in the Resonance of an Impact Oscillator," *Phys. Lett.* A91(1), pp. 5-8, 1982.

[63] Timoshenko, S. P. and Goodier, J. N., *Theory of Elasticity*, Third Edition, McGraw-Hill Inc., 1970.

[64] Tongue, B. H., "Characteristics of Numerical Simulations of Chaotic Systems," *J. of Applied Mechanics*, Vol. 54, pp. 695-699, 1987.

[65] Tung, P. C. and Shaw, S. W., "The Dynamics of an Impact Print Hammer," *J. of Vibration, Acoustics, Stress and Reliability in Design*, Vol. 110, pp. 193-200, 1988.

[66] Tung, P. C. and Shaw, S. W., "A Method for the Improvement of Impact Printer Performance," *J. of Vibration, Acoustics, Stress and Reliability in Design*, Vol. 110, pp. 528-532, 1988.

[67] Whiston, G. S., "Global Dynamics of A Vibro-Impacting Linear Oscillator," *J. of Sound and Vibration*, Vol. 118, No.3, pp. 395-429, 1987.

[68] Wolf, A. Swift, J. B., Swinney, H. L. and Vastano, J. A., "Determining Lyapunov Exponents form Time Series," *Physica*, 16D, pp. 285-317, 1985

[69] Yorke, J. and Li, T.-Y., "Period Three Implies Chaos," *Am. Math. Monthly*, Vol. 82, pp. 985-992, 1975.